12-2021

Theoretical investigation of the Co-C bond activation in methylcobalamin and adenosylcobalamin-dependent systems: mechanistic insights.

Arghya Pratim Ghosh
University of Louisville

THEORETICAL INVESTIGATION OF THE Co-C BOND ACTIVATION IN METHYLCOBALAMIN AND ADENOSYLCOBALAMIN-DEPENDENT SYSTEMS: MECHANISTIC INSIGHTS

By

Arghya Pratim Ghosh
B.Sc., Visva-Bharati University, 2014
M.Sc., Visva-Bharati University, 2016
M.S., University of Louisville 2020

A Dissertation
Submitted to the Faculty of the
College of Arts and Sciences of the University of Louisville
in Partial Fulfillment of the Requirements
for the Degree of

Doctor of Philosophy in Chemistry

Department of Chemistry
University of Louisville
Louisville, Kentucky

December 2021

THEORETICAL INVESTIGATION OF THE Co-C BOND ACTIVATION IN METHYLCOBALAMIN AND ADENOSYLCOBALAMIN-DEPENDENT SYSTEMS: MECHANISTIC INSIGHTS

By

Arghya Pratim Ghosh
B.Sc., Visva-Bharati University, 2014
M.Sc., Visva-Bharati University, 2016
M.S., University of Louisville 2020

A Dissertation Approved on

November 17, 2021

By the following Dissertation Committee

Dr. Pawel M. Kozlowski (Dissertation Director)

Dr. Craig A. Grapperhaus

Dr. Lee M. Thompson

Dr. Badri Narayanan

DEDICATION

This dissertation is dedicated to my respected father, Sh. Indranath Ghosh who always

encouraged and motivated me for pursuing higher education in science

ACKNOWLEDGEMENTS

This thesis is a result of a combined effort of many people, all of whom I would like to acknowledge for their guidance, faith, and support in helping me with finishing it. I start with my advisor and mentor, Dr. Pawel M. Kozlowski. I am truly grateful and extremely indebted to him for allowing me to be a part of his computational bio-inorganic chemistry research team. His guidance, expertise, patience, and support throughout my graduate studies have been critical to my journey as a graduate student. It was a wonderful experience working with him. I look forward to his advice and valuable suggestions in the future as well.

I want to convey my deepest appreciation to my committee members Dr. Craig Grapperhaus, Dr. Lee Thompson, and Dr. Badri Narayanan, for their valuable suggestions and advice during my Ph.D. I am also extremely grateful to my collaborators, Dr. Maria Jaworska, Dr. Piotr Lodowski, Dr. Szymon Malinowski, Dr.Sarah Edwards, and Dr.Justyna Jaroszynska-Wolinska. Special gratitude goes to Dr. Piotr Lodowski, whose expertise, insights, and valuable suggestions have been crucial in our collaborations. Finally, my sincere regard goes to my master's project advisor Dr. Manas Ghosh and Dr. Pranab Sarkar, for always encouraging me to do good science and pursue Ph.D.

I would also like to thank the Department of Chemistry for offering me the teaching assistantship position during my graduate research. It would not be possible without the generous support from the department. Without the necessary help and faithful efforts of

iv

the staff of the Chemistry Department, especially that of Sherry Nalley, my life as a graduate student would have been more difficult. In addition to these, I am extremely thankful to the Cardinal Research Cluster (CRC) at the University of Louisville and Lipscomb High-Performance Computing Cluster at the University of Kentucky Information Technology Department for providing access to high-performance computing facilities. I am truly grateful to Mr. Harrison Simrall from Cardinal Research Cluster (CRC) for his invaluable help with the CRC-related technical issues.

I consider myself fortunate to have some good colleagues who were very helpful and supportive throughout my journey. Dr. Abdullah Mamun, my good friend, ex-roomie, and a great colleague who was extremely helpful throughout my graduate journey. He was my first 'go-to' person for any problem inside and outside the lab. Thank you for helping me with research, teaching me how to drive, and taking me to groceries whenever I asked. I had a very pleasant experience working with Dr. Megan J. Toda and Saurav Parmar, who are excellent friends and wonderful colleagues. Dr. Brady Garabato, thank you for giving me your desktop and helping me with many technical problems.

My stay in Louisville was enriched and enjoyable because of some people I met who will always be in my heart. Avinash uncle and Madhu aunty, words cannot explain how much you mean to my wife and me. Thank you for making us a part of your family and giving us so much love. I will always cherish our relationship and every moment we spent in your house. Chinmay, Kritika, Deepika, and Vasu, you guys brought so much joy to my life. You guys are more than friends. I would also like to acknowledge Hari, Anthony, Opu, Ramya, and Anwar for their friendship.

ABSTRACT

THEORETICAL INVESTIGATION OF THE Co-C BOND ACTIVATION IN
METHYLCOBALAMIN AND ADENOSYLCOBALAMIN-DEPENDENT
SYSTEMS: MECHANISTIC INSIGHTS

Arghya Pratim Ghosh

November 17, 2021

The vitamin B_{12} derivates, otherwise known as cobalamin (Cbl), are ubiquitous

organometallic cofactors. The biologically active forms of Cbl, such as methylcobalamin

(MeCbl) and adenosylcobalamin (AdoCbl), act as cofactors in different physiological

reactions for both prokaryotes and eukaryotes. A crucial aspect of the Cbl-mediated

systems is the activation of the organometallic Co-C bond that plays a critical role in its

catalytic activity. One of the most remarkable features of this Co-C bond is its unusual

activation in AdoCbl-dependent enzymatic reactions, where a trillion-fold rate acceleration

of the Co-C bond cleavage is observed inside the enzyme compared to the isolated AdoCbl.

Although several hypotheses have been proposed previously, none can fully explain the

trillion-fold rate acceleration that is observed for the Co-C bond cleavage. Thus, the

factor(s) responsible for the unusual activation of the Co-C bond in the AdoCbl-dependent

enzyme remains elusive. Nonetheless, this Co-C bond of MeCbl and AdoCbl cofactors is

also known for its unique ability to be activated both thermally and photolytically within

the enzymatic environment as well as in solutions. Even though the photochemistry of

Cbl-dependent systems has been known for almost five decades, it has recently received

a lot of attention due to its potential role in light-activated drug delivery, biomimetic catalysis, and a variety of other applications. Therefore, with these applications in mind, understanding the mechanistic insight into the activation of the Co-C bond is paramount for gaining a comprehensive knowledge of these reactions.

In this dissertation, the mechanistic details of the activation of the Co-C in the photolysis and native catalysis of MeCbl and AdoCbl-dependent systems have been investigated using hybrid quantum mechanics/molecular mechanics (QM/MM) simulations, density functional theory (DFT), and time-dependent density functional theory (TD-DFT) methodologies. Overall, this dissertation is divided into six chapters. Chapter one gives an introduction, a historical overview of B_{12} chemistry, and possible applications in therapeutics and optogenetics. Chapters two and three discuss the photoactivation of the Co-C bond in MeCbl-dependent methionine synthase (MetH) and explore the role of the enzymatic environment on photoreaction. The photochemical data of isolated MeCbl cofactor in solution were also discussed and compared with the enzymatic environment to understand the effect of protein binding on the photolysis of Co-C bonds. The influence of mutation on the photolysis of Co-C is discussed in chapter three. Overall, in these two chapters, it was shown that the enzymatic environment affects the photolysis of the Co-C bond by modulating the electronically excited state. Chapter four provides an in-depth insight into the aerobic photolysis of MeCbl, with emphasis placed on the mechanistic details of the insertion of O_2 in the activated Co-C bond. It was shown that the photochemical properties of MeCbl can also be modulated in the presence of molecular oxygen, i.e., in aerobic conditions.

While chapters two to four cover the light-activation of the Co-C bond, chapter five focused on the activation of the Co-C bond during the native catalysis of AdoCbl-dependent methylmalonyl CoA mutase (MCM). The QM/MM methodology has been used to investigate the factor(s) responsible for the unusual activation of the Co-C bond that is observed in the enzyme as compared to AdoCbl in solution. While there are at least three previously reported hypotheses for the activation of the Co-C$_{5'}$ bond including, substrate-induced conformational changes, electrostatic interaction between the Ado group and the enzyme, and involvement of tyrosine residue, none of these can explain this unusual activation. Thus, how the arrival of the substrate triggers the activation of the Co-C$_{5'}$ bond remains an open issue.

TABLE OF CONTENTS

LIST OF TABLES

LIST OF FIGURES

LIST OF SCHEMES

CHAPTER I

INTRODUCTION

1.1. Vitamin B_{12} and its derivatives: A brief history

The journey of B_{12} chemistry started in 1925 with a serendipitous encounter, when Whipple, Minot, and Murphy found an antianemic factor in the raw liver that can reverse anemia in dogs and humans.[1] This discovery brought a monumental change in the treatment of "pernicious anemia" because, before this discovery, death was inevitable. As a result, Whipple, Murphy, and Minot shared the 1934 Nobel Prize in Physiology or Medicine for their life-saving discovery found in the liver.[2] This discovery prompted an upsurge in the research activities in this area, which helped in flourishing this field in many notable contributions, such as the initial isolation of vitamin B_{12} by Folkers, Sharp, Dohme, and Smith in 1948 and the crystallization of B_{12} by a British scientist Dorothy Crowfoot Hodgkin.[3-5] This crystallization of the complex structure of vitamin B_{12} is considered a breakthrough in B_{12} chemistry.[6] Later on, Woodward and Eschenmoser, in 1972, reported the first total synthesis of the B_{12} cofactor.[7] All the aforementioned discoveries have led the ground for an explosion of work on chemical, biochemical, as well as enzymatic aspects of B_{12} cofactors. Vitamin B_{12} and its derivatives, commonly known as cobalamins (Cbls) (Figure 1.1), are among nature's most complex organometallic compounds, which play a critical role in the metabolism of microorganisms, animals and humans.
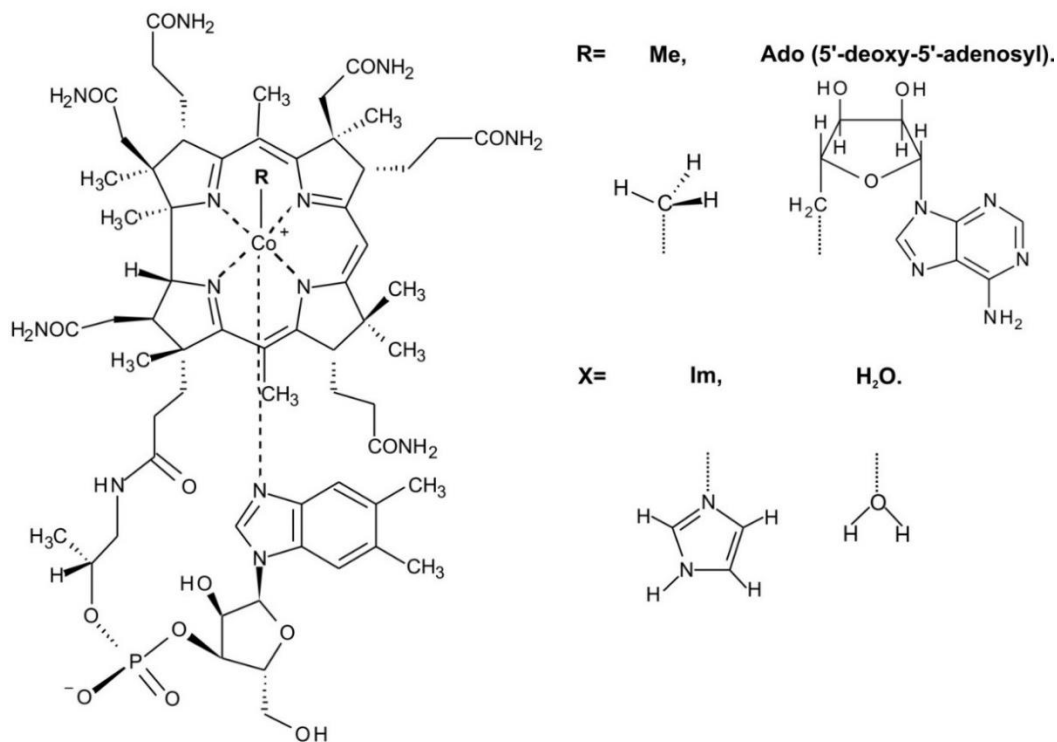
Figure 1.1. Left: General molecular structure of cobalamins. Right: Molecular structure of upper axial ligands for methylcobalamin (R=Me) and adenosylcobalamin (R=Ado). Molecular structure of lower axial ligands for base-on (X=Im) and base-off (X=H$_2$O) model structures.

However, unlike the microorganisms that can fully synthesize B$_{12}$ *de novo*, higher organisms such as mammals do not possess mechanisms to synthesize it within their bodies.[8-10] Instead, they uptake their required Cbls from dietary sources. A complex metabolic mechanism is employed [9, 11] to ensure efficient uptake of dietary Cbls, which selects for Cbls and delivers them to cells, where Cbls are transformed into the physiologically relevant cofactors methylcobalamin (MeCbl) and adenosylcobalamin (AdoCbl). These two biologically active cofactors catalyze two essential physiological reactions in mammals, as well as in bacteria.[12] In humans, the AdoCbl-dependent methylmalonyl-CoA mutase (MCM) catalyzes the radical rearrangement of methylmalonyl-CoA (MCoA) to succinyl- CoA (SCoA).[13-15] This conversion is critical in

the catabolism of branched-chain amino acids, odd-chain fatty acids, and cholesterol.[16] On the other hand, MeCbl serves as a cofactor for methionine synthase (MetH), which catalyzes the synthesis of methionine (Met) by the methylation of the homocysteine (Hcy).[17-18] This reaction is necessary for maintaining a balanced distribution of cellular folate derivatives and preventing Hcy buildup.[19]

1.2. General molecular structure of B$_{12}$ derivatives

Cbls belongs to the porphyrinoid family, comprised of a negatively charged corrin macrocycle with several side chains of acetamide and propionamide groups bound to the periphery of the corrin ring.[20-23] Like porphyrin, the corrin ligand is also a part of linearly π-conjugated systems that belong to the family of tetrapyrrolic macrocycles.[24] Centralized in the corrin ring is low-spin cobalt (Co) ion, which is equatorially coordinated to four nitrogen of the macrocycle.[25] The Co(III) form is further coordinated to upper and lower axial ligands in the Co(III) state. The upper axial position is commonly known as the β axial site, whereas the lower axial position is generally referred to as the α axial site (Figure 1.1). In what is known as the base-on conformation, the metal center is ligated with 5,6-dimethylbenzimidazole (DBI) as the lower ligand. Regardless of its oxidation state, the Co ion is always ligated with the four pyrrolic nitrogen of the corrin ring. In addition to the base-on conformation found in both solution and enzymes, Cbls can be found in different conformations[26] depending on their environment. In very acidic condition aqueous solution (i.e., ~pH 2), the protonated DBI group can be replaced with a weakly coordinated water molecule.[21, 27-28] This is known as the base-off configuration.

Upon binding with enzymes, the DBI base of the lower axial face can be detached and replaced with the imidazole (Im) moiety of a histidine (His) residue of the protein. This is

known as base-off/His-on configuration, exemplified by MetH.[17, 29] On the other hand, the upper axial position can be coordinated with various ligands, such as cyano (CN), hydroxyl (OH), methyl (Me), adenosyl (Ado), (Figure 1.1), etc.[4, 23, 30] Depending on the nature of the upper axial ligand, Cbls are distinguished from each other and can also be classified as B_{12} derivatives into alkyl and non-alkyl Cbls. The former compounds include Ado groups or Me as an upper axial ligand, which act as a cofactor in numerous enzymatic reactions. These two are the only naturally occurring bio-inorganic cofactor with an organometallic metal-carbon bond (Co-C bond in this case) that participates in enzymatic reactions. On the other hand, vitamin B_{12}, commonly known as cyanocobalamin (CNCbl) with the CN^- group as upper axial ligand, is classified as non-alkylcobalamin. The other known examples of non-alkyl Cbls are aquacobalamin (H_2OCbl), hydroxocobalamin (HOCbl), and azidcobalamin (N_3Cbl).[31] The Co atom in Cbls resides in the low spin, +3 oxidation states under nonreducing circumstances, with two axial ligands appended from the corrin macrocycle's periphery.[23] Furthermore, there are two further low-oxidation forms of Cbls, namely, cob(I)alamin (Co^I) and cob(II)alamin (Co^{II}), that are important in enzymatic processes. For example, one-electron reduction of cob(III)alamin (Cbl^{III}) by a reducing agent or homolytic cleavage of the Co-C bond can produce Cbl^{II}. On the other hand, one-electron reduction of cob(II)alamin or heterolytic cleavage of the Co-C bond generates Cbl^I.[32]

1.3. Functional and biological importance of B_{12}-dependent enzymes

Since its discovery, B_{12} has been best known for its role as a cofactor in enzymatic catalysis. So, historically the main focal point of B_{12} research has been related to its functions and reactivity in biologically essential reactions.[8, 10, 12, 19, 32-42] B_{12} derivatives are

classified as isomerases, methyltransferases, or reductive dehalogenases based on the types of biological reactions they catalyze. Cbl-dependent methyltransferases (MeTrs) that catalyze Me transfer reaction plays a vital role in amino acid metabolism and CO_2 fixation in many organisms that are especially important for anaerobic organisms in their energy generation processes.[34, 42] AdoCbl-dependent isomerases play a role in DNA replication and repair (ribonucleotide reductase). In addition, they are involved in various radical events such as 1,2 rearrangement reactions, heteroatom eliminations, and intramolecular amino group migrations.[34, 38, 43-48]

On the other hand, the dehalogenases class of enzyme, which plays a crucial role in dehalorespiration, is well-reputed for its involvement in detoxifying aliphatic and aromatic chlorinated organic compounds.[34, 42, 49-50] The dehalorespiring bacteria have been shown to play an essential role in the transformation and detoxification of chlorinated compounds such as perchloroethylene or trichloroethene.[51-53] Their ability to degrade halogenated pollutants has ecological benefits because bacteria can be efficiently used in environmental detoxification via bioremediation. So, B_{12}-dependent systems play a crucial role in catalyzing many biologically important reactions. Thus, their role as a cofactor for numerous enzymatic reactions has been explored and discussed in the literature.

Nevertheless, there are only two B_{12}-dependent enzymes found in mammals, the MeCbl-dependent MetH and AdoCbl-dependent MCM.[17, 51, 54] MetH catalyzes methionine biosynthesis by transferring the Me group from methyltetrahydrofolate (CH_3-H_4folate) to thiolate of Hcy via the demethylation of the tetrahydrofolate (H_4-folate).[29, 34, 55-56] While Met is a necessary amino acid, H_4-folate is involved in the manufacture of amino acids, purines, and pyrimidine and is thus needed for nucleic acid synthesis. Although it is unclear

how the MetH activates the methyl donor during the reaction, the catalytic process begins

with the displacement of the Me group, which is associated with the activation of the

organometallic Co-C bond. The scheme of this catalytic process is shown in Figure 1.2.
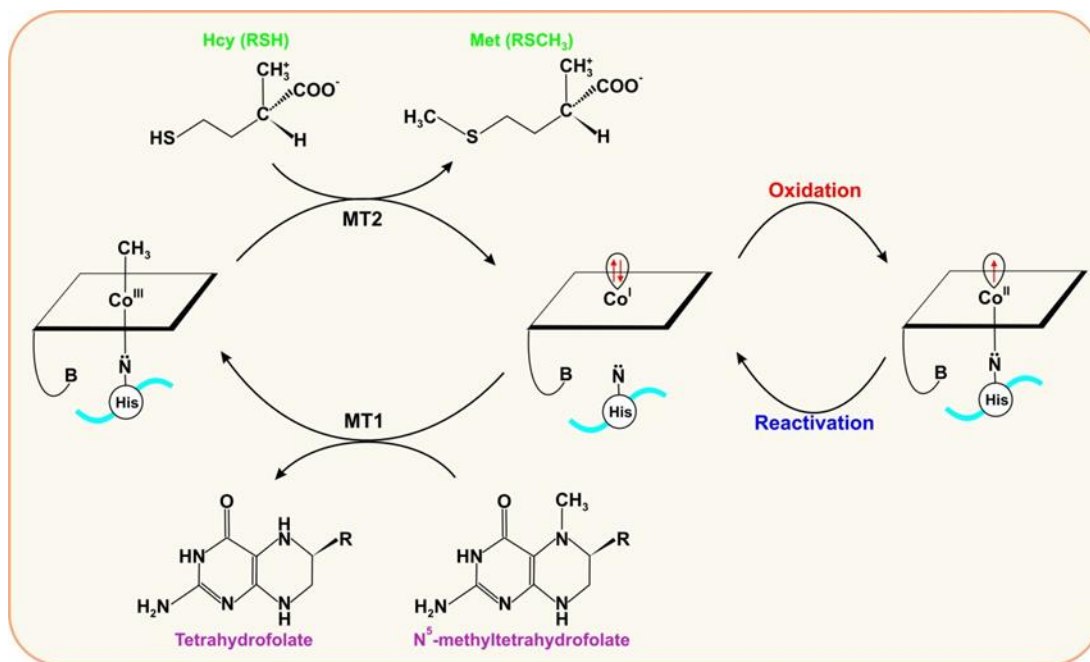
Figure 1.2. General mechanism of the catalytic cycle of methyl-tetrahydrofolate to homocysteine for MeCbl-dependent MetH.

While the MeCbl-dependent MetH catalyzes the methyl transfer reaction via a

formally heterolytic rupture of the Co-C_5 bond, the AdoCbl-dependent MCM serves as a

radical reservoir and catalyzes several radical-mediated enzymatic reactions.[12, 15, 18, 55-57]

These include heteroatom elimination, 1,2-amino shift, and carbon skeleton rearrangement.

Among coenzyme B_{12}-dependent enzymes, MCM is one of the widely investigated

enzymes, that catalyze the reverse isomerization of MCoA to SCoA (Figure1.3). Unlike

the MeCbl-dependent MetH, the MCM's catalytic process starts with the homolytic

cleavage of the Co-C bond. In mammals, it converts MCoA to SCoA during the catabolism

of odd-chain fatty acids and cholesterol.[39] Any abnormalities in MCM activity could result

in a metabolic disorder known as acidosis. Thus, given the undeniable importance of B_{12} and its derivatives in medical therapy, such as anti-tumoral antibodies,[58-59] as well as in various critical biological reactions, it remains a fascinating topic of research.
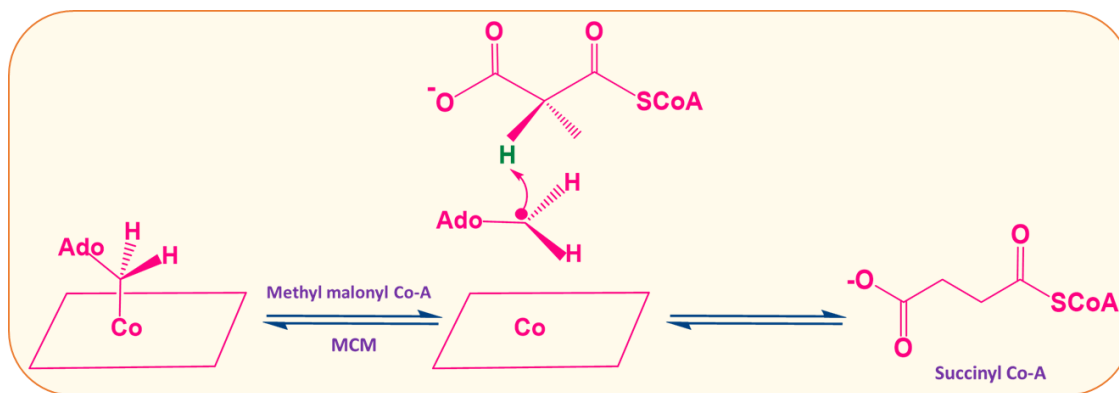
Figure 1.3. Scheme of native catalysis reactions catalyzed by MCM

1.4. Current understanding towards the Co-C bond activation in B_{12}-dependent mutases during the native catalysis

AdoCbl-dependent mutases belong to the isomerases class of B_{12} enzyme that catalyzes the carbon-skeleton rearrangements.[14, 48, 60-61] The initial step in these reactions is the homolytic cleavage of the Co-C bond, followed by subsequent hydrogen abstraction from the substrate (Figure 1.4). The homolytic cleavage of the Co-C bond produces the Co(II)/5-deoxyadenosyl (Ado•) radical pair (RP), which instantly abstracts an H-atom from an inactivated C-H bond in the substrate and generate a substrate radical. The radical substrate then subsequently undergoes a 1,2 rearrangement and re-abstracts an H-atom from 5'-deoxyadenosine to generate the Ado•, which subsequently recombines with cob(II)alamin to complete the enzyme cycle.[32, 39, 62] A critical aspect of AdoCbl-dependent enzymatic reactions is that the H-atom abstraction by Ado• and the homolysis of the

organometallic Co-$C_{5'}$ bond are coupled, as reported from an investigation based on kinetic isotopic effect (KIE) studies through pre-steady state stopped-flow experiment.[63-66] The UV-spectral change during the catalytic reaction of AdoCbl-dependent MCM and GLM with a deuterated substrate shows a substantially lower rate, revealing the abstraction steps of the H-atom is the rate-limiting step of the reaction, supporting the kinetic connection of two processes.[63, 67]
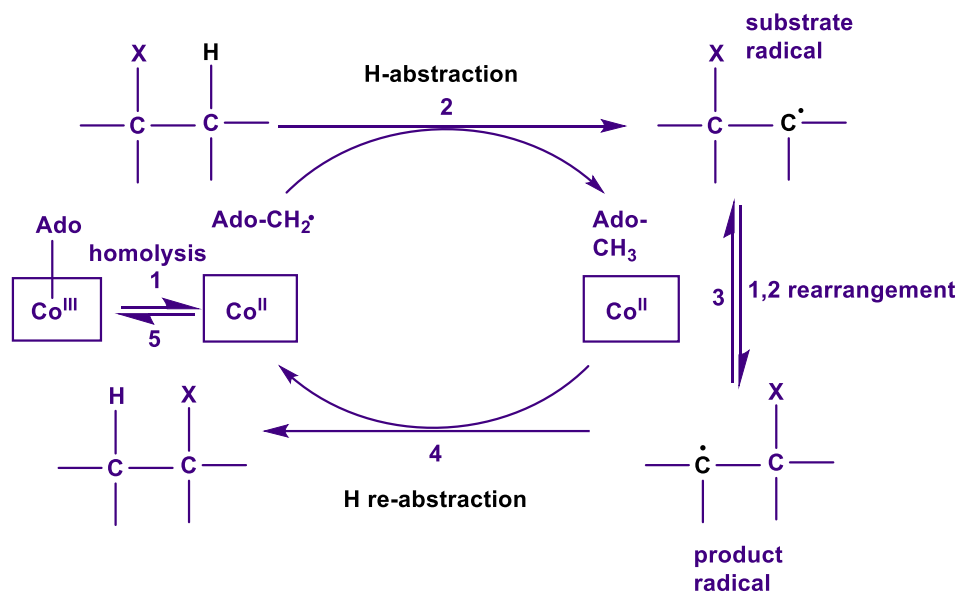
Figure 1.4. Mechanistic pathway of the native catalytic cycle of AdoCbl-dependent enzymes.

The most important feature of the catalytic reaction of AdoCbl-dependent mutases is the unusual activation of the Co-$C_{5'}$ bond. While upon binding with the substrate, the cleavage of the Co-$C_{5'}$ bond in B_{12}-dependent mutases occurs on the millisecond timescale, the homolysis of isolated AdoCbl in solution is very slow.[45, 68-69] The half-life of this bond homolysis in an isolated AdoCbl cofactor is almost six months.[45, 69] Based on kinetic studies, it has been found that the homolysis of the Co-$C_{5'}$ bond in several coenzyme B_{12}-dependent mutases attains a high catalytic rate (k_{cat}) of 2-300 s^{-1}. Thus, it appears that in

AdoCbl-dependent enzymatic reactions, the homolysis of the Co-C$_5$ bond occurs at a trillion-fold faster rate than thermal homolysis in solution.[68, 70] This is the most fascinating, as well as still not fully understood, aspect of AdoCbl-dependent enzymatic reactions. Therefore, the fundamental question is, "what triggers the activation of this Co-C$_{5'}$ bond in AdoCbl-dependent mutases?" Thus, to understand the unusual activation of the Co-C bond and the origin of this large catalytic effect inside the enzyme, it is essential to elucidate the complete mechanism of the Co-C$_{5'}$ bond activation at the molecular level.

Based on kinetic and computational studies, many different mechanistic proposals regarding the unique labilization of the Co-C$_{5'}$ bond have been discussed.[71-81] Earlier, it was suggested that the protein might increase the corrin ring folding and weaken the upper axial Co-C bond by compressing and distorting the corrin ring and Ado fragment.[82] This compression can cause destabilization of the ground state and strain to the Co-C$_{5'}$ bond. Furthermore, the puckering of the corrin-ring pucker also depends on the lower-axial ligand. However, several experimental and theoretical studies later refute the strain hypothesis.[83] These studies found that changing the lower axial ligand from the native dimethyl benzimidazole (DBI) to a smaller ligand does not affect the strength of the Co-C$_{5'}$ bond, and the lower axial base does not affect the Co-C bond strength in the ground state. Furthermore, crystal structures of various AdoCbl-dependent enzymes, such as ethanolamine ammonia-lyase (EAL), diol dehydratase (DDH), and glycerol dehydratase (GDH), show that substrate binding does not change the structure of the corrin ring, and the Co-N$_{Im}$ bond is longer than isolated AdoCbl in solution, proving the strain hypothesis invalid.[84-85]

More recently, another hypothesis was put forward by Warshel and his group, which suggests that the origin of the catalytic power in AdoCbl-dependent enzymes is associated with the electrostatic interaction between the ribose of the Ado group and the amino acid residues of the enzyme active site.[71-72]. In addition to these, it has also been suggested that the catalytic power originates from binding the substrate molecule to the apoenzyme.[75, 86] It has further been postulated that the binding of the substrate triggers the radical formation by inducing the destabilization of the Co-$C_{5'}$ bond.[76, 85] However, no consensus was reached based on this mechanism. Moreover, a study based on the AdoCbl-dependent DDH suggests that a major conformational change can also be witnessed in the substrate-free enzyme upon the binding of AdoCbl cofactor with the apoenzyme, which leads to the labilization of the Co-$C_{5'}$ bond.[76, 84] Thus, one cannot draw any logical conclusion into how the conformational change induced by substrate binding affects the catalytic activity and the unique labilization of the Co-$C_{5'}$ bond of AdoCbl-dependent enzymes.

The x-ray structures of AdoCbl-dependent enzymes further reveal that the binding of the substrate also induces a large conformational modification to the enzyme and its active site residues. It has been noticed that in several coenzyme B_{12}-dependent enzymes, a tyrosine residue (Tyr), in particular, is situated in the vicinity of the AdoCbl cofactor at an average distance of 7.5 Å from the Co atom of the corrin ring.[86] The phenoxyl oxygen of this Tyr is directed toward the cofactor or the substrate molecule. Moreover, it has been reported that a site-specific mutation of a Tyr residue (by a phenylalanine residue) induced a significant drop in the catalytic activity of the enzyme of AdoCbl-dependent MCM. Based on these observations, another hypothesis in understanding the catalytic origin of

AdoCbl-dependent enzymes has been put forward.[79-81] It has been proposed that a conformational change upon substrate binding results in the displacement of phenoxyl hydrogen of the Tyr residue, which is in the vicinity of the AdoCbl cofactor, toward the substrate. This displacement of phenoxyl hydrogen can induce an intramolecular electron transfer (ET) from the Tyr residue to the AdoCbl cofactor. This ET to the cofactor can significantly reduce the bond dissociation energy (BDE) of the Co-C$_{5'}$ bond, which may lead to the acceleration in the catalytic rates (k_{cat}). It is important to mention that the role of Tyr residue as a redox center has been discussed before in many biological processes, such as in cytochrome c oxidase, photosystem I/II, ribonucleotide reductase.[87-91] Regardless of all these different proposals, a consensus has not been reached about the origin of the unique catalytic power AdoCbl-dependent enzymes, and thus, it demands further investigations.

1.5. Photo-activation of the Co-C bond in Cbl-dependent systems

Since the discovery of vitamin B$_{12}$, it has been a subject of extensive research and is mainly known for its biochemical role as a cofactor in thermally driven enzymes. However, in 1958 for the first time, Barker reported the light-sensitivity of B$_{12}$ when he found that the pseudo vitamin B$_{12}$ undergoes decomposition upon irradiation with visible light from a tungsten lamp.[92] Although initially it was considered an unwanted side reaction, in 1960, the same group of researchers conducted a detailed study to explore the photochemical cleavage of Cbl.[93] In another study, Dolphin, Pratt, and co-workers showed that while the alkyl-Cbls were photolytically unstable, the non-alkyl Cbls were insensitive to light.[94-95] Since these critical contributions, the photochemistry of Cbls gained interest among the scientific community.

In the 1990s, Matthews and co-workers used spectroscopic techniques such a UV-Vis spectroscopy and stopped-flow spectroscopy to investigate the photolytic cleavage of MeCbl inside MetH.[96-97] It was shown that UV or visible light absorption results in partitioning between relaxation through vibrational modes to the ground state and bond homolysis. The photolytic cleavage resulted in the formation of Co(II)/CH$_3$ RPs, which are surrounded by a cage provided by the protein residues. This prevents the diffusive loss of the methyl radical, which results in the recombination of RPs. Thus, the quantum yield of the photolysis is dictated by the competition between radical escape and recombination of RPs. It was further suggested that a mutation of these residues that surround the upper face of the MeCbl cofactor could increase the exposure of methyl radical and increase the rate of photolysis of MeCbl.[96-97]

With the advancement of laser spectroscopic techniques, the photochemistry of Cbls has continued to intrigue researchers more than ever before. Sension and co-workers have been using ultrafast transient absorption spectroscopy (TAS) to investigate the photolytic properties of Cbls since the late 1990s.[97-101] They demonstrated that the photolysis of MeCbl is sensitive to the excitation wavelength. Excitation at 400 nm results in the formation of two distinct photoproducts, bond homolysis and a metastable state, which has an absorption spectrum consistent with the formation of cob(III)alamin. On the other hand, following excitation with 500 nm results in only the formation of metastable cob(III)alamin without prompt photolysis.[100] They have also investigated the photolytic properties of AdoCbl in solution and the protein environment in GLM to study how the protein-coenzyme interaction affects photoreactivity. It was shown that, unlike MeCbl, in the photolysis of AdoCbl, the quantum yields of RP formation are unaffected by the

excitation wavelength.[99] Based on the TAS, it appears that the enzymatic environment modulates the low-lying excited states and stabilizes the product of photolysis. This stabilization makes the recombination of RPs less favorable. It was reported that that the enzymatic environment reduces the rate constant for geminate recombination by ~30% in AdoCbl-dependent GLM when compared with the isolated cofactor.

The photolytic properties of AdoCbl-dependent enzymes, such as EAL have been extensively studied experimentally. In a key study, Robertson and Warncke sought to look into RP formation that results from photolytic cleavage of the Co-C$_{5'}$ bond of AdoCbl in EAL using TAS.[102-103] The following conclusion is among the major findings of the study. It was shown that photolysis of AdoCbl in EAL leads to a quantum yield for cob(II)alamin that is 3-fold smaller than for AdoCbl in aqueous solution, indicating that the protein binding site suppresses photoproduct, namely RP formation. It is also important to note that this study considered the role of the substrate in photolysis as it is well-known that substrate binding is a key step in the native catalytic cycle. Interestingly it was found that, unlike true substrates, the substrate analog for TAS experiments does not induce the RP stabilizing changes in EAL. In another study, Warncke and co-workers used time-resolved, full-spectrum electron paramagnetic resonance (EPR) spectroscopy to further probe the substrate-triggered Co-C$_{5'}$ cleavage and RP formation in AdoCbl-dependent EAL.[104] It was shown that substrate binding to holo-EAL did not convert the protein to a structural state that would stabilize the RP photoproduct. Accordingly, a major conclusion of the study was that a change in protein structure is not a basis of Co-C$_{5'}$ bond cleavage in native catalysis.

Scrutton and Jones also studied EAL, especially to determine how the substrate affects the native catalytic cycle, using pre-steady-state magnetic field effect (MFE) investigations.[105] First, it should be noted that in all MFE experiments, RP formation is singlet-born in Cbls. Stopped-flow MFE studies were insensitive to magnetically induced changes in the net forward rate of Co-C$_{5'}$ homolytic bond cleavage. A magnetic dependence in the continuous-wave Co-C$_{5'}$ photolysis of free AdoCbl in 75% glycerol was observed. However, magnetic dependence was not observed in the thermal Co-C$_{5'}$ homolysis in EAL with the substrate. It was concluded that the RP formation after homolysis of the Co-C$_{5'}$ suppressed geminate recombination to the extent that an MFE could not be observed. In another study, Scrutton and co-workers investigated the effect of protein dynamics on geminate RP by determining the influence of viscosity on the cw-photolysis rate and its MFE.[106] This was achieved by using a specially configured MFE stopped-flow spectrophotometer to determine the magnitude of MFE of isolated AdoCbl and AdoCbl in EAL. It was found that the magnitude of the MFE increases with viscosity in isolated AdoCbl, whereas the magnitude of the MFE remains constant, at around 18% when protein-bound. This seemed to indicate that viscosity, and hence protein dynamics, affect the transient RP dynamics in the EAL active site on a timescale likely to be not much more than a few ns. It was reported that the majority of the geminate pairs have recombined within 3 ns using a 375 nm laser flash in a fs pump-probe spectrometer experiment. This is similar to GLM, where there is also a marked delay in the appearance of the Cbl^{II} photoproduct after photolysis.[99]

In addition to the Cbl-dependent enzymes, recently, an entirely new field of Cbl chemistry, namely B$_{12}$ photoreceptors, has emerged with the discovery and X-ray structure

determination of CarH.[107] It is a bacterial enzyme that mediates light-dependent gene regulation in photoprotective cellular responses. This was an exciting discovery for the B_{12} community because, while the light sensitivity of the $Co-C_{5'}$ bond in coenzyme B_{12} has been known for almost five decades, photolytic properties were not associated with controlled reactivity until CarH. When exposed to sunlight, it undergoes significant conformational changes, allowing it to biosynthesize carotenoids.[108-111] CarH-Dark State (CarH-DS) forms a tetramer in the dark after AdoCbl binds to the enzymes, which can adhere to DNA and stop transcription. When AdoCbl is exposed to light, the Co-C link cleaves, releasing radical pairs that break the tetramer into monomers and trigger transcription by detaching from DNA (Figure 1.5).
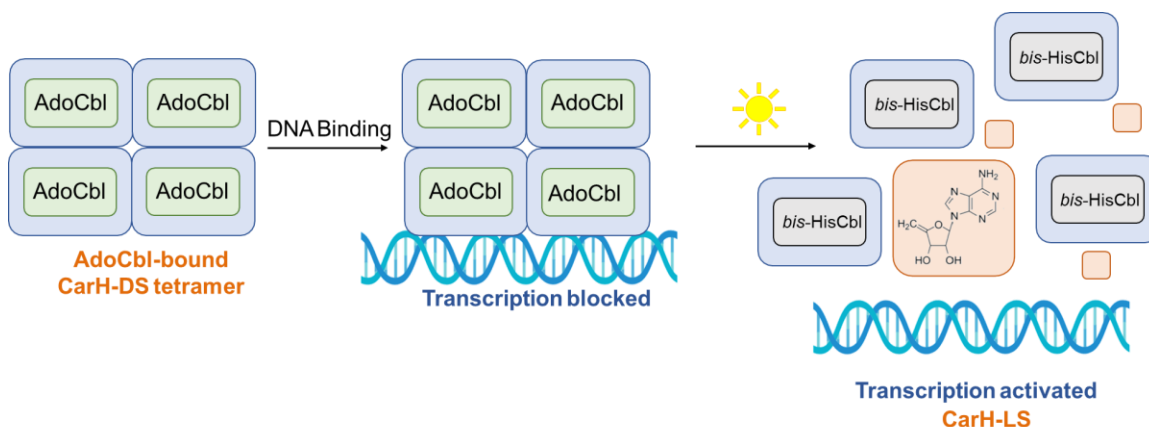
Figure 1.5. Photochemical mechanism of Co-C bond cleavage in AdoCbl-dependent CarH.

Each monomer contains a DNA binding domain, a helical bundle, and a Cbl binding domain. Monomers form head-to-tail dimers combined to form the tetramer, and DNA binds to CarH-DS and prevents the transcription of biosynthetic genes in the absence of daylight. As a result, photolysis of AdoCbl in biological media plays an important role and can be used for a variety of reasons. Nevertheless, the photolytic properties of Cbls-

dependent systems have been investigated using various experimental approaches to date. The main finding of these investigations is that the photophysical properties of Cbls can be modulated by the nature of axial ligands and the cofactor's environment. While these experimental studies have investigated the photoactivation of the Co-C bond in several Cbl-dependent enzymes, the photochemistry of B_{12}-dependent systems, particularly MeCbl-dependent systems, has not been investigated theoretically and must be addressed further using advanced theoretical calculations.

1.6. Motivation: Applications of photolytic and catalytic properties of Cbl-dependent systems

Coenzyme B_{12} dependent systems act as a radical reservoir in several biological and chemical reactions essential to life, including energy generation.[31, 38-39, 42, 59, 112] It can be used for a variety of applications, including bio-fuel conversion, catalyst design, and artificial enzyme design, to name a few. AdoCbl-dependent enzymes catalyze several important chemical reactions with numerous industrial applications using radical chemistry. For example, alcohol to aldehyde conversion and glycerol dehydration.[113-114] Glycerol is produced as a byproduct of biofuel production. Over the last decade, increased biofuel production has resulted in an oversupply of glycerol. Because of the increased glycerol production, developing biological processes for harnessing it and converting it to valuable products like 1,3-propanediol (1,3-PDO) and 2,3-butanediol (2,3-BDO) has gotten a lot of attention in industrial biotechnology. 1,3-PDO, for example, is a valuable chemical product that may be utilized as a solvent in the cosmetics business, and its international demand has increased by 150 percent in recent years. Through the unique activation of the Co-C bond, AdoCbl-dependent enzymes can substantially reduce the

activation energy and hence speed up processes. As a result, many AdoCbl-dependent enzymes could be employed as green catalysts in the microbial conversion of glycerol which demands a thorough understanding of B_{12}-dependent processes. Therefore, a comprehensive understanding of the catalytic activation of the Co-C bond can be critical in developing genetically engineered microorganisms consisting of the gene of AdoCbl-dependent enzymes for 1,3-PDO bioproduction. Furthermore, the B_{12}-dependent systems also possess complex photolytic properties through the light-sensitive Co-C bond. Studies have revealed that the light sensitivity of B_{12}-dependent systems can be used to develop phototherapeutic applications.[115-118] The upper axial position can be used to attach various drug molecules, which can then be triggered by the photoactivation of the Co-C bond. In those circumstances, the main problem is to locate a suitable candidate that can be activated by light while remaining within the tissue's optical window. Attaching fluorophore molecules to Cbls has been found to overcome this problem.[116,117] The fluorophores molecule can operate as an antenna, capturing long-wavelength light between 600 and 900 nm and transmitting the energy to Cbls, causing the Co-C bond to be activated and the drug to be liberated.[117] This phototherapeutic has a wide range of applications, from cancer therapy to tissue engineering; therefore, theoretical understanding of the photoactivation of the Co-C bond is crucial. Thus, the activation of the Co-C bond in B_{12}-dependent native catalytic and photolytic reactions has been investigated from a computational perspective.

Herein in this dissertation, the mechanistic details of the activation of the Co-C in the photolysis and native catalysis of MeCbl and AdoCbl-dependent systems have been investigated using hybrid quantum mechanics/molecular mechanics (QM/MM) simulations, density functional theory (DFT), and time-dependent density functional

theory (TD-DFT) methodologies. Chapters two through four of this dissertation were devoted to investigating the light-induced activation of the Co-C bond in B_{12}-dependent systems and how different factors, such as the enzymatic environment, mutation, and aerobic condition, influence the photoactivation of the Co-C bond in B_{12} cofactors.

In chapter two the photoactivation of Co-C bond inside MeCbl-dependent MetH was explored employing QM/MM approach. Subsequently, the photochemical data of isolated MeCbl cofactor in solution were also discussed. The first objective of this chapter is to explore the mechanism of the light-induced activation of the Co-C bond in enzyme-bound MeCbl. The second aim of this chapter is to understand the influence of the enzymatic environment on the photoactivation of the Co-C bond. Toward this, the photochemical data of enzyme-bound MeCbl was compared with the isolated MeCbl cofactor to understand the effect of protein binding on the photolysis of Co-C bonds.

In chapter 3, we further applied QM/MM-based methodology to explore and understand how the mutation in the cap domain of MetH controls the photoreactivity of the protein-bound MeCbl cofactor. We have introduced mutation on the phenylalanine 708 positions (F708) and replaced it with alanine (A708) residue. The ground state and excited state properties of both wild-type and mutated enzymes were computed based on the combined density functional theory/molecular mechanics (DFT/MM) and time-dependent DFT (TD-DFT/MM), respectively.[119] To explore the effect of mutation on the photoactivation of the Co-C bond in MeCbl-bound MetH, the photochemical data of wildtype (WT)-MetH and F708A-MetH were compared.

At last, the implication of the Co-C photoactivation in the aerobic photoreaction of MeCbl was investigated in chapter four. While many experimental and computational

studies have been conducted to investigate the inherent process of anaerobic photolysis of Cbls, the mechanism of photodissociation of the Co-C bond in the presence of oxygen has yet to be thoroughly investigated. Thus, the purpose of chapter four is to unravel the mechanism of oxygen insertion in the aerobic photolysis of MeCbl. The mechanism of the photoreaction is explored by analyzing the PEC and S_0 PES of $(Im-[Co^{III}(corrin)]-CH_3)^+ + O_2 \rightarrow (Im-[Co^{II}(corrin)])^{+\bullet} + {}^\bullet OO-CH_3$ reaction, as well as the S_1 PES for $(Im-[Co^{III}(corrin)]-OO-CH_3)^+$.

While chapters two through four deal with the photoactivation of the Co-C bond, chapter five focuses on the catalytic activation of the Co-C bond in the AdoCbl-dependent methylmalonyl CoA mutase (MCM). The most remarkable aspect of the AdoCbl-dependent enzyme-catalyzed reaction is the observed trillion-fold rate enhancement as compared to the uncatalyzed reaction in solution.[13, 120] Although there have been a few previously reported hypotheses for $Co-C_5$ bond activation, none of them can explain this unusual activation. As a result, it is unclear how the arrival of the substrate activates the $Co-C_5$ bond. Thus the main objective of this chapter is to advance the current understanding of the catalytic activation of the Co-C bond in AdoCbl-dependent MCM and unravel the mystery behind the unusual activation of the Co-C bond.

CHAPTER II

EXPLORING THE LIGHT-INDUCED ACTIVATION OF THE Co-C BOND IN MECBL-DEPENDENT METHIONINE SYNTHASE: ROLE OF ENZYMATIC ENVIRONMENT

2.1 Background

[1]MeCbl-dependent MetH is one of the widely studied Cbl-dependent enzymes that is found both in bacteria and mammals.[17, 56] As discussed in chapter 1, MeCbl is a biologically active form of vitamin B_{12} that acts as a cofactor in a class of enzymes that catalyze complex molecular transformation such as amino acid metabolism or CO_2 fixation in many organisms. It is an octahedral Co(III) complex where a methyl group is axially coordinated to the Co metal center as an upper axial ligand by an organometallic σ Co-C bond and 5,6-dimethylbenzimidazole (DBI) ligand as the lower axial base (Figure 1.1).[34, 62, 121] MetH enzyme catalyzes the transfer of a methyl group from MeCbl to Hcy, resulting in Met and cob(I)alamin intermediates. The resulting cob(I)alamin is remethylated by CH_3-H_4Folate or CH_3-THF substrate to produce MeCbl and H_4Folate (Figure 1.2).[18] The displacement of a methyl group from the MeCbl cofactor, associated with the cleavage of the Co-C bond, constitutes the crucial step in this catalytic cycle. In the case of MeCbl-

---

[1] The discussions in this chapter are based on the publication *"Ghosh, A. P., Mamun, A. A., Lodowski, P., Jaworska, M., & Kozlowski, P. M. (2018). Mechanism of the photo-induced activation of Co-C bond in methylcobalamin-dependent methionine synthase.* J. Photochem. Photobiol., B, 189, 306-317"

dependent MetH, this cleavage is formally heterolytic or homolytic, depending on the proposed mechanism, whereas the cleavage of the Co-C bond in AdoCbl-dependent enzymes is homolytic.[34, 39, 51] However, unlike the native catalysis, the Co-C bond of the MeCbl cofactor inside MetH can also be cleaved homolytically by light to generate a $Co(II)/CH_3$ RP (Scheme2.1).[96-97, 122] Sension and co-workers have probed excited state dynamics and photolytic properties of MeCbl in solution as well as inside the enzymatic environment using ultrafast laser spectroscopy.[97, 100, 123] Employing TAS, it was shown that photolysis of MeCbl is wavelength-dependent. Photolysis of MeCbl at an excitation wavelength of 400 nm causes 25% prompt bond homolysis, resulting in Co/CH_3 (RP) and 75% formation of the metastable state consistent with cob(III)alamin intermediate, where the axial ligand is weakly bonded. On the other hand, excitation at 520 nm results in metastable cob(III)alamin photoproduct formation without prompt photolysis. This metastable photoproduct branches between photolysis (14%) and recovery of MeCbl to the ground state.[100] Unlike MeCbl, the quantum yield of Co-C bond cleavage in AdoCbl is wavelength-independent.
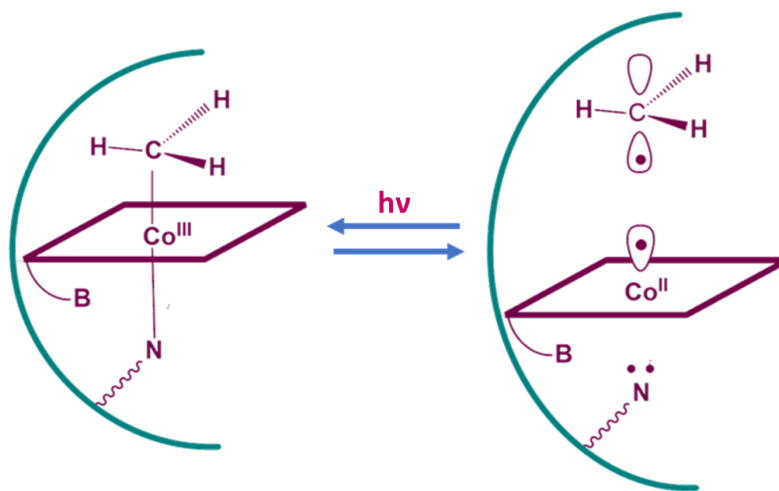
Scheme 2.1. Cleavage of Co-C bond by light in MetH without substrate.

The photodissociation mechanism of the Co-C bond depends on several factors. The influence of the axial base and the cofactor's environment is the most important. In strongly acidic conditions, the lower axial base of the MeCbl cofactor is detached and replaced with a water molecule to adopt the base-off form. The mechanism of Co-C bond photolysis in solution is different based on whether MeCbl is in the base-on or base-off configuration.[124] The absence of the trans-nitrogenous ligand in base-off MeCbl changes its electronic structure, which opens a channel for internal conversion. Ultimately, this reduces the rate of geminate recombination. Unlike the base-off form, a competition between geminate recombination and the diffusive separation of the RP was observed in base-on MeCbl in the solution.

The nature of the protein environment influences the reactivity of the Co-C bond as well as the photolytic properties of Cbls.[96, 125] The rate of photolysis in the MeCbl-dependent enzyme, MetH, is slower when it is compared with the isolated cofactor in the solution. It appears that the enzyme protects the MeCbl from photolysis by decreasing the rate of the reaction by almost 50-fold.[96] There are two main factors that are inhibiting the photolysis of MeCbl when it bounds to the protein. First, the excited state relaxation rate increases by binding of MeCbl with the protein, while the rate of bond homolysis decreases. The second factor that affects the photolysis is the cage effect of the protein. In an enzyme-bound MeCbl, the protein residues form a cage that surrounds the methyl group, preventing the diffusive loss of the radicals. This has been evidenced by the increase in the rate of recombination inside the enzyme.[96-97] A similar situation is also observed in solution, where solvent molecules form a cage, which prevents the escape of methyl radical after photolysis of the Co-C bond. Although several experimental studies have been

reported the aforementioned observations, there is still a lot to explore about the effect of the enzymatic environment and the mechanism of photoinduced activation of the Co-C bond in MeCbl-dependent MetH.

Along with these experimental studies, quantum chemical calculations were also conducted to investigate the electronic structure and photochemical properties of cobalamins in solution as well as in the enzymatic environment.[121-122, 126-130] Due to the size and the complexity of the molecule, density functional theory (DFT)[131-132] and time-dependent DFT (TD-DFT)[133-136] have been used to explore the ground and excited-state properties of Cbls, respectively. Accordingly, using TAS and theoretical studies, it was shown that the crucial step in photolytic cleavage could be explained by carefully scrutinizing the electronic properties of the S_1 excited state. To that end, the S_1 potential energy surface (PES) was used to describe the pathways of photodissociation and the associated mechanism. The S_1 PES was characterized as having two minima regions, namely metal-to-ligand charge transfer (MLCT) and the ligand field (LF). RP generation occurs from the LF region.[122, 130, 137-138] The challenge in describing the photodissociation mechanism is connecting these two minima regions. Two possible pathways were identified, Path A and Path B, for the base-on form of MeCbl, and both pathways, are active. In the base-off (axial nitrogenous ligand replaced by water) form of MeCbl, only Path B, where the Co-C bond elongates first, was found to be active.

While these theoretical studies have explored the photolytic properties of isolated MeCbl in solution, the photochemistry of MeCbl inside MetH has not been explored from a theoretical point of view. The present work has been completed to carefully investigate the ground and electronically excited states of the MeCbl-dependent enzyme MetH, using

23

a combined quantum mechanics/molecular mechanics (QM/MM) method[139] to explore its photochemical and photophysical properties.

2.2 Computational Methodology

2.2.1 QM/MM

In computational chemistry, there are various methodologies based on various levels of theory to study complex biological and bioinorganic systems. Methods used to study enzymes include molecular dynamics (MD), molecular mechanics (MM), and QM/MM.[140-141] MD simulation is commonly used to study the motions of molecules in complicated biological systems using classical mechanical force fields. MM, however, is objectively geared more towards determinations of molecular equilibrium structures. Molecular modelers make use of a force field to predict the geometry of a novel molecule, usually containing atoms in the order of more than ~10,000 atoms, by generating data related to bond parameters from other related molecules. The force field equations are empirical and derived on the assumption that atoms in a molecule behave as balls joined by springs. A large molecule is treated as a system consisting of the same features, which are present in small molecules but put together in different ways. MM methods are very versatile primarily because the derived force field parameters are transferable from molecule to molecule. However, there are limitations in the use of mechanical force fields, and changes in the electronic structure including bond breaking and formation, electron transfer, and electronic excitations cannot be characterized by MM and MD methods.

QM/MM is a method that combines QM (electronic structure methods) and MM (empirical force field) to study large systems including enzymes.[73,139, 141-143] QM methods

are used to determine the electronic structure of molecules whereas MM methods are used to determine the potential energy as a function of nuclear coordinates. In general, a QM/MM set-up can be described as follows, the chemically important part of the system such as the active site is treated with the QM method and the remainder of the system is treated with an MM method. The main advantage of the QM/MM method on large systems is that it can deliver a relatively low computational cost compared to a previously impossible calculation with QM methods alone, as well as accuracy that typical MM methods cannot match.

In the QM/MM method, the molecular structure can be partitioned into different "layers" through a boundary between the subsystems, and each layer is treated with a different level of theory.[138-139] The electronically prominent region, which typically includes the key components of the active site such as the cofactor and substrate, is treated with a QM method and is referred to as the high layer (HL). The low layer (LL) contains the protein residues and sometimes a portion of a large substrate of cofactor. The LL is typically treated with a classical MM method. In addition, a middle layer might (ML) be defined depending on the system under study.

For a typical two layers, subtractive QM/MM as implemented in ONIOM involves three calculations and the final energy of the entire system is given by following equation[138,139]

$$E_{total} = E_{MM,real} + E_{QM,model} - E_{MM,model} \quad ....(1)$$

First, the energy of the overall real system is calculated at the MM level of theory. Then the energy of the model system (HL) is calculated both at QM and MM levels of theory.

Finally, to avoid double-counting, the energy of the model system (HL) calculated at the MM level of theory is subtracted. The subtractive QM/MM scheme is very straightforward in terms of implementation because QM/MM electrostatics are treated with a fixed atomic charge in the core and environment. This method does not take into account the polarization of the QM wavefunction. In ME, all the bonded (like stretching, bending, and torsional) and non-bonded (like electrostatic and van der Waals) interactions between the two layers are treated at the MM level of theory. In the case of a three-layer calculation, further simplification of the active site is rendered utilizing an additional ML. The ML can be treated with MM or an inexpensive semiempirical QM (SQM) level of theory such as PM6. For a three-layer ONIOM calculation, the energy of the entire system is given by the following equation,

$$E_{total} = E_{MM,real} + E_{SQM,medium} + E_{QM,model} - E_{MM,medium} - E_{SQM,model} \ldots\ldots\ldots\ldots\ldots(2)$$

2.2.2 Model preparation and QM/MM Setup

In this study ONIOM-based, DFT/MM framework[119] and TD-DFT/MM calculations have been performed to investigate the mechanism of Co-C bond photolysis and the electronic structure of MeCbl-bound MetH. The high-resolution crystal structure of MeCbl containing a fragment of MetH (PDB ID: 1BMT) was used as the initial structure.[29] The crystal structure of MetH from *Escherichia coli* was determined at a resolution of 3.0 Å and revealed a unique feature of MetH, the conformational change of MeCbl when it binds with MetH. In the enzyme, the DBI group, which is axially attached to the Co center of corrin ring in the base-on form of MeCbl, is displaced from the Co center and is replaced by the imidazole (Im) moiety from a histidine (His) residue of the protein.

The crystal structure of chain A of MeCbl-dependent MetH was obtained from the Protein Data Bank to build the computational model. All experimental artifacts were removed from the crystal structure. The structure was protonated using GaussView 5 and PropKa 3.0 software,[144] assuming the normal protonation states of all residue (except His). For His, the protonation states were determined by visual inspection of local H-bonding residues and using PropKa 3.0 software. The protonation states of the His are determined by the protonation of the nitrogen at particular positions, namely δ and α. If the protonation occurs at δ, then its referred to as HID, and if the protonation occurs at the α position of nitrogen, it is referred to as HIE. The His759, which is axially coordinated with the Co of the corrin ring, was protonated at the N_δ position; hence it is treated as HID. This structure of MeCbl-bound MetH was then minimized at the MM-level of theory using the AMBER force field (FF). This minimized structure was used for the QM/MM calculations. The model system was partitioned into three layers. The methyl group, Co atom, corrin ring, and the Im moiety of His759, which are important to describe the photodissociation mechanism, were included in the HL. The remaining part of the cofactor, including the nucleotide tail along with the side chains, was added to the ML, and the rest of the protein was included in the LL. The model contained a total of 4031 atoms, where 1640 atoms (within the 20 Å from the Co center) were kept unfrozen while the remaining 2391 atoms were kept frozen throughout the course of the calculations. All the QM/MM calculations reported in this study were performed using Gaussian 09 software.[145]

2.2.3 DFT/MM Calculations

DFT was applied using the GGA-type BP86 functional[146-147] for the high layer portion of the model system. Which contains the methyl group, Co atom, corrin ring, and

the Im moiety of His759. The accuracy of DFT is largely dependent on the selection of the proper functional. Previous benchmark studies have shown that in the case of cobalamins, a pure GGA-type functional such as BP86 can accurately describe the structural parameters and bond dissociation energies (BDEs).[148-151] From our previous benchmark studies, targeting the Co-C BDEs and the electronically excited states of cobalamins, we have confidence that this level of theory is appropriate for this system. Semi-empirical PM6 level of theory was used for the middle layer.[152] The low-layer was treated with the MM level of theory using the AMBER FF (FF99SB).[153] To keep consistency with the previous studies, the TZVPP basis set was used for Co, C, N, O atoms[154-155] and TZVP for H atoms. Three-layer ONIOM (DFT:PM6: AMBER) mechanical embedding (ME) was carried out for the geometry optimization of the MeCbl-bound MetH structure. The MM parameters for the cofactor were obtained from Marques *et al*. Starting from the equilibrium geometry, the ground-state (S_0) potential energy curves (PECs), as a function of Co-C bond length, were constructed by systematic elongation of the Co-C bond with a step size of 0.1 Å for MeCbl-bound MetH and the solution-based Im$-$[Co^{III}(corrin)]$-$Me$^+$ model complex. The 3D PESs were also constructed for MeCbl inside enzyme and Im$-$[Co^{III}(corrin)]$-$Me$^+$ by simultaneously elongating the Co-C and Co-N$_{Im}$ bond lengths with a step size of 0.1 Å.

2.2.4 TD-DFT/MM Calculations

To describe the photodissociation mechanism, it is crucial to explore the low-lying excited states with a proper level of theory. For MeCbl, TD-DFT was benchmarked against high-level *ab initio* CASSCF/MC-XQDPT2 and EOM-CCSD wavefunction-based methods.[121, 156] It was shown that using BP86 functional in the TD-DFT framework can accurately describe the low-lying excited states. For MeCbl, the S_1 state was characterized

as having an MLCT character, which is consistent with TAS and resonance Raman experiments.[157-158]

TD-DFT/PM6/MM framework was applied to construct the manifold of low-lying excited states PECs and PESs. Single point ONIOM (TD-DFT:PM6: MM) calculations were used to construct the PECs along the Co-C bond length and the S_1 PES as a function of the Co-C and Co-N_{Im} bond lengths. For the PECs, the single-point calculations were performed for each optimized structure of the ground state PEC to compute the manifold of low-lying singlet and triplet excited states, which indicate that vertical excitations were calculated without relaxing the geometry of the excited state.

To understand the nature of the electronic transitions, each excited state was scrutinized with a detailed analysis of the relevant orbitals involved in the electronic transition. Additional single-point calculations were performed to analyze the molecular orbitals. Orbital analysis has revealed that the MLCT region of the S_1 PES involves an electronic transition from Co d-orbitals to the corrin π^*. The electronic excitation in the LF region of the S_1 PES occurs from the Co d and corrin π orbitals to the $\sigma^*(d_z^2)$ orbital. This σ^* orbital is mainly an anti-bonding combination of the p orbital of carbon and the d_z^2 orbital of Co.

2.3 Results and Discussion

2.3.1 Ground State Geometry

The structure of MeCbl-bound MetH was optimized, followed by frequency calculations using the DFT/PM6/AMBER level of theory (Figure 2.1). The absence of imaginary frequencies has confirmed that the structure has been optimized properly. By

comparing the structural parameters of the optimized geometry with the experimental values obtained from the crystal structure, we found that the computed values agree well with experimental data (Table 2.1). While the optimized value for axial Co-C bond distance (1.98 Å) matches very well with the experimental bond distance (1.96 Å) in the enzyme, the Co-N_{Im} bond length observed a slight deviation of 0.08 Å from its experimental value.
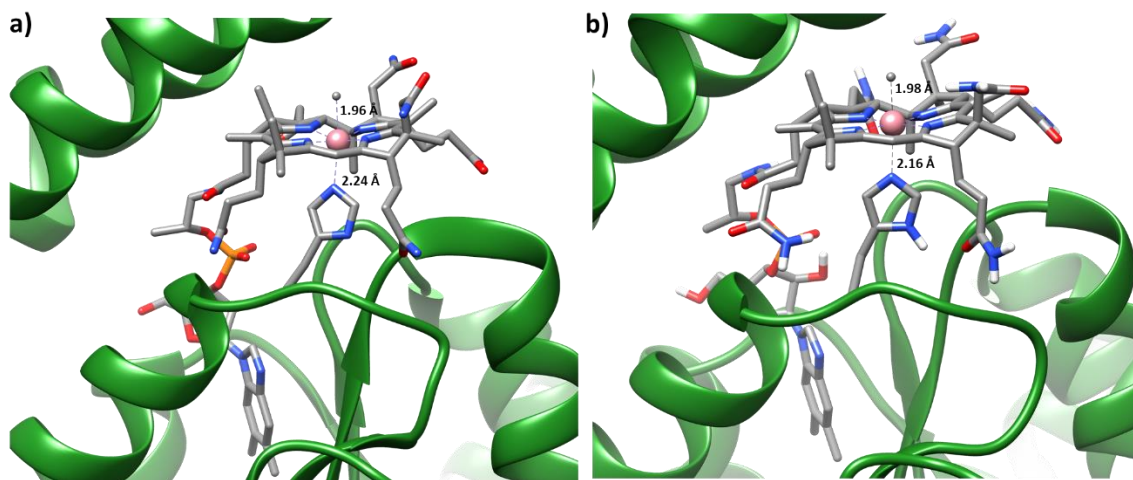
Figure 2.1 (a) Crystal structure of MetH (PDB ID: 1BMT) obtained from the protein data bank. (b) Optimized structure of MeCbl-dependent MetH using DFT/PM6/MM level of theory.

The calculated Co-N_{Im} bond length in the optimized structure was 2.16 Å, while the experimental bond distance for the axial Co-N_{Im} bond was 2.24 Å (Table 2.1). This small deviation of 0.08 Å arises because the Co-N_{Im} bond is much weaker than the Co-C bond. We have also compared the axial Co-N_{Im} bond distance with the results obtained from the calculations of our previous study of the base-on form of MeCbl inside solution, where the lower axial ligand is imidazole moiety. The optimized Co-N_{Im} bond distance in base-on MeCbl at S_{0min} was 2.17 Å, where the Co-N_{Im} bond distance in MeCbl-bound MetH was

2.30 Å. This result also points out that the length of the Co-N$_{Im}$ bond of base-on MeCbl and MeCbl-bound MetH depends on its local environment.

	MeCbl-bound MetH				Im-[Co^{III}(corrin)]-Me$^+$			
	Optimized Structure	I (S$_{0min}$)	I (S$_{1min}$)	Crystal Structure	I (S$_{0min}$)	I (S$_{1min}$)	expt [a]	expt [b]
Bond Distances, Å								
Co-C	1.976	2.000	2.000	1.957	1.986	2.006	1.972	1.979
Co-N$_{Im}$	2.164	2.300	2.100	2.241	2.175	2.055	2.093	2.163
Co-N$_{21}$	1.908	1.924	1.932	1.925	1.881	1.880	1.905	1.877
Co-N$_{22}$	1.958	1.952	1.957	2.015	1.938	1.975	1.900	1.921
Co-N$_{23}$	1.932	1.942	1.946	2.016	1.937	1.979	1.923	1.918
Co-N$_{24}$	1.902	1.903	1.910	1.914	1.878	1.879	1.863	1.874
Bond Angles, deg								
C-Co-N$_{Im}$	173.9	174.8	175.7	167.4	177.3	164.6	173.4	174.6
N$_{21}$-Co-N$_{23}$	173.7	173.9	173.7	172.9	173.1	173.1	173.4	173.4
N$_{22}$-Co-N$_{24}$	171.5	172.0	171.3	177.8	172.6	171.5	172.2	171.4
Torsion Angles, deg								
N$_{21}$-N$_{22}$-N$_{23}$-N$_{24}$	-1.7	-1.6	-1.7	4.8	-4.1	-3.7	-3.9	-4.6
N$_{21}$-N$_{22}$-N$_{23}$-Co	0.8	-0.1	1.1	4.9	-1.9	-0.5	-2.1	-1.4

Table 2.1 Selected Geometrical Parameters for the MeCbl-bound MetH and Im−[CoIII(corrin)]−Me$^+$ Model Complex.

2.3.2 Low-lying Excited States Along with Co-C Bond

To be consistent with our previous investigations of the photolytic properties of Cbls, the electronically excited low-lying singlet and triplet states were calculated along the Co-C bond employing the method mentioned in Section 2.2.4 The PECs were computed by systematic elongation of the Co-C bond. A step size of 0.1 Å was used to stretch the Co-C bond. All the corresponding geometries (S$_0$) of MeCbl-bound MetH were then

optimized at each point using ONIOM(DFT/PM6/AMBER)-ME level theory. The single

point ONIOM(TD-DFT/PM6/AMBER) calculation was performed for each optimized

structure of the ground state to compute the manifold of low-lying singlet and triplet

excited states, which indicate that vertical excitations were calculated without relaxing the

geometry of the excited state. We have generated the PECs of vertical singlet and triplet

excited states up to the energy value of 3.6 eV for MeCbl inside MetH (Figure 2.2). This

was compared with the excited states computed for a base-on model of MeCbl in solution

from our previous work. There is no significant difference between energy curves (Figure

2.2) of MeCbl inside MetH and the isolated base-on MeCbl. For both of them, none of the

singlet states have repulsive character, while the repulsive character of the triplet was found

to the among low-lying triplet states. For MeCbl-bound MetH, this state, with a $^3(\sigma_{Co-C} \rightarrow$

$\sigma^*_{Co-C})$ character, dropped in energy along Co-C coordinate and at a Co-C bond distance

of ~2.5 Å it becomes lowest in energy. In our previous studies of MeCbl in the base-on

form, we have predicted the repulsive nature of this $^3(\sigma_{Co-C} \rightarrow \sigma^*_{Co-C})$ state using a UDFT

framework. Despite having similar orbital contributions in both of the repulsive states, the

energy in the TD-DFT state drops faster due to the instability of a single-determinant wave

function at a longer Co-C distance. It should be noted that this triplet state does not properly

level-off as a function of Co-C distance due to the single-determinant based wave-function

used in TD-DFT calculations.
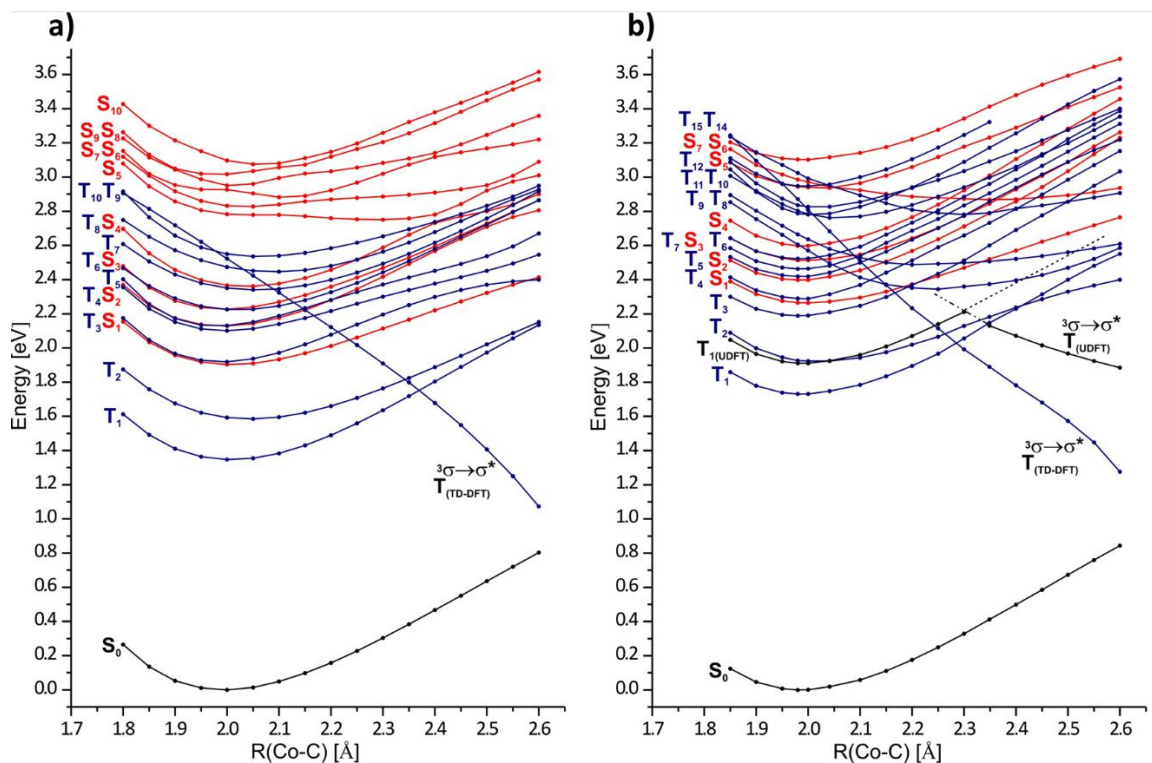
Figure 2.2. Potential energy curves for the ground (black) and vertical singlet (red) and triplet (blue) excited states as functions of Co-C bond length for **(a)** MeCbl-dependent MetH and (b) Im−[Co^{III}(corrin)] −Me$^+$ model complex in water.

A detailed analysis of electronic transitions is important to understand the photolysis of MeCbl-bound MetH. We have characterized the eleven lowest vertical singlet excited states based on the orbital analysis (Table 2.2), and corresponding figures of these orbital can be found in Figure A1. The excitation energy for the S_1 state for MeCbl-bound MetH is 1.9 eV. The orbital characterization for this electronic transition indicates that the dominant character of the S_1 state is MLCT. The electronic transitions in the S_1 state are 87% $d_{xz}+ \pi \rightarrow \pi^*$, 10% $d_{xy}+n+ \pi \rightarrow \pi^*$. These transitions are mainly from metal d orbital to the corrin π^*. The excitation energy for the next excited singlet S_2 and S_3 are 2.12 eV and 2.22 eV, respectively. In the S_2 state, the main contribution in electronic transition is coming from HOMO to LUMO with 79% $d_{yz}+ \pi \rightarrow \pi^*$ type excitation, while in the S_3

state, the electronic transitions are characterized as 45% % $d_{xy}+n+\pi \rightarrow \pi^*$ and 37% $d_{xy} \rightarrow$ π^*. The excitation energies for MeCbl inside MetH are comparatively smaller than the computed verticle excitation energy of isolated MeCbl in base-on form. We have also observed that a large amount of anti-bonding σ^* character, almost 64% $d_{yz}+\pi \rightarrow \sigma^*(d_z^2)$, appears for transition in S_{10} excites state.

	E[eV]	f	λ[nm]		%	Character	Exp. [nm]
S_1	1.90	.0033	651	H-2→L	10	$d_{xy}+n+\pi\rightarrow \pi^*$	
				H-1→L	87	$d_{xz}+\pi\rightarrow \pi^*$	
S_2	2.12	.0279	582	H-3→L	09	$d_{xy}\rightarrow\pi^*$	
				H-1→L+2	04	$d_{xz}+\pi\rightarrow d_{xz}+\pi^*$	
				H→L	79	$d_{yz}+\pi\rightarrow \pi^*$	
S_3	2.22	.0208	556	H-3→L	37	$d_{xy}\rightarrow\pi^*$	552
				H-2→L	45	$d_{xy}+n+\pi\rightarrow \pi^*$	
				H→L	10	$d_{yz}+\pi\rightarrow \pi^*$	
S_4	2.36	.0439	523	H-3→L	49	$d_{xy}\rightarrow \pi^*$	
				H-2→L	35	$d_{xy}+n+\pi\rightarrow \pi^*$	
S_5	2.78	.0061	445	H→L+1	84	$d_{yz}+\pi \rightarrow d_{xy}+n+ \pi^*$	
				H→L+2	03	$d_{yz}+\pi \rightarrow d_{xz}+\pi^*$	
S_6	2.83	.0035	437	H-2→L+1	10	$d_{xy}+n+\pi \rightarrow d_{xy}+n+ \pi^*$	
				H-1→L+1	69	$d_{xz}+\pi \rightarrow d_{xy}+n+ \pi^*$	
				H→L+2	11	$d_{yz}+\pi \rightarrow d_{xz}+\pi^*$	
S_7	2.92	.0079	423	H-5→L	30	Im $\pi\rightarrow \pi^*$	
				H-4→L	32	$d_{xy}+\pi \rightarrow \pi^*$	
				H→L+2	26	$d_{yz}+\pi\rightarrow d_{xz}+\pi^*$	

Table 2.2 Eleven lowest vertical singlet electronic transitions and orbital characterization based on the single point TD-DFT/MM calculations of MeCbl-dependent MetH.

2.3.3 Potential energy surfaces as a function of axial bond lengths

From our previous investigations, we know that axial bond lengths experience the largest structural change upon excitation while the corrin structure is almost unchanged.

This theoretical observation corroborates with the experimental results from XANES spectroscopy reported for CNCbl.[159] Therefore, to elucidate the photodissociation mechanism of the Co-C bond of MeCbl inside the enzyme, PESs for S_0, S_1, has been constructed as a function of axial bonds.

The methodology used for calculating the vertical excitation has been outlined in Section 2.2.4 The energy minimum of the S_0 PES occurs around the Co-C bond distance of 2.00 Å and Co-N$_{Im}$ length of 2.3 Å (Figure 2.3a). The lowest energy region in the S_1 PES (Figure 2.3a) occurs at almost the same Co-C bond distance as the S_0 PES and a slightly changed Co-N$_{Im}$ bond length at 2.1 Å. The topology of the S_1 PES has few intermediates (Figure 2.4a), which are important in exploring the photodissociation of the
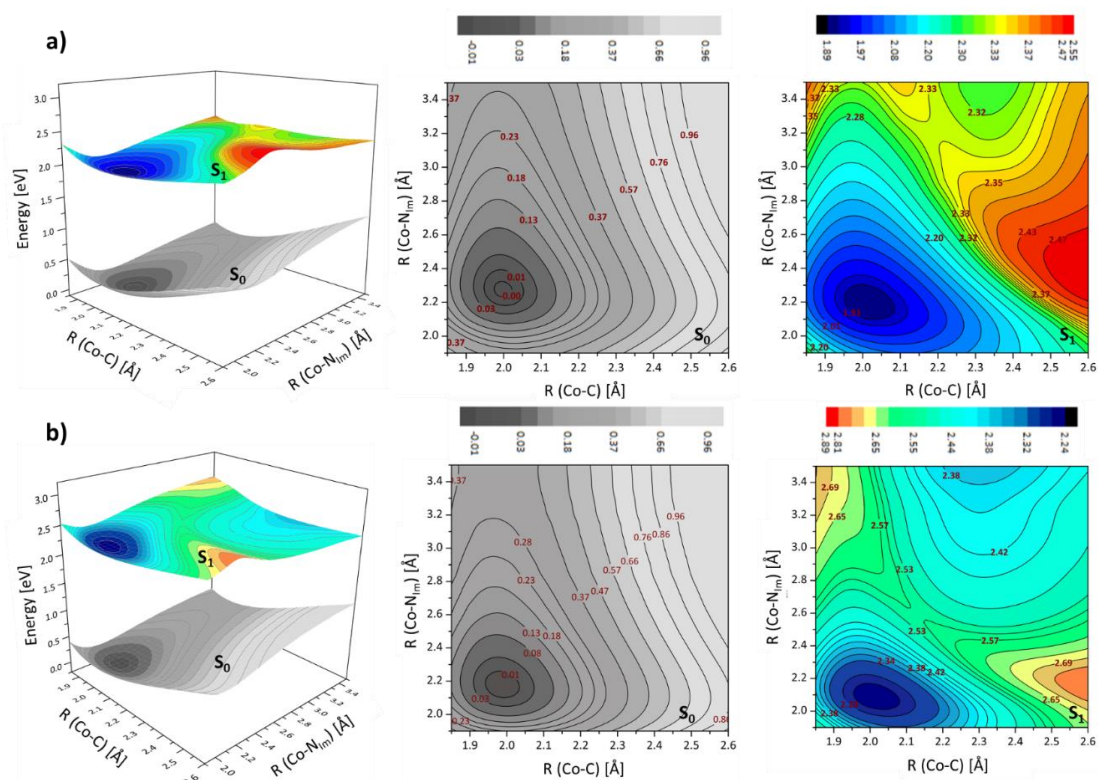
Figure 2.3. Potential energy surfaces for the S_0 with vertical projections of the S_1 state plotted as functions of axial bond lengths along with the corresponding S_0 and S_1 contour PESs with color codes for **(a)** MeCbl-dependent MetH **(b)** Im−[Co^{III}(corrin)]−Me$^+$ base-on model complex in water.

Co-C bond. The most remarkable feature of S_1 PES is that it identifies two separate regions which are relevant to the photodissociation. These two regions are separated by a seam, which indicates an intersection between two excited states through a minimum energy crossing point (MECP), see Figure 2.4a. The first region is the MLCT state, which corresponds to slightly shorter axial bond lengths (Figure 2.4a). Excitation in the MLCT
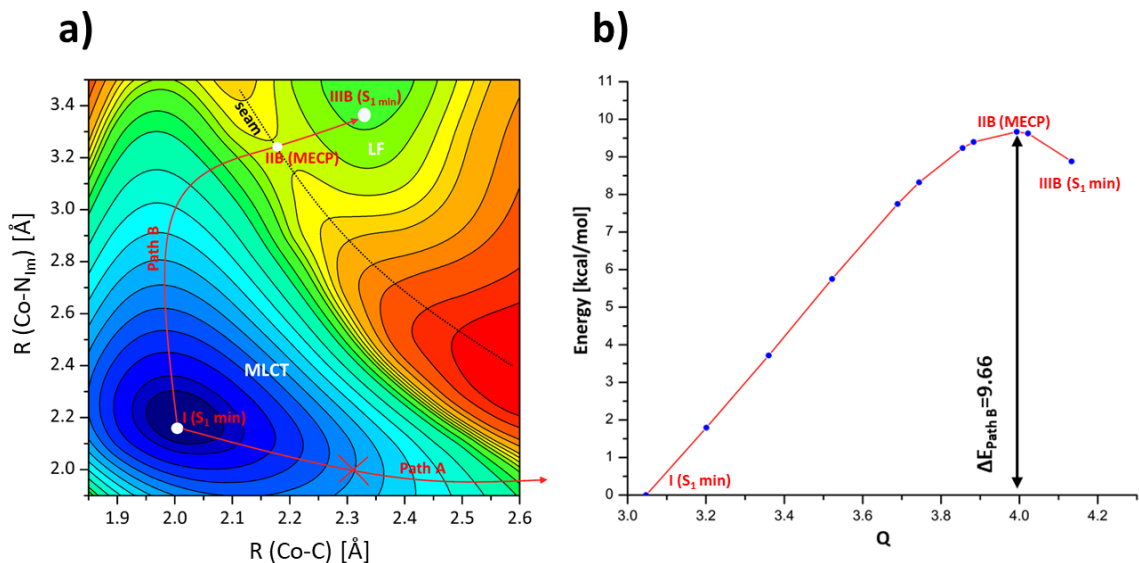
Figure 2.4. (a) Scheme of photoreaction of MeCbl inside MetH on the S_1 PES with minima regions, separated by a seam, where MLCT minimum is denoted as I (S_{1min}) and LF minimum is denoted IIIB (S_{1min}) and (b) minimum energy paths (Path B) between MLCT and LF state plotted as a function of energy versus Q value.

the region is associated with $d_{xz}/d_z^2 + \pi \rightarrow \pi^*$ or $d_{xz} + \pi \rightarrow \pi^*$ type transition (Figure 2.5). The second dominant region on the S_1 PES is the LF state, which is characterized as $d_{yz} + \pi \rightarrow \sigma^*(d_z^2)$ excitation, corresponding to longer axial bond lengths. The electronic transition in the MLCT energy minima (I(S_{1min}), Figure 2.5) of the S_1 PES corresponds to 87% $d_{xz} + \pi \rightarrow \pi^*$ and 10 % $d_{xy} + \pi \rightarrow \pi^*$ type transition. The energy minimum of the LF state is located at a Co-C bond of 2.35 Å and a Co-N_{Im} bond of 3.4 Å. The electronic excitation in the LF state has a dominant HOMO to LUMO character with 95% $d_{yz} + \pi \rightarrow$

d_z^2 at IIIB(S_{1min}) (Figure 2.5). At the MECP, IIB, the excitations are HOMO to LUMO+1 and HOMO to LUMO. The corresponding optimized ground state geometries of selected points on the S_1 PES (Figure 2.4a), **(a)** I (S_{1min})**, (b)** IIB (S_{1min})**, (c)** IIIB (S_{1min}) are depicted in Figure A2. The LF (IIIB(S_{1min})) energy minima of the S_1 PES is higher in energy than MLCT minima (I(S_{1min}) by an amount of 9.45 kcal/mol. The S_1 PES of base-on isolated MeCbl (Figure 4b) was compared with the S_1 PES of MeCbl inside the MetH.
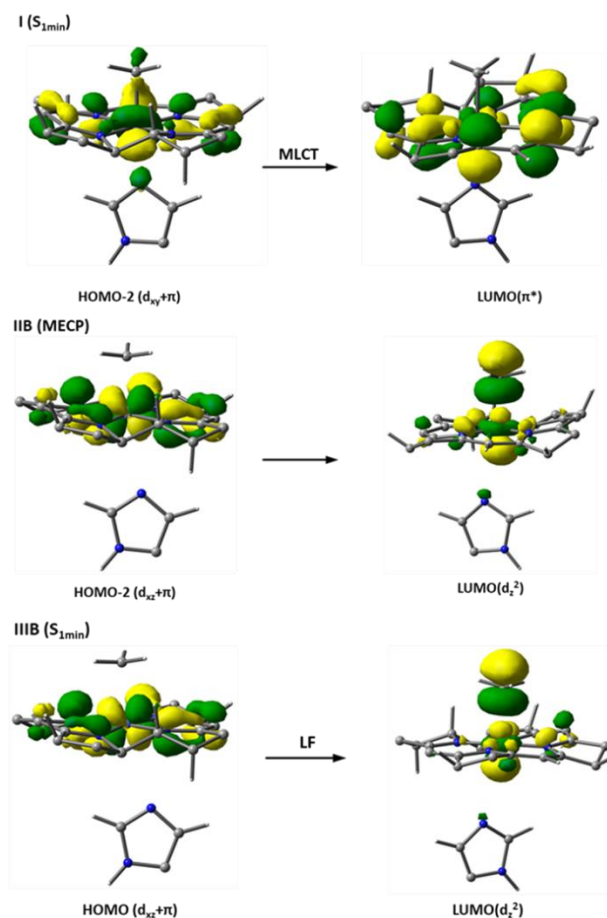
Figure 2.5. HOMO and LUMO molecular orbitals are involved in electronic excitations corresponding to selected points on the S_1 PES (Figure 2.4a) along Path B.

We have found two energy minima in the S_1 PES of base-on MeCbl. The LF minima is also higher in energy than MLCT minima for isolated base-on MeCbl. In the case of

MeCbl inside MetH, the energy difference between the MLCT and LF minima region in the S_1 PES is very high compared to the base-on MeCbl. The LF region is energetically more stabilized in base-on MeCbl inside solution than MeCbl inside enzyme. These results clearly depict that the enzymatic environment is playing a role in the destabilization of LF.

2.3.4 Pathways of photodissociation: mechanism of photoreaction

S_1 PESs have been analyzed to explore the mechanistic insight of the photodissociation of cobalamin. The computed PESs along the axial bond distances are the result of the crossing of two different electronic states, MLCT and LF. The energetic difference between these two electronic states, MLCT and LF, in the S_1 PES guides the photodissociation pathway. For base-on MeCbl, it was found the photoreaction involves two pathways, Path A and Path B (Figure 2.6a). Path A is associated with the initial elongation of the Co-C bond followed by a detachment of the Co-N_{Im} bond. Path B involves the first detachment of the Co-N_{Im} bond from the energy minima associated with the MLCT electronic state, followed by a lengthening of the Co-C bond. While the intermediates involved in both the dissociation pathway are different, the initial and final products are the same. Energetically the MLCT region is lower than the LF electronic state in both MeCbl inside MetH and base-on MeCbl in solution. This indicates that the MLCT to LF transition is an uphill process.

The analysis of the energetics based on S_1 PES of MeCbl inside MetH indicates that the photoreaction could only proceed through Path B, which is associated with the initial elongation of Co-N_{Im} bond from the MLCT minimum (I, $S_{1\ min}$, Figure 2.4a). After the initial displacement of the Co- $N_{Im,}$ the photoreaction proceeds through the seam, which is an intersection between the MLCT and LF electronic state and follows the minimum
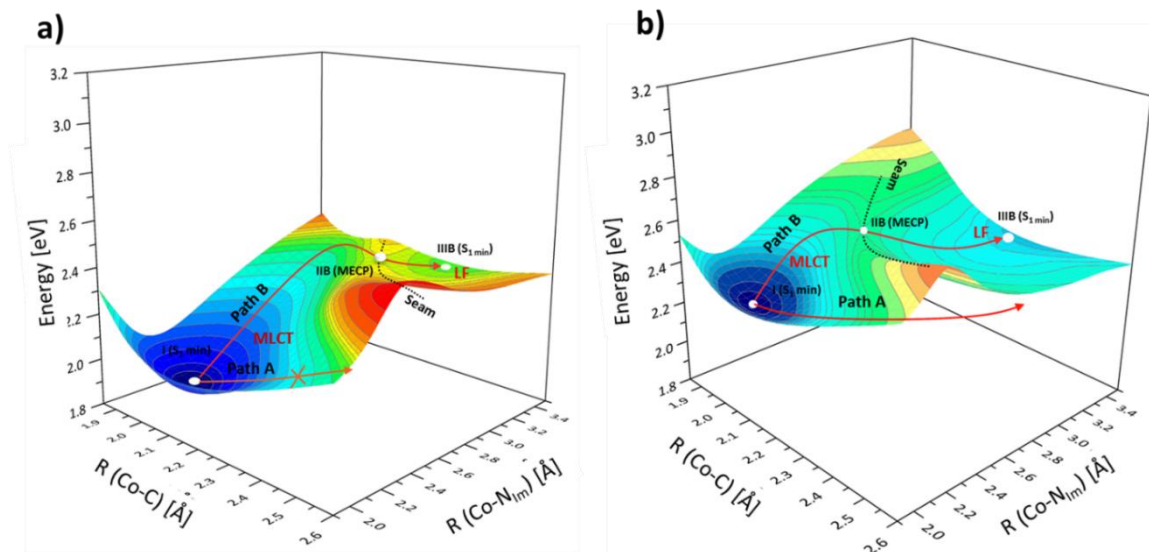
Figure 2.6 Potential energy surfaces of S_1 state as a function of axial bond lengths with photoreaction pathway depicted by red arrows for (a) MeCbl inside Methionine Synthase (b) Im−[Co^{III}(corrin)] −Me$^+$ base-on model complex in water.

energy crossing point (MECP), IIB, located on the seam. We have generated the energy

profile (minimum energy pathway) of photodissociation along Path B (Figure 2.4b) as a

function of Q (Q = $\sqrt{R_{Co-C}^2 + R_{Co-N_{Im}}^2}$). The calculated energy barrier between I($S_{1\,min}$) and

IIB (MECP) on the S_1 PES is 9.66 kcal/mol. From the intermediate state, IIB (MECP), on

S_1 PES, it goes into the minimum energy region in the LF electronic state. As previously

mentioned, the LF state is associated with an anti-bonding orbital of the ligand (Figure

2.5). Finally, the photodissociation occurs from the LF region (Figure 2.7).

The photodissociation along Path B, which involves the elongation of the Co-N$_{Im}$

bond from the MLCT minima (I $S_{1\,min}$), proceed through the MECP at IIB along the seam

to LF minima of S_1 PES at IIIB ($S_{1\,min}$), as shown in Figure 2.4a and 2.6a. The energetic

barrier of Path B is 9.66 kcal/mol (Figure 2.4b). At the MECP (IIB), the Co-N$_{Im}$ bond

distance is long, around 3.2 Å, and the Co-C bond is essentially the same length as at I (S_1

$_{min}$), ~2.15 Å. After the photoreaction reaches IIB, the displacement of the Co-N$_{Im}$ bond is

barrierless. From IIIB (S$_{1\ min}$), the photodissociation of the Co-C bond occurs, generating

Co(II)/CH$_3$ RPs. The RPs can undergo diffusive loss or recombination of Co(II)/CH$_3$ RP

may take place through deactivation to the ground state, as shown in Figure 2.7.
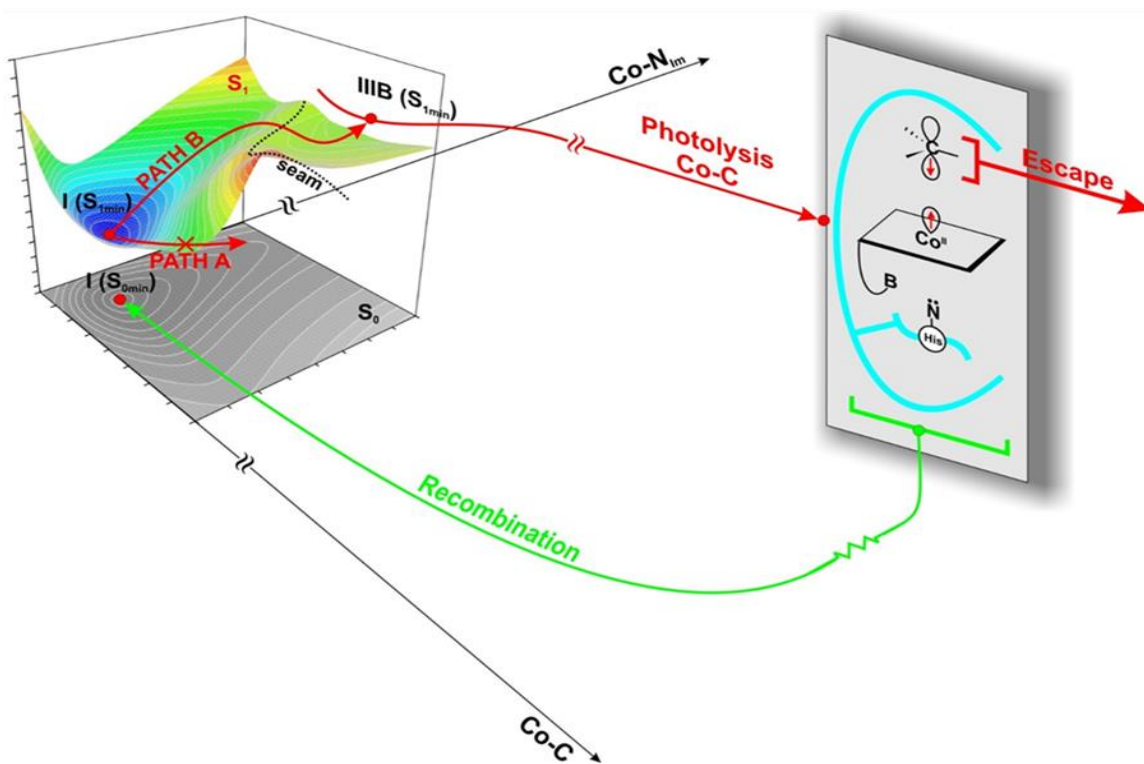
Figure 2.7. Schematic representation of photoreaction for MeCbl-bound MetH.

Recombination of RP will occur after the re-attachment of axial ligands with the corrin

ring. On the other hand, Path A, which initiates from the MLCT minimum (I S$_{1\ min}$),

involves the detachment of the Co-C bond followed by elongation of the Co-N$_{Im}$ bond. The

barrier associated with the crossing of the seam in Path A is high in energy. As we can see

in Figures 2.6a, the energetic barrier associated with Path A is relatively higher than Path

B, which makes it an energetically unfavorable pathway to connect the MLCT to the LF

state. Therefore, the photodissociation in MeCbl inside MetH proceeds via only Path B,

which involves the displacement of the axial base through the minimum energy along the seam followed by a detachment of the Co-C bond.

2.3.5 Comparison with Experiment

Femtosecond to nanosecond TAS has been applied to explore the photolytic properties of the MeCbl cofactor in solution as well as inside the enzymatic environment. As has been pointed out, the photolysis of MeCbl is wavelength-dependent. While excitation at 400 nm results in partitioning between bond homolysis and formation of the metastable state, the formation of the metastable state results from excitation at 520 nm in the visible αβ-band. The TD-DFT/PM6/MM calculation has revealed that upon excitation from the singlet ground state, the S_4 state is initially populated as indicated by the calculated higher oscillator strength value (Table 2.2). The analysis of orbitals involved in the electronic transitions to the S_4 state indicated it is primarily associated with $d_{xy} \rightarrow \pi^*$ transitions with 49% of HOMO-3 to LUMO character. This type of electronic transition, characterized as MLCT, can be associated with a metastable state found in the experimental studies of the MeCbl cofactor. Walker *et al.* have reported a formation of metastable cob(II)alamin in visible α/β-band with an excitation wavelength of 552 nm in their TAS study of MeCbl-bound MetH. In our excited state calculation (Table 2.2), we have also found a metastable state S_3 at an excitation wavelength of 557 nm. Although the S_3 state has a high value of oscillator strength, the initial excitation from a singlet ground state of MeCbl bound MetH corresponds to the S_4 state as it has a noticeably higher value of transition dipole moment compared to other energetically close low-lying excited states. The excitation energies of S_1-S_4 are close to each other, which indicates fast deactivation to the lowest S_1 state. The excitation near the D/E band (at 400 nm) results in a partitioning,

which comes from the direct excitation of two or more excited states. Our TD-DFT/PM6/MM calculations found that the excitation near 400 nm produced excited states which belong to the S_9, S_{10}, S_{11} states (Table 2.2). Energy proximity between these excited states would cause vibrational level overlap, resulting in deactivation to the lowest excited S_1 state. The orbital characterization of these states has shown that these excited electronic states have dominated the LF character, which has an inclination for the weakly attached axial base with Co. Considering this, the excited states after excitation at 400 nm undergo relaxation directly to the LF minimum on the S_1 PES. Depending on wavelength excitation, the photochemical process can be initiated from the MLCT or directly from the LF state of S_1 PES, with the fact that only the LF S_1 state is responsible for homolysis of Co-C bond and radical recombination. Prior to the photolysis from LF minima of S_1 state, the photoreaction involves few intermediates. Based on our calculation, we have identified that the intermediates involved in the photoreaction are MLCT and LF state (Figure 2.8). Experiments have reported that absorption of visible light at 400 nm also leads to the kinetic partitioning between vibrational relaxation to S_0 state and the formation of Co(II)/CH$_3$ RP, which is associated with LF minima of S_1 PES (IIIB $S_{1\ min}$).

After the molecule reaches the LF minimum of S_1 PES (IIIB $S_{1\ min}$), either it could relax down to the S_0 state through the deactivation process, or the homolysis of bond can take place through the diffusive escape of methyl radical. As the axial base is partially attached to Co, the deactivation process of the excited state is associated with the deformation of the corrin structure and coordination sphere of Co. The bending of the N-Co-N angle is most likely involved in the process of ground-state relaxation of the excited molecule from the LF minima of S_1 PES (IIIB $S_{1\ min}$). Due to the dominant anti-bonding

character of the LF state, the ground state relaxation could also proceed through the de-excitations from the $(d_{yz})^1 (d_z^2)^2$ excited state configuration to a ground state Co(II), $(d_{yz})^2$ (dz^1). The RP is held within the cage formed by protein residues while inside the enzyme. In the case of the isolated MeCbl cofactor, the RP exists within the cage formed by a solvent molecule. After the formation of these RP, a competition between RP recombination and radical escape has been observed by the experimental studies. TAS study of MeCbl-bound MetH has been indicated that the branching ratio and the initial production of cob(II)alamin are not affected by the enzymatic environment, but it protects the MeCbl-bound MetH from photolysis.
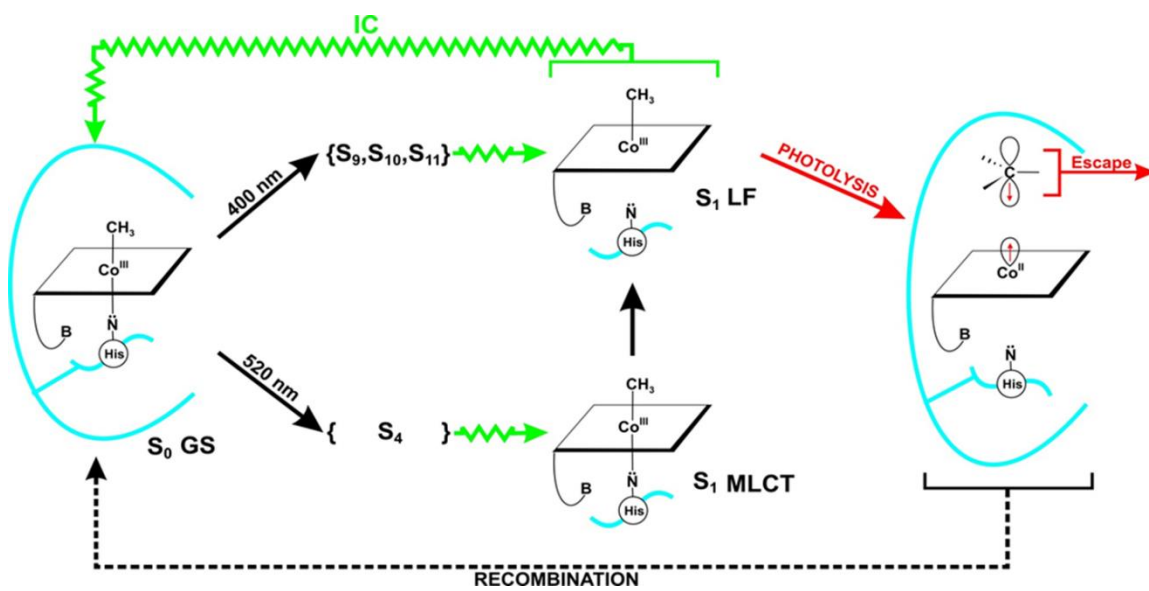
Figure 2.8 Mechanism of MeCbl photolysis in MetH and post-homolysis photolytic events (cage escape, internal conversion), as described in Section 2.3.5.

The enzymatic environment impedes the diffusion of methyl radical and enhances the rate of recombination of RP, which protects MeCbl from photolysis and decreases the rate of photoreaction by ~50 fold.[96] Based on experimental studies, the following factors that could inhibit the photolysis of MeCbl inside MetH, (i) the protein environment could

43

alter the excited state partitioning by increasing the rate of ground-state relaxation and decreasing the rate of bond homolysis (ii) the lower axial His ligand which is hydrogen-bonded with neighboring serine and aspartate residue forms a "ligand triad." This "ligand triad" could also protect the MeCbl-bound MetH from photolysis.[160] (iii) the protein residues form a cage that prevents the diffusive separation of methyl radical and increase the rate of radical recombination. Based on our calculation and careful analysis of S_1 PES of MeCbl-bound MetH, we can predict that it is easier to generate RP in solution than inside enzyme because the LF state is more stabilized in solution than inside enzyme. Therefore, the enzymatic environment plays a role in the destabilization of the LF state.

2.3.6 Implications of MeCbl photochemistry inside the enzyme: influence of enzyme on the photoactivation

Considering the one photolytic pathway for Co-C bond dissociation in MeCbl-bound MetH, a more general scheme has been presented for a lucid understanding of MeCbl photochemistry inside MetH (Figure 2.8). Based on our TD-DFT/PM6/MM calculations, it was found that the initial excitation at 520 nm of MeCbl-bound MetH primarily populated the S_4 or S_2 states as indicated by oscillator strength. The excited states associated with the excitation at 520-530 nm have dominant MLCT character, while the excited states that developed from excitation near 400 nm wavelength have associated with the LF region of S_1 PES. The similar excitation energies of S_1-S_4 electronic states have indicated a fast relaxation to the S_1 state. As the photolysis of MeCbl-bound MetH is guided by the energetics of MLCT and LF electronic states of S_1 PES, the computed S_1 PES of MeCbl-bound MetH was compared with the results of the base-on MeCbl to investigate the effect of enzymatic environment on the photochemistry of MeCbl.

Although the topology of S_1 PES for MeCbl-bound MetH and isolated base-on MeCbl is nearly indistinguishable, the energetics of MLCT and LF electronic states of S_1-PES are different. The LF state is energetically shallow and higher in energy than MLCT for both MeCbl-bound MetH and base-on MeCbl, which made the MLCT region more stabilized. However, for the MeCbl-bound MetH, the energy difference between the minima of MLCT and LF electronic state is four times higher than the energy difference of the base-on MeCbl. This higher energetics of LF state is the reason why we found only one pathway (Path B) for the photodissociation of MeCbl-bound MetH, which is associated with the detachment of axial base followed by elongation of the Co-C bond. While in base-on MeCbl, where the LF is comparatively lower in energy, it has two possible photodissociation pathways (Figure 2.6b). Therefore, the LF region is sensitive to environmental conditions, and in MeCbl-bound MetH, the enzymatic environment engendered the destabilization of LF, which affects the photolytic properties of MeCbl-bound MetH.

2.4 Conclusion

The purpose of the present computational study was to investigate the mechanism of light-induced activation of the Co-C bond in MeCbl-bound MetH to provide a detailed insight into the enzymatic effect on the photochemistry of MeCbl. The computed S_1 PES have been analyzed to identify probable photodissociation pathways (Path A and Path B) and intermediates that are involved in the photolysis of MeCbl-bound MetH. Regardless of the pathway and the environment, that is either in solution or inside the enzyme, the photodissociation of MeCbl starts from the MLCT region of S_1 PES which is associated with the excitation at α/β band of visible light. Excitation at 400 nm results in partitioning

between ground state relaxation and homolysis of Co-C bond, which has dominant LF character as suggested by orbital analysis. A detailed analysis of the energetics of S_1 PES has been performed to identify the most favorable path for photodissociation. Path B, which is associated with the first elongation of the Co-N_{Im} bond followed by a subsequent detachment of the Co-C bond, is the energetically favorable and active pathway for photolysis of MeCbl inside MetH. The computed photochemical data of MeCbl-bound MetH was compared with the isolated MeCbl cofactor in the base-on form to investigate the effect of the enzymatic environment on the photolysis of MeCbl. On the S_1 PES, the LF electronic state is higher in energy than the MLCT state for both MeCbl in solution and inside MetH; thus, the MLCT region is energetically more stabilized. The energy difference between the minima of the MLCT and LF electronic state for MeCbl bound MetH is 9.45 kcal/mol, which is almost four times higher than the energy difference between the MLCT and LF region for a base-on form of MeCbl in solution. This difference in the destabilization of LF in comparison to MLCT can affect the formation of RP in the LF state; hence it can prevent the photolysis of MeCbl-bound MetH. Furthermore, this study provides an insight into the effect of the environment on the S_1 PES as well as the photoactivation of the Co-C bond of MeCbl.

CHAPTER III

EFFECT OF MUTATION ON THE PHOTOACTIVATION OF Co-C BOND: A CASE STUDY OF MECBL-DEPENDENT METHIONINE SYNTHASE

3.1 Background

[2]As discussed in Chapter 2, the photoactivation of the Co-C bond and the photolytic properties of MeCbl depend on the cofactor's environment, whether it is in solution or inside the enzymatic environment. The TAS study has shown that the enzyme protects the MeCbl cofactor against photolysis by enhancing the intrinsic rate of geminate recombination and preventing the diffusive loss of methyl radical.[97, 161] Based on the experimental results, it appears that MeCbl-bound MetH decreases the photoreaction rate by almost 50-fold.[96] Several factors are responsible for inhibiting the photodissociation of organometallic Co-C bonds inside the protein environment, a few of which are enumerated here. First, upon binding with protein, the enzymatic environment expedites the ground-state relaxation rate and decreases the RP formation rate. Second, the protein could also deter the oxidation of methyl radical by prohibiting the oxygen from the Cbl binding pocket of MetH. Third, the protein environment plays a role in destabilizing the ligand field (LF)

---

[2] The discussions in this chapter are based on the publication *"Ghosh, A. P., Mamun, A. A., & Kozlowski, P. M. (2019). How does the mutation in the cap domain of methylcobalamin-dependent methionine synthase influence the photoactivation of the Co–C bond?* Phys. Chem. Chem. Phys., *21(37), 20628-20640 "*

electronic state, which could plausibly affect the formation of Co(II)/CH$_3$ RP in the LF state and alter the photochemical yield of cob(II)alamin.[162] Alongside these aforementioned factors, Matthews and co-worker, have affirmed that the hydrophobic residues of the cap domain which surrounds the upper face (or β face) of MeCbl cofactor is protecting the photolysis of MeCbl by caging the methyl radical and inducing the geminate recombination of the Co(II)/CH$_3$ RP.[96] To be precise, phenylalanine708 (F708) and leucine 715 (L715) are situated above the methyl group in MeCbl-bound MetH, impeding the cage escape by limiting the solvent accessibility of the methyl group. They have also demonstrated that the mutation in the cap domain of MeCbl-bound MetH, particularly at the F708 position, will dramatically increase the rate of photolysis by almost 62-fold.

To further validate this hypothesis, it is important to understand the influence of mutation on the photo-reactivity of MeCbl-bound MetH at a molecular level. Toward this, a detailed understanding and delineated description of excited-state based on quantum mechanical (QM) calculation is indispensable. In this present study, we have introduced mutation on the F708 position and replaced it with alanine (A708) residue, and these amino acid residues were kept in the HL throughout the calculations of this chapter (Figure 3.1). The ground state and excited state properties of MetH were computed based on the combined density functional theory/molecular mechanics (DFT/MM) and time-dependent DFT (TD-DFT/MM), respectively. The computed photochemical data of wildtype (WT)-MetH and F708A-MetH were also compared to investigate the influence of mutation on the photoactivation of the Co-C bond in MeCbl-bound MetH.

3.2 Computational methodology

ONIOM-based[119, 141] DFT/MM, and TD-DFT/MM methods were applied to investigate the photodissociation mechanism of Co-C bond in MeCbl-bound MetH as well as the influence of mutation on the light-induced activation. The x-ray structure of the MeCbl-binding domain of MetH (PDB code:1BMT, @ 3 Å resolution)[29] was used as a
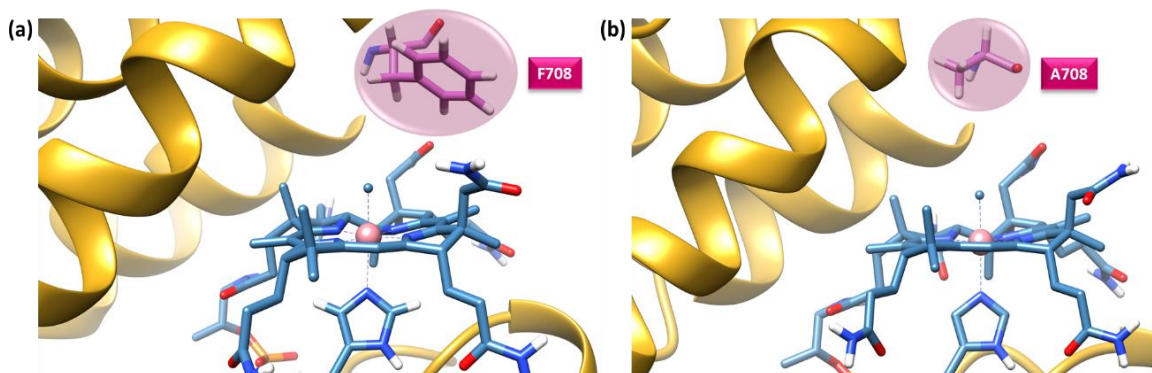
Figure 3.1. The active site of MeCbl-dependent MetH. MeCbl cofactor, Phe, Ala amino group is depicted as a ball and stick model and protein residue using ribbon **(a)** WT-MetH **(b)** F708A-MetH

structural model to perform the QM/MM calculations. The crystal structure contains two independent chains (chains A & B), and each chain includes the entire MeCbl cofactor independently. For building the computational model, one independent chain (chain A) was used to prepare the initial model using UCSF Chimera.[163] Upon binding with the enzyme, the MeCbl cofactor undergoes a structural change, leading to the displacement DBI group. The DBI group, which is axially ligated to the Co center of corrin ring in the base-on form of isolated MeCbl cofactor, is replaced by the Im group of histidine759 (H759) residue of the protein.

3.2.1 Model Building and QM/MM set up

To investigate the effect of the mutation on the photoactivation of the Co-C bond in MeCbl-bound MetH, we have prepared two different models of MeCbl-bound MetH for

carrying out the QM/MM calculations. The mutation was introduced at the F708 position of MeCbl-bound MetH and replaced by alanine (A708). These two models, WT-MetH and F708A-MetH, were then protonated using PROPKA 3.0 software[144] via the PDB2PQR web server. The protonation states of axially coordinated H759 residue are determined by the protonation of nitrogen either at α or δ position. Based on the protonation of nitrogen at a particular position, it refers to HID (for N_δ position) or HIE (N_ε position). In both models (WT-MetH and F708A-MetH), the H759 was protonated at the N_δ position, therefore, treated as HID. These protonated structures were then minimized with the MM level of theory using the AMBER force field. Finally, these minimized models were used to generate QM/MM input.

The energy minimized structure of WT-MetH and F708A-MetH were further partitioned into three layers for carrying out ONIOM (DFT/TD-DFT:PM6:MM)-ME calculations. In this ONIOM-ME calculation, the truncated cofactor (Co atom and corrin ring) without the side chains of corrin ring, methyl group, the amino acid residue at 708 positions (F708 in WT-MetH and A708 in F708A-MetH), and the Im moiety of H759 were included in the HL. It is worth mentioning that the atoms which are chemically important to describe the photoreaction were placed into the HL (Figure 3.2). The rest of the cofactor, the nucleotide tail, and all side chains were included in the ML, and the remaining protein part was placed in the LL. In total, the models of WT-MetH and F708A-MetH contain 4032 and 4022 atoms, respectively. Protein residues within 20 Å of the Co center were used for geometry optimization and kept unfrozen and remaining atoms were kept frozen. All ONIOM calculations were performed using the Gaussian 09 software package.[145]

3.2.2 Ground State Calculations
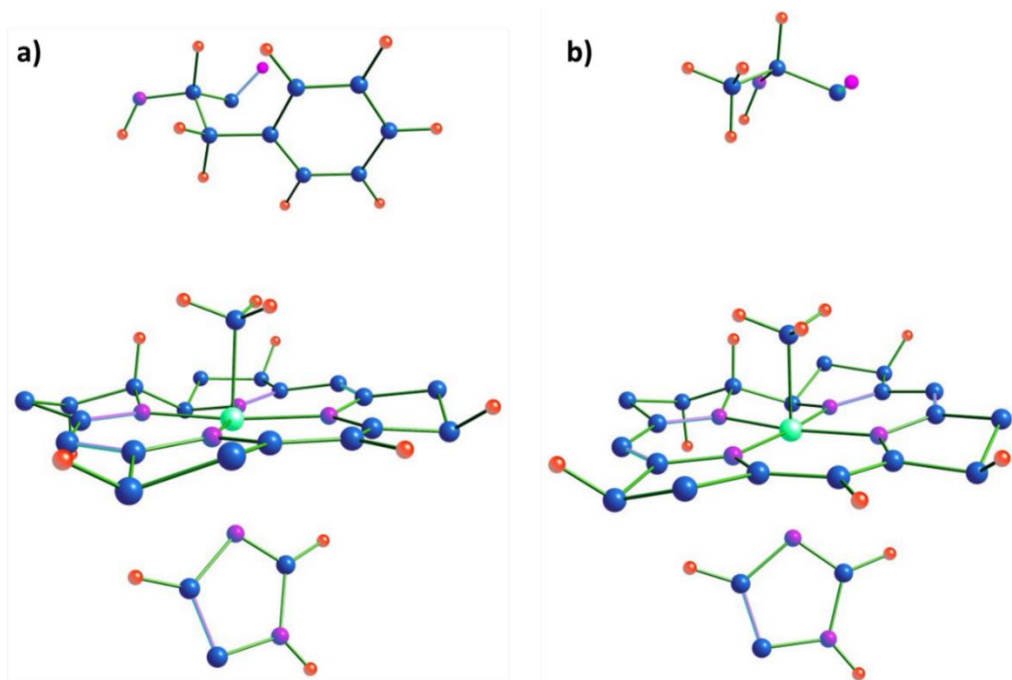
Figure 3.2. Active site figures treated with QM level of theory in the QM/MM calculations (a) WT-MetH and (b) F708A-MetH.

The models of MeCbl-bound MetH, WT-MetH, and F708A-MetH were optimized using DFT:PM6:MM level of theory. In DFT, the accuracy of the calculations solely depends on the proper choice of a functional. Based on our previous benchmark studies, it has been shown that a pure GGA-type functional, like BP86, gives a more reliable and accurate description of geometrical parameters of Cbls as well as Co-C bond dissociation energy (BDE).[147-149] Thus, the use of BP86[147] as a DFT functional is crucial for our studies. Consistent with our previous results,[162, 164-166] the TZVP basis set was used for the H atom, and the TZVPP basis set was used for Co, C, O, and N atoms.[154] Semi-empirical (PM6) level of theory was used to study the middle layer of our models, while the low layer, which contains the protein part of our models, was treated with MM level of theory using the ABMER (FF99SB)[153] force field as implemented in Gaussian 09 program. The AMBER parameters assigned for the MeCbl cofactor were obtained from Marques et al.[167] The

equilibrium geometry was used to compute the ground state (S_0) 3D-PESs as a function of Co-C and Co-N_{Im} for WT-MetH and F708-MetH. These two axial bond lengths are sensitive to the cofactor environment as well as excitations with light. Thus, S_0 PES for WT-MetH and F708A-MetH were constructed by simultaneous elongation of Co-C and Co-N_{Im} bond with a step size of 0.1 Å.

3.2.3 Excited State Calculations

A detailed understanding of the S_1 excited state is paramount in exploring the photoactivation of the Co-C bond. Toward this, S_1 PES has been constructed in the TD-DFT:PM6:MM framework. TD-DFT has been benchmarked against ab initio methods like CASSCF/MC-XQDPT2 and EOM-CCSD, which revealed that using BP86 functional with TD-DFT can give a proper description of low-lying excited states such as $S_1 \ldots S_n$.[128, 156] The S_0 optimized geometry of WT-MetH and F708A-MetH was used to generate the S_1 PESs. Single point TD-DFT:PM6:MM calculations on each point of optimized S_0 PESs were used to construct the S_1 PESs without relaxing the excited state geometry. A detailed orbital analysis was carried out on each point of S_1 PESs to dissect the nature of electronic transitions. The S_1 PES is the outcome of crossing two different electronic states, MLCT and LF. The electronic excitation in the LF states involves Co d and corrin π to σ^* type transition, where the σ^* is the combination anti-bonding p orbital of carbon and Co d_Z^2 orbital. The orbital analysis has predicted that the electronic transition in the MLCT region involves excitation from Co d-orbitals to corrin π^*. However, a more careful analysis of the electron density difference (EDD) between S_0 and S_1 states suggests this is not completely metal to ligand transition. Figure A3 has provided a graphical description of EDD between S_0 and S_1 state at S_1 PES. This EDD plot clearly depicts that the electron

density is not only decreasing on the Co atom but also along with the N_{Im}-Co-C_{Me} bond. On the other hand, the electron density increases on the corrin ring. Therefore, the electron density is shifted from both the Co and NIm-Co-CMe axial bonding to the corrin ring upon electronic excitation. This type of electronic transition is defined as σ bond-ligand CT type transitions (SBLCT).[129] However, considering the importance of the MLCT component in this transition, it will be more pertinent to describe this state as a mixed MLCT/SBLCT character. But for consistency with experimental results, we simply use MLCT.

3.3 Results and Discussion

3.3.1 Ground State Geometry

The minimized structure of WT-MetH and F708A-MetH were used for geometry optimization. The geometry optimization was carried out at DFT:PM6:MM level of theory. Frequency calculations have confirmed that the geometries of WT-MetH and F708A-MetH have optimized to a stationary point, as no imaginary frequencies were found. The geometrical parameters of the optimized structure agreed well with experimental parameters (Table 3.1). In the optimized geometry of WT-MetH, the calculated Co-C and Co-N_{Im} bond lengths are 1.99 Å and 2.29 Å, respectively. On the other hand, for F708A-MetH, the computed Co-C and Co-N_{Im} bond lengths are 1.99 Å and 2.26 Å, respectively (Table 3.1). The computed structural parameters of the base-on form of the MeCbl cofactor inside the solution, where the axial ligand is Im group, were compared with MeCbl-bound MetH. The noticeable difference was observed in the lower axial bond distance, while in the optimized MeCbl cofactor, the lower axial Co-N_{Im} bond length is 2.17 Å, in WT-MetH and F708A-MetH the Co-N_{Im} lengths in 2.29 Å and 2.26 Å, respectively. This indicates

that the lower axial Co-N_{Im} bond lengths in MeCbl inside solution and MeCbl inside enzyme are sensitive towards the local environment.

	Crystal structure	WT- MetH			F708A-MetH		
		Optimized Structure	I (S_{0min})	I (S_{1min})	Optimized Structure	I (S_{0min})	I (S_{1min})
Bond Distances (Å)							
Co-C	1.957	1.999	2.000	2.000	1.976	2.000	2.000
Co-N_{Im}	2.241	2.296	2.300	2.100	2.164	2.300	2.100
Co-N_{21}	1.925	1.895	1.895	1.903	1.894	1.893	1.901
Co-N_{22}	2.015	1.949	1.949	1.957	1.955	1.954	1.960
Co-N_{23}	2.016	1.941	1.941	1.947	1.947	1.946	1.954
Co-N_{24}	1.914	1.886	1.886	1.892	1.889	1.888	1.893
Bond Angles (°)							
C-Co-N_{Im}	167.4	169.7	169.6	170.7	170.3	170.1	171.1
N_{21}-Co-N_{23}	172.9	173.8	173.8	173.6	173.9	174.0	173.5
N_{22}-Co-N_{24}	177.8	172.1	172.2	170.8	172.4	172.6	171.4
Torsion Angles (°)							
N_{21}-N_{22}-N_{23}-N_{24}	4.8	-3.4	-3.4	-3.4	-1.9	-1.8	-2.2
N_{21}-N_{22}-N_{23}-Co	4.9	0.002	-0.1	1.3	0.7	0.5	1.6

Table 3.1. Selected geometrical parameters for both the WT-MetH and F708A-MetH.

3.3.2 Excited states: energy profile and topology of S_1 PES as a function of axial bond lengths

Based on TAS and XANES experiments, it is apparent that the Co-CN and Co-NIm axial bonds experience most structural changes upon electronic excitation, while the corrin macrocycle is only slightly perturbed.[159] Therefore, to clarify the light-induced activation of the Co-C bond in MeCbl-bound MetH, the construction of the excited state PESs as a function of axial bond lengths is indispensable. To explore the effect of the mutation on

the photolysis of the Co-C bond, the S_0 and S_1 PESs of WT-MetH were compared with F708-MetH. The detailed methodology regarding the construction of S_1 PESs has been discussed in Computational Methods (Section 3.2.3).

The S_1 PES of WT-MetH carries two minima regions, namely MLCT and LF (Figure 3.3a). Unlike the MLCT region, which is associated with shorter Co-C bond length, the LF excitation corresponds to a longer Co-C and Co-N_{Im} bond distance. These two
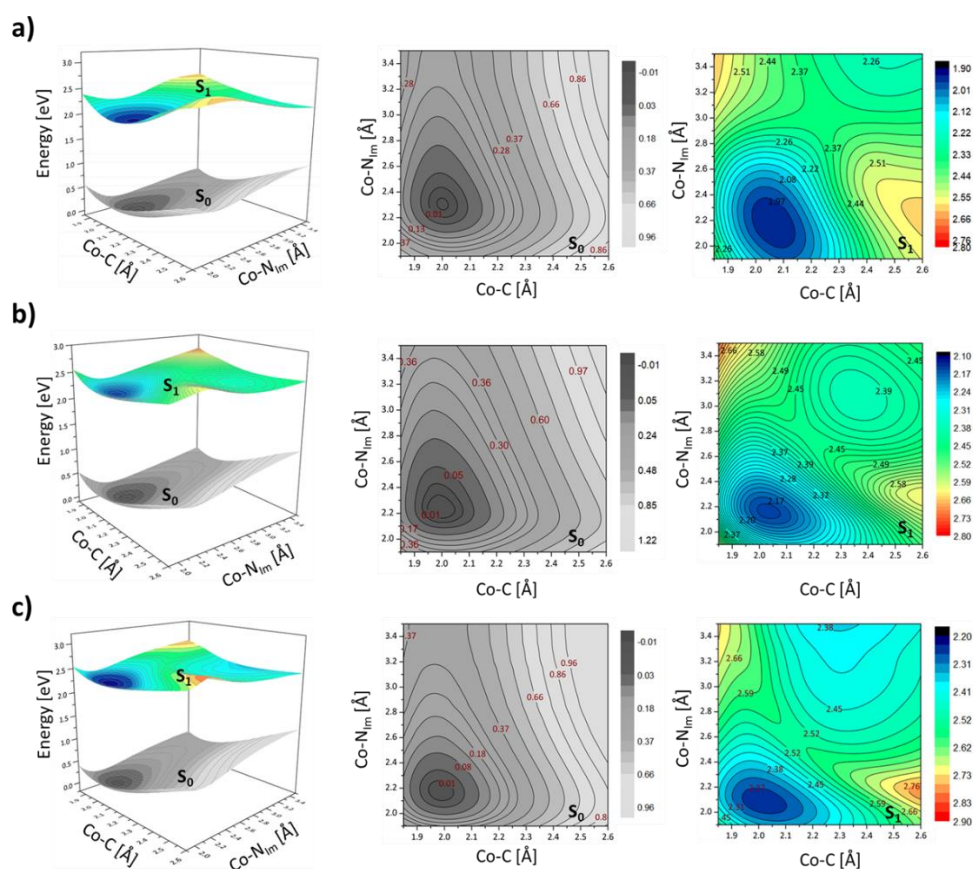
Figure 3.3. Potential energy surfaces for the S_0 with vertical projections of the S_1 state plotted as functions of axial bond lengths along with the corresponding S_0 and S_1 contour PESs **(a)** WT-MetH **(b)** F708A-MetH **(c)** Im−[Co^{III}(corrin)]−Me$^+$ base-on model complex in water.

energy minima result from the intersection between two different electronic states and separated by a seam through an MECP (IIB, Figure 3.4a). In the case of WT-MetH, the

MLCT minima I (S_{1min}) at S_1 PESs located at a similar Co-C bond distance as S_0 PES and a marginally longer Co-N_{Im} bond distance (Figure 3.4a). The second minima on S_1 PES, the LF IIIB (S_{1min}) localized at a Co-C bond length 2.5 Å and Co-N_{Im} 3.5 Å (Figure 3.4a). The electronic excitation in the MLCT region is associated with d + $\pi \rightarrow \pi^*$ type transition, whereas the transition in LF electronic state has a dominant d + $\pi \rightarrow \sigma^*$ (d_z^2) character. Figure 3.5 shows the molecular orbitals involved in the electronic transition from $S_0 \rightarrow S_1$ for selected points on the S_1 PES (Figures 3.4a and 3.4b). The electronic transitions for the MLCT I (S_{1min}) and LF IIIB (S_{1min}) have been characterized as 72% d_{xz} + $\pi \rightarrow \pi^*$ and 98% d_{yz} + $\pi \rightarrow \sigma^*$ (d_z^2) type transition, respectively (Figure 3.5a). The electronic excitation at IIB (MECP) has a dominant HOMO-1 to LUMO character with 95% d_{xz} + $\pi \rightarrow \sigma^*$(d_z^2) transition (Figure 3.5a). Figure A4 has depicted the corresponding ground state optimized geometries of the selected points in Figure 3.4a.
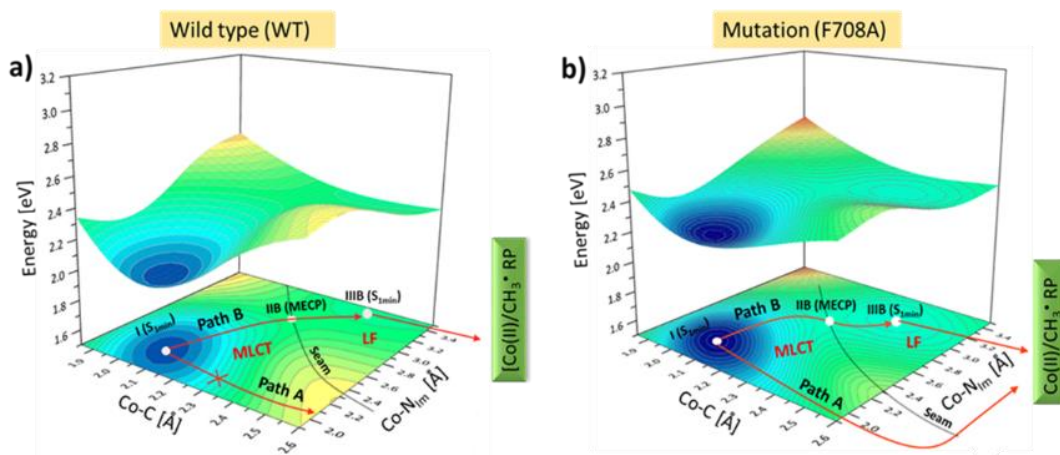
Figure 3.4. Potential energy surfaces of S_1 state as a function of axial bond lengths with photoreaction pathway depicted by red arrows for **(a)** WT-MetH **(b)** F708A-MetH.

The S_0 and S_1 PESs of F708-MetH were analyzed and compared with WT-MetH. While the topology of S_0 PESs are almost identical for both WT-MetH and F708-MetH and

contains a single energy minimum at Co-C bond length of 2.0 Å and Co-N$_{Im}$ 2.3 Å, the noticeable differences are evident on the S$_1$ PESs. The S$_1$ PES of F708-MetH also contains two energy minima, separated by a seam (Figure 3.3b). The MLCT minima I (S$_{1min}$) for F708A-MetH was localized at a Co-C bond length 2.0 Å and Co-N$_{Im}$ bond distance at 2.1 Å (Figure 3.4b, and Figure A4). The axial bond lengths for LF IIIB (S$_{1min}$) are 2.4 Å and 3.1 Å for Co-C and Co- N$_{Im,}$ respectively (Figure 3.4b, Figure A4). The electronic transition in MLCT minima I (S$_{1min}$) is 77% d$_{xz}$ + $\pi \rightarrow \pi^*$ and in LF minima IIIB (S$_{1min}$), the electronic excitation correspond to 98% d$_{yz}$ + $\pi \rightarrow \sigma^*$ (d$_z^2$ (Figure 3.5b). At the IIB (MECP), the excitation has dominant metal d orbital $\rightarrow \sigma^*$ (d$_{xz}$ + $\pi \rightarrow \sigma^*$ (d$_z^2$)) contribution (Figure 3.5b).

Although the analogous S$_1$ PES of the base-on isolated MeCbl cofactor also carries two different minima regions (Figure 3.3c) the topology and the energetics of the S$_1$ PES for base-on MeCbl are markedly different from its WT-MetH and F708A-MetH counterparts. While noticeable differences are observed between the S$_1$ PES of WT-MetH and isolated MeCbl cofactor (as discussed in chapter 2), the topology and the energy difference between MLCT (I (S$_{1min}$)) and LF minima (IIIB (S$_{1min}$)) are similar for F708A-MetH and base-on MeCbl inside the solution. This indicates that the mutation on the F708 position in the cap domain is playing a role in stabilizing the LF electronic state.

3.3.3 Long-range Charge Transfer Analysis

In TD-DFT methodology, the long-range charge transfer (LR-CT) is a great matter of concern.[168] This concern mainly arises due to the LR excitations, which are basically the result of the poor overlap between the occupied and virtual orbitals. Density-based matrix (D$_{CT}$) calculation was carried out using the DctViaCube software suite[169] to ensure that selected S$_0 \rightarrow$ S$_1$ transitions are not affected by LR-CT issues.[170-171] D$_{CT}$ is the spatial

distance between the two barycenters of density depletion (R_+) and density augmentation zone (R_-). D_{CT} calculation was performed on several points of S_1 PES (for both WT-MetH and F708-MetH) to diagnose the extent of charge transfer based on the ground and excited
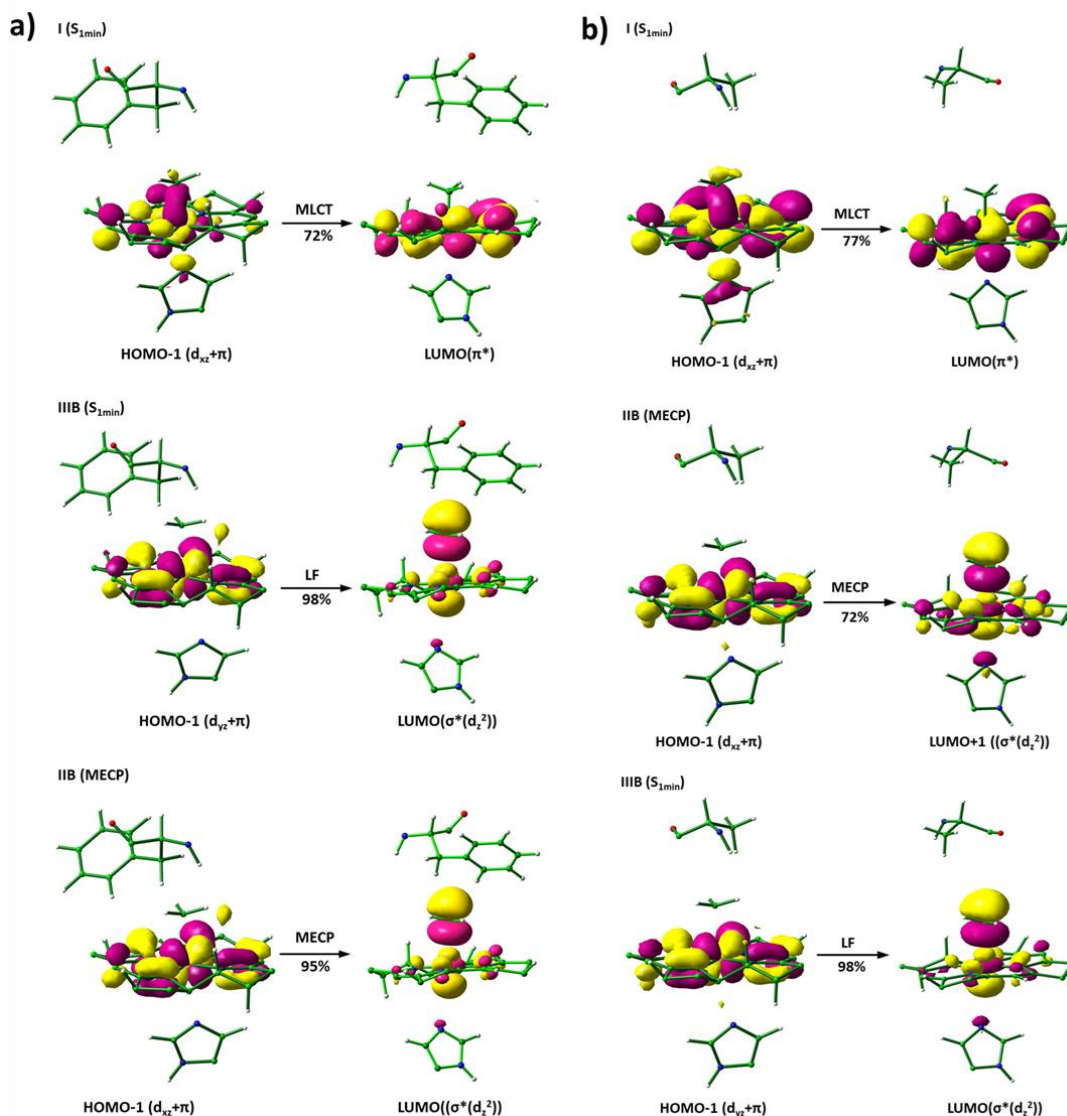
Figure 3.5. HOMO and LUMO molecular orbitals involved in electronic excitations from $S_0 \rightarrow S_1$ for selected points on the S_1 PES (Figure 3.4a and 3.4b) along Path B for (a)WT-MetH (b) F708A-MetH.

state densities. Few selective parameters were considered in D_{CT} calculation for successfully implementing the CT diagnoses. These parameters are the charge transfer

length between the density depletion (R_+) and density augmented zone (R_-) (D_{CT}), the total transferred charge (q), the half of the centroid axis along with the charge transfer (H), and the difference between D_{CT} and H (t). A relatively smaller value of t and H>D_{CT} indicates a significant overlap between occupied and virtual orbitals.[170]

For WT-MetH, the electronic transition between corrin and the F708 residue and electronic excitation involving corrin ring and A708 group in the case of F708A-MetH are typically characterized as LR-CT type excitations. These LR-CT transitions can have a negative impact on the S_1 PESs. Detail orbital analysis of corresponding electronic excitations was performed, and proper electronic transitions have been selected to construct a reliable S_1 PES to ensure that LR-CT transitions had no negative impact on the computed PESs. Several points on the S_1 PES was have been analyzed with D_{CT} diagnosis to further ensure that the selected transitions were not results of LR-CT type excitation (Table 3.2). The calculated values of H, negative t value, and the length of charge transfer (D_{CT}), which are below the threshold number reported in previous studies, reflect the proper overlap between the involved occupied and virtual orbitals. Therefore, taking all these above into account, we have confidence that S_1 PES for WT-MetH and F708A-MetH wasn't affected by LR-CT type excitations and was correctly constructed using TD-DFT:PM6:MM methodology.

3.3.4 Mechanism of photodissociation: comparison of WT-MetH and F708A-MetH photoreaction

A systematic approach was used to analyze the constructed PESs in order to gain insight into the mechanism of photoactivation of the Co-C bond for Cbls. The shape of the S_1 PES is the result of the crossing between two different electronic states, MLCT and LF.

	Selected Points		f	λ[nm]		%	Character	D_{CT}	q	H
	Co-C	Co-N$_{Im}$								
MLCT	2.00	2.10	.0113	579	H-1→L	72	$d_{xz}/d_z^2 + \pi \to \pi^*$	0.27	0.91	1.71
					H-4→L	13	$d_{yz} + \pi \to \pi^*$			
MLCT	2.00	2.30	.0020	560F	H-3→L	72	$d_{xz}/d_z^2 + \pi \to \pi^*$	1.55	0.92	2.85
					H-1→L	11	$d_{xz} + \pi \to \pi^*$			
MLCT	2.10	2.10	.0084	586	H-1→L	82	$d_{xy} + \pi + \to \pi^*$	0.25	0.91	1.69
					H-2→L	04	$d_{xz}/d_z^2 + \pi \to \pi^*$			
LF	2.50	3.30	.0029	860	H-1→L	98	$d_{xz} + \pi \to d_z^2$	0.33	0.73	1.54
LF	2.50	3.50	.0032	882	H-1→L	98	$d_{yz} + \pi \to d_z^2$	0.30	0.83	2.45

b)

	Selected Points		f	λ[nm]		%	Character	D_{CT}	q	H
	Co-C	Co-N$_{Im}$								
MLCT	2.00	2.10	.0066	588	H-1→L	77	$d_{xz}/d_z^2 + \pi \to \pi^*$	0.27	0.98	2.28
					H-2→L	08	$d_{yz} + \pi \to \pi^*$			
MLCT	2.00	2.30	.0025	568	H-2→L	72	$d_{xz}/d_z^2 + \pi \to \pi^*$	0.15	0.81	1.48
					H-1→L	08	$d_{xz} + \pi \to \pi^*$			
MLCT	2.10	2.10	.0087	596	H-1→L	84	$d_{xy} + \pi + \to \pi^*$	0.25	0.87	1.73
					H-2→L	04	$d_{xz}/d_z^2 + \pi \to \pi^*$			
LF	2.50	3.30	.0028	859	H-1→L	98	$d_{xz} + \pi \to d_z^2$	0.60	0.96	2.20
LF	2.50	3.50	.0030	877	H-1→L	98	$d_{yz} + \pi \to d_z^2$	0.83	0.78	1.29

Table 3.2. Charge transfer diagnostics to characterize the selected points on the S_1 PES for a) WT-MetH b) F708A-MetH

The key challenge in describing the photoreaction mechanism is to connect these two minima regions through a minimum energy path (MEP). Energetics and connections between these two electronic states depict the pathway of photodissociation. Based on our previous studies, two different pathways, namely Path A and Path B, have been identified for the photodissociation of the Co-C bond. The energetic profile of the photodissociation is different for each Path. Path A involves the initial elongation of the Co-C bond from the MLCT (I (S_{1min})) prior to the detachment of the Co-N$_{Im}$ bond, while the Path B is associated

with the initial detachment of the Co-N_{Im} bond from the MLCT ($I(S_{1min})$) followed by subsequent elongation of Co-C bond. Although the intermediates involved in the photoreaction are different for both the pathways, the initial and final products are similar. The scheme of photoreaction is depicted in Figure 3.4.

In the case of WT-MetH, the LF state is energetically higher than the MLCT state by an amount of 7.4 kcal/mol. This indicates that the MLCT to LF transition is an uphill process. The photodissociation in WT-MetH can only proceed through Path B, which involves the first lengthening of the Co-N_{Im} bond from the minima region associated with the MLCT electronic state (I (S_{1min})) (Figure 3.4a). After the initial detachment of the Co-N_{Im} bond, the photoreaction proceeds through MEP along the seam and cross energy barrier at the MECP (II) (Figure 3.4a). The energy profile of the photoreaction was constructed as a function of Q, where Q is defined as $Q = \sqrt{R_{Co-C}^2 + R_{Co-N_{Im}}^2}$. The calculated energy barrier to cross the MECP (IIB) along path B is 10 kcal/mol (Figure 3.6). At this intermediate state, the Co-N_{Im} bond is long (about 3.00 Å), whereas the Co-C bond is 2.25 Å (Figure A4). Once the intermediate reaches the MECP (IIB), the detachment of the axial base takes place in a barrierless fashion. After crossing the energy barrier (IIB, MECP), the photoreaction leads to the LF (IIIB (S_{1min})) minima of S_1 PES. The photodissociation of the Co-C bond primarily occurs from this LF electronic state by generating the Co(II)/CH_3 RP. After the formation of RP, either it can undergo a diffusive loss through the 'cage' formed by the protein residues of the cap domain, or it could recombine through the deactivation to the ground state.
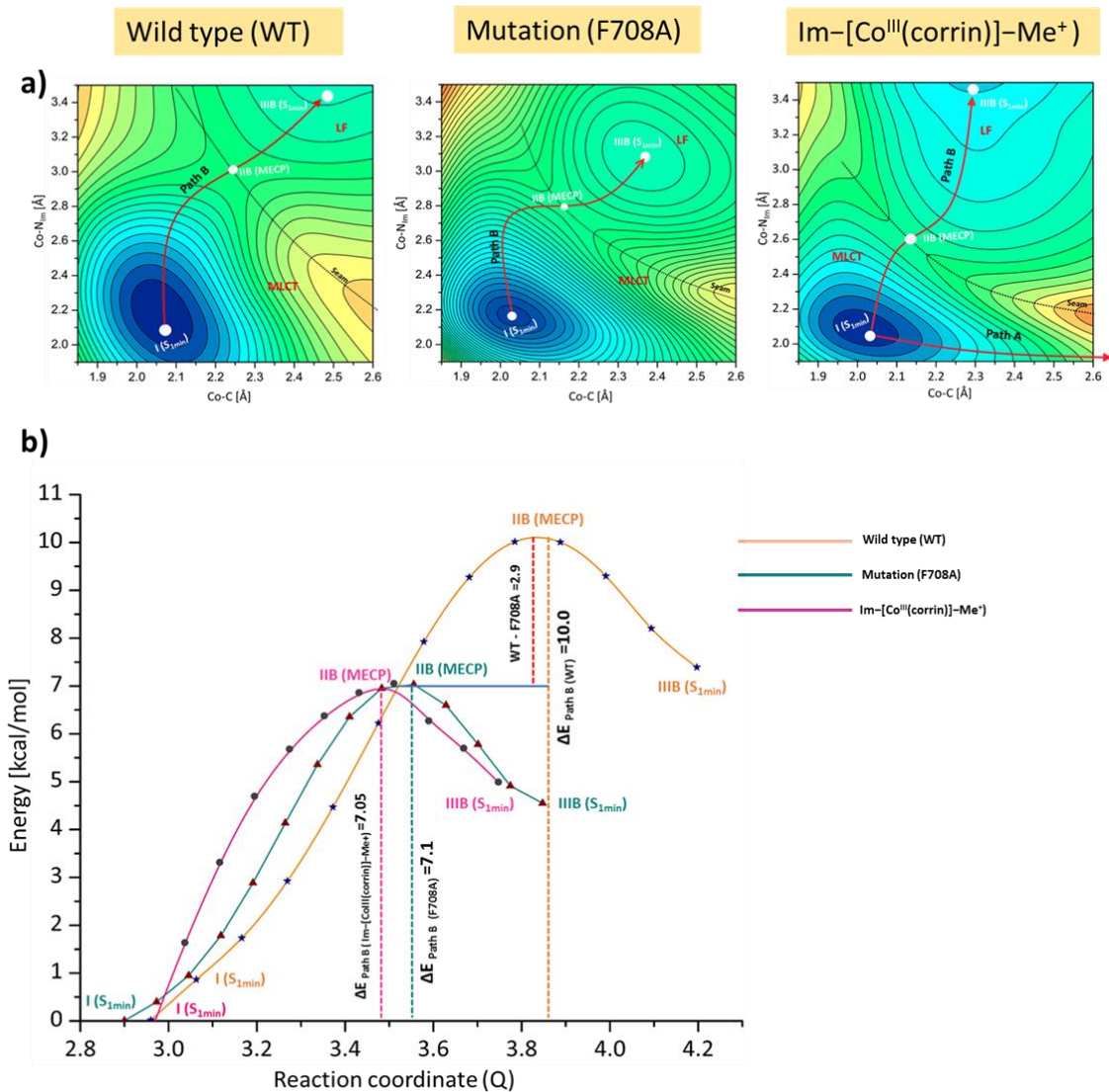
Figure 3.6 (a) Scheme of photoreaction along Path B for both WT-MetH and F708A-MetH as well as Im−[Co^{III}(corrin)]−Me$^+$ base-on model complex in solution on the S$_1$ PES with minima regions, separated by a seam, where MLCT minimum is denoted as I (S$_{1min}$) and LF minimum is denoted IIIB (S$_{1min}$) and **(b)** minimum energy paths (Path B) between MLCT and LF state plotted as a function of energy versus Q value.

On the other hand, the photoreaction involving Path A is not effective and energetically unfavorable due to the steep increase in energy associated with the displacement of the Co-C bond (Figure 3.4a) (see chapter 2, section 2.3.4). Hence, the

photodissociation in WT-MetH proceeds only through Path B, which involves the detachment of the Co-N_{Im} bond prior to the elongation of the Co-C bond.

For F708A-MetH, the S_1 PES is energetically unique in comparison to WT-MetH as the LF electronic state is energetically stabilized than its WT counterpart. The energy difference between the MLCT and LF minima in F708A-MetH is 2.3 kcal/mol (Figure 3.7b). In contrast to WT-MetH, for F708A-MetH, both Path A and Path B are feasible for the photodissociation of the Co-C bond (Figure 3.4b). However, Path B, which is associated with the first elongation of Co-N_{Im} bond from the MLCT (I, S_{1min}) minima and proceeds through the intermediate state at IIB, is energetically most favorable and effective for the Co-C bond photolysis. The energy barrier to cross the MECP (IIB, Figure 3.4b) along path B is 7.1 kcal/mol (Figure 3.6). After crossing the MECP (IIB) on S_1 PES, the photoreaction proceeds to the LF minima region (IIIB, S_{1min}), where the axial base nearly dissociates and generates the Co(II)/CH_3 RP. Upon the formation of RP, it will follow the same mechanism as WT-MetH towards the photodissociation of the Co-C bond. Therefore, for F708A-MetH the Path A remains ineffective, and the photoreaction will proceed through Path B, which is energetically favorable for the light-induced activation of the Co-C bond.

3.3.5 Comparison with Experiment

3.3.5.1 Transient Absorption Spectroscopy

The photoactivation of the Co-C bond and the photolytic properties of the MeCbl cofactor in solution as well as inside enzymes have been investigated using TAS techniques.[96-97, 172] It has been shown that absorption of visible light at 400 nm results in

the formation of the excited state. This excited state leads to the kinetic partitioning between the formation of Co(II)/CH$_3$ RP and the deactivation to the ground state through vibrational relaxation. In our previous TD-DFT/MM calculation, we have reported that this excited state has a dominant LF character associated with d$_{yz}$ + π→σ* (d$_z^2$) type electronic
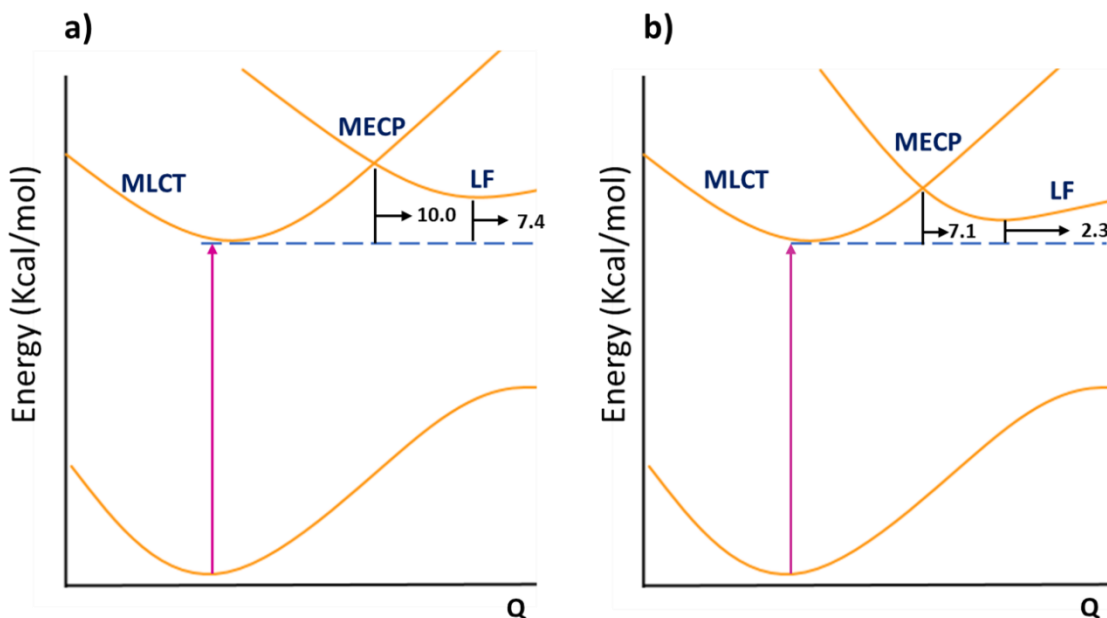
Figure 3.7. Relative energetics of the MLCT and LF state for (a) WT -MetH (b) F708A -MetH.

transition. Based on this observation, we have proposed that for MeCbl-bound MetH (for both WT-MetH and F708A-MetH), photolysis of Co-C bond occurs from the LF minima region of S$_1$ PES (IIIB, S$_{1min}$) at wavelength near-UV D/E band (~400 nm).[162] Therefore, the experimentally observed partitioning at 400 nm is associated with IIIB (S$_{1min}$) at S$_1$ PES. From this IIIB (S$_{1min}$) state, either deactivation to the ground state through internal conversion or the formation of Co(II)/CH$_3$ RP can take place. The deactivation process could take place through two different channels. The first deactivation channel involves the corrin ring distortion after the partial detachment of the axial base at LF minima, IIIB

(S_{1min}). As the axial base is either partially or completely dissociates at IIIB (S_{1min}) (Figure A4), the deactivation occurs through the deformation of the corrin ring and coordination sphere of the Co atom. The bending of the N-Co-N bond is most likely responsible for this deactivation process. Another channel of deactivation is the de-excitation from LF minima, IIIB (S_{1min}) to ground state by changing the electronic configuration from $(d_{yz})^1 (d_z^2)^2$ to $(d_{yz})^2 (d_z^2)^1$.[173] Once the RP is formed from the LF minima (IIIB (S_{1min})), a competition between geminate recombination of RP and diffusive loss of methyl radical has been observed by experiments. In MeCbl-bound MetH, the RP is trapped inside a cage, formed by the protein residues of the cap domain. This cage provides a relatively unreactive environment that protects the photolysis of the MeCbl cofactor by impeding the radical escape and enhancing the rate of recombination.[96-97] Prior to the photodissociation from the LF minima (IIIB (S_{1min})), the photolysis involved few intermediates. A detailed schematic representation of the photoreaction and involved intermediates has been outlined in Figure 3.8.

3.3.5.2 Influence of Mutation on the Photolysis of Co-C bond

The enzymatic environment inhibits the photolysis of MeCbl by preventing the radical escape of methyl radical and increasing the rate of geminate recombination. It has been reported that for WT-MetH, the protein environment is preventing the photodissociation of the Co-C bond and decreasing the rate of photolysis by ~50 fold.[96] Based on our calculation and the analysis of S_1 PES, we can argue that it is easier to generate RP in solution than inside enzyme as the enzymatic environment alter the formation of Co(II)/CH$_3$ RP by destabilizing the LF state (Figure 3.6).
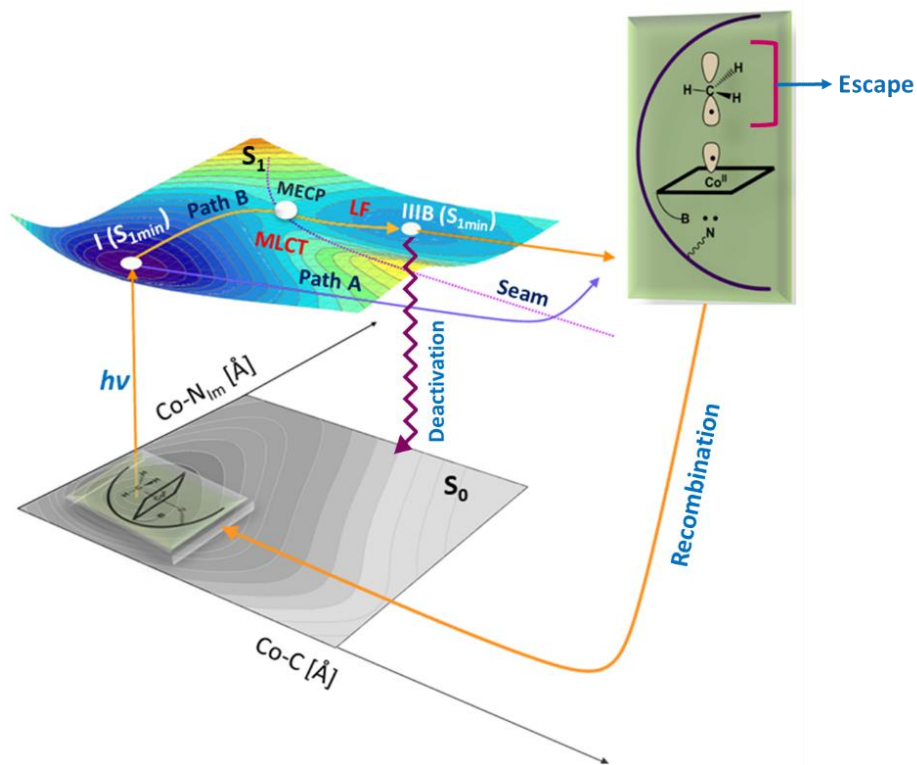
Figure 3.8. Schematic representation of photoreaction for MeCbl-bound MetH for both Path A and B

However, for F08A-MetH, it has been reported that the mutation compromises the protein cage and increases the rate of radical escape. To further investigate the influence of mutation, we have analyzed the trajectory of the radical escape. The topology of the CH_3 radical escape is depicted in Figure 3.9. It shows that for the WT-MetH with increasing Co-C bond distance, the corresponding bond angle of N_{Im}-Co-C is decreasing to an extent where the radical escape is not occurring in the N_{Im}-Co-C straight line. A similar trend was observed for the F708A-MetH. Therefore, introducing mutation to F708 residue (F708A) does not influence the trajectory of the radical escape; rather, it modulates the energetic of the excited states. This is evident based on constructed S_0 and S_1 PES from QM/MM calculations. In fact, in F08A-MetH rate of photolysis increases by a factor of 62 as compared to WT-MetH.[96] This finding corresponds well with our calculated results. Based

on the combined QM/MM calculation, we can suggest that the cap domain mutation influences the two main factors, namely the *rate of geminate recombination* and the *formation of RP*, which affect the photolysis of Co-C bond in MeCbl-bound MetH.
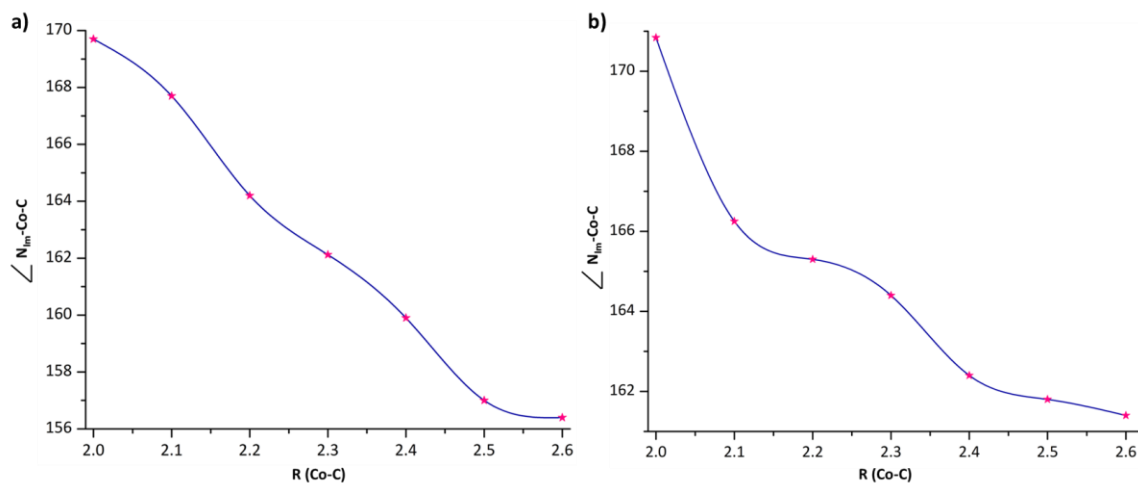
Figure 3.9. The changes of N_{Im}-Co-C bond angles along with the Co-C bond length elongation for **(a)** WT-MetH and **(b)** F708A-MetH. QM/MM calculations were performed to elongate the Co-C bond length from 2.00 A to 2.60 A with a step size of 0.1 A. At each point, the bond angle of N_{Im}-Co-C was determined and plotted as a function of Co-C bond length to show the escape of the CH_3 radical pair along the designated line.

The rate of geminate recombination for both WT-MetH and F708A-MetH has been computationally estimated by considering the radiative decay from the S_1 LF state to the S_0 state. The Einstein coefficient A, also known as deactivation rate constant (k_{fl}), has been used to calculate the rate of geminate recombination.[174-175] The deactivation rate constant (k_{fl}) can be expressed as $k_{fl} = A = \frac{2\pi v^2 e^2}{c^3 \varepsilon_0 m_e} * f$, where v is the emission wave number, f is the oscillator strength, m_e is the mass of an electron, c is the speed of light, and ε_0 is the vacuum dielectric constant. Our calculation suggests that the rate of geminate recombination for WT-MetH is almost 20% higher than the F708A-MetH. The higher deactivation rate constant for WT-MetH indicates a greater extent of geminate recombination, which in turn

decreases the ultimate rate of photolysis. Hence, the mutation in the cap domain increases the rate of photolysis in F708-MetH by impeding the rate of geminate recombination. The protein environment could also affect the photolysis by altering the primary photochemical yield for RP. In F708A-MetH, the protein environment is altering the photochemical yield of RP by reducing the energy difference between MLCT (I, S_{1min}) and LF minima (IIIB, S_{1min}) (Figure 3.7b) and lowering the energy barrier for photoreaction (Figure 3.6b). In WT-MetH, the energy difference between MLCT (I, S_{1min}) and LF minima (IIIB, S_{1min}) (Figure 4) is almost three times higher than the energy difference of F708A-MetH (Figure 3.7). This indicates that the mutation on F708 engendered a stabilization in the LF state, which affects the photoactivation of the Co-C bond.

This led us to propose that the photoactivation and the low-lying excited states can be modulated by introducing a mutation in the cap domain of the Cbl-binding module of MetH. This study has further implications for other Cbl-dependent enzymes. Specifically, for AdoCbl-dependent EAL, it has been shown that a glutamate residue (E287) is in van der Waals contact with the Ado group of AdoCbl cofactor, and it has substantially impacted the low-lying excited states.[176] As a result, mutation of E287 with a more hydrophobic residue results in a 15 nm blue shift of the absorption spectrum.[177] However, the detailed mechanism of this change in the absorption spectrum has not been explicitly reported yet. The present study has shown that the potential effect of the mutation is to influence the photoactivation of the Co-C bond by modulating the energetics of MLCT and LF state of S_1 PES. This theoretical insight can also be helpful to investigate further the effect of the mutation on the photolytic properties of vitamin B_{12}-dependent enzymes.

3.4. Summary and Conclusion

In this study, we have provided a theoretical analysis of how the mutation in the cap domain of MetH controls the photoreactivity of the protein-bound MeCbl cofactor. The photochemical data of WT-MetH and F708A-MetH have been compared to understand the effect of the mutation on the photoactivation of the Co-C bond. The photodissociation mechanism for the Co-C bond can be explained by analyzing the low-lying excited state. The S_1 PES for both WT-MetH and F708A-MetH contains two minim regions, namely MLCT and LF. Based on the energetics of computed S_1 PES, two distinct mechanistic pathways (Path B and Path A) have been identified to connect the MLCT and LF electronic state for describing the photoactivation of the Co-C bond. Path B, which is associated with initial detachment of Co-N_{Im} bond followed by subsequent displacement of Co-C bond, has been identified as an energetically favorable pathway of photodissociation for both WT-MetH and F708A-MetH. In contrast, Path A will remain inactive for photolysis. However, for base-on MeCbl in solution, both Path A and Path B are active for the photolysis of the Co-C bond.

Hybrid QM/MM calculations revealed that the mutation F708A has a significant impact on the topology of S_1 PES as well as on the rate of photolysis. It has been proposed that the mutation F708A can affect the photolysis of enzyme-bound MeCbl in three possible ways: (1) altering the photochemical yield of Co(II)/CH_3 RP by decreasing the energy difference between MLCT and LF minima. The energy difference between MLCT and LF minima for WT-MetH is almost three times higher than its mutant counterpart (F708-MetH). (2) The mutation of F708A also decreases the energy barrier for photoreaction. (3) The mutation decreases the rate of geminate recombination. For F708A-MetH, the deactivation rate constant is almost 20% lower than WT-MetH, which indicates

a higher rate of photolysis for F708A-MetH. These observations also complement the experimental studies, which reported a significant rate enhancement of photolysis by ~ 62-fold for F708A-MetH. Considering all of these, we can clearly conclude that mutation in the cap domain of the Cbl-binding module of MetH can influence the photoactivation of the Co-C bond in enzyme-bound MeCbl by altering the rate of photolysis.

CHAPTER IV

PHOTOACTIVATION OF THE Co-C BOND IN THE PRESENCE OF OXYGEN: UNRAVELING THE PHOTOREACTION MECHANISM IN THE AEROBIC PHOTOLYSIS OF METHYLCOBALAMIN

4.1 Introduction

The photolytic properties of Cbls have been thoroughly investigated both experimentally and computationally, both in solution as well as inside enzymes.[92, 94-95, 125, 172, 178-187] These investigations have concluded that the photo-reactivity of Cbls is influenced by the nature of axial ligands and the cofactor's environment. For instance, while the biologically active forms of Cbls with alkyl axial ligands, MeCbl and AdoCbl, as well as their analogs, are exemplified by ethylcobalamin (EtCbl) or propylcobalamin (PropCbl) are considered to be photolytically active; in contrast, the non-alkyl Cbls are photostable.[98, 157, 188-190] In addition, the cofactor's environment also influences the photoactivation of the Co-C bond in both MeCbl and AdoCbl. While the enzymatic environment prevents the photolysis of MeCbl, it affects the photoactivation of the Co-C bond in AdoCbl-dependent enzymes.[96, 99, 162, 164-165, 179, 191] As concluded in Chapters 2 and 3 that the photolysis of MeCbl involves two primary intermediates, namely MLCT and ligand LF excited electronic states. Based on the energetics of these two electronic states, two possible pathways of the photodissociation were identified, namely Path A and Path B (Figure 2.6b). In Path A and Path B, the photoreaction is initiated from the MLCT state (MLCT minimum, denoted $I(S_{1min})$ in Figure 2.6b) of the S_1 PES. Then, it proceeds to the LF region by crossing the MECP energy barrier (MECP = minimum energy crossing point)

associated with the intersection of MLCT/LF PESs. However, the intermediates involved in both routes are different. While the photoreaction in Path A initially proceeds along the Co-C bond followed by the displacement of the Co-N_{Im} bond, the photodissociation along Path B involves the initial elongation of the Co-N_{Im} bond (or detachment of axial base) followed by the labilization of the Co-C bond (Figure 2.6b). After the system reaches the LF state, two processes are possible: deactivation to the ground state and the photodissociation of the Co-C through the formation of Co(II)/CH_3 RP (Scheme 4.1). Alternatively, once the RP is formed, it can either diffuse through the solvent cage or can be de-excited to the ground state by changing the electronic configuration from $(d_{yz})^1(d_z^2)^2$ to $(d_{yz})^2(d_z^2)^1$ associated with Co(II).

Apart from the nature of axial ligands and cofactor's environment, the photochemical and photophysical properties of Cbls can also be modulated in the presence of molecular oxygen, i.e., in aerobic conditions.[94, 181, 192-196] Whereas many experimental and computational investigations have been carried out to explore the inherent mechanism of the anaerobic photolysis of Cbls, the mechanism of the photodissociation of the Co-C bond in the presence of oxygen is still not well explored. Previous studies have suggested that the key species in the aerobic photolysis of Cbls involves intermediate with the Cbl-OO-R linkage.[195-196] The DFT and TD-DFT calculations have demonstrated that light is only needed to activate the Co-C bond via electronic excitation towards the formation of the Co/CH_3 radical pair (RP).[197] Co(II) de-excitation occurs from this configuration by transferring the electron from Co d_z^2 to d_{yz} orbital. Such change in electronic configuration, namely from $(d_{yz})^1(d_z^2)^2$ to $(d_{yz})^2(d_z^2)^1$, can facilitate the reaction with triplet oxygen. It has been further proposed that the insertion of O_2 should occur in the ground state; however,

the detailed mechanistic pathway has not been fully explored yet. Herein we provide a more in-depth insight into the aerobic photolysis of MeCbl, emphasizing the specific steps involved in the insertion of O_2 in the elongated Co-C bond.
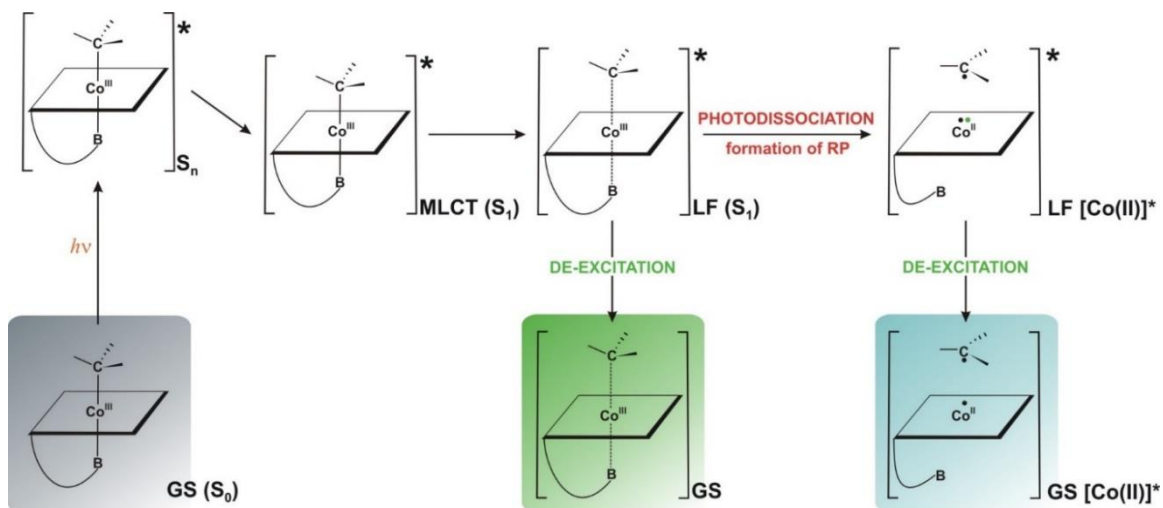
Scheme 4.1 General scheme of the mechanism of MeCbl photolysis without the presence of oxygen.

4.2. Model system and computational details

The structural model of MeCbl was extracted from high-resolution X-ray crystallographic data available for MeCbl.[23] The initial structure of MeCbl was truncated and simplified to reduce computational cost. All the side chains of the corrin macrocycle and the nucleotide loop were replaced with hydrogen atoms. The nucleotide loop contains a phosphate group (PO_4^-); thus, its removal results in a positive charge in the truncated model. Next, the DBI group, which is axially ligated through the lower axial face of the corrin ring, was replaced with imidazole (Im). The size of the truncated MeCbl has 54 atoms, and such a structural model will be denoted as $^+$ throughout our study. Based on the truncated structure, a model complex of the reaction product with molecular oxygen was

73

used in the calculations. These are denoted as $(Im–[Co^{III}(corrin)]-OO-CH_3)^+$ or $([Co^{III}(corrin)]-OO-CH_3)^+$ for base-on and base-off forms, respectively (Figure 4.1).
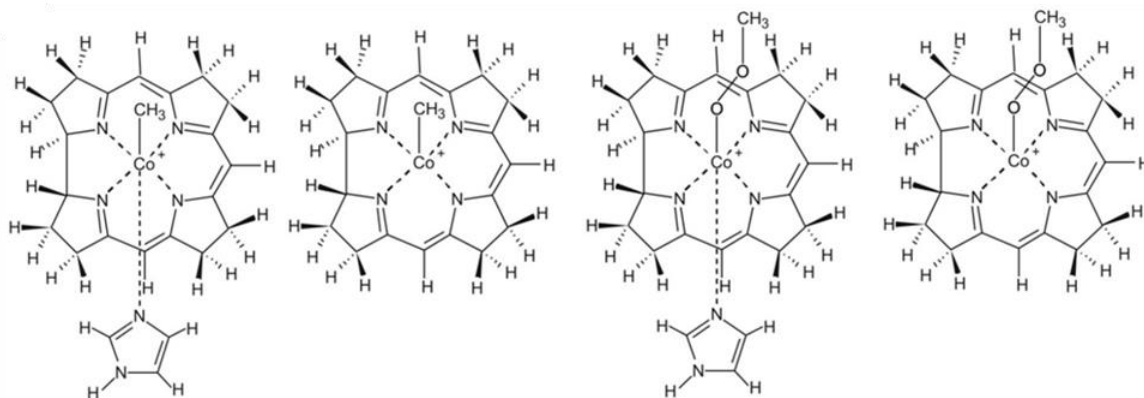
Figure 4.1. Structures of base-on and base-off forms of the model complexes employed in the calculations: $(Im–[Co^{III}(corrin)]–CH_3)^+$, $([Co^{III}(corrin)]–CH_3)^+$, $(Im–[Co^{III}(corrin)]–O–O–CH_3)^+$ and $([Co^{III}(corrin)]–OO–CH_3)^+$.

In accordance with previous studies, all calculations were carried out using the DFT[198] and TD-DFT[133-134] framework using nonhybrid (GGA) BP86 exchange-correlation functional.[146-147] In all calculations performed in this chapter, the TZVP basis set was used for H atoms and TZVPP[199] for Co, C, N, and O atoms, as implemented in the TURBOMOLE [200-201] and Gaussian 09 suite of programs.[145] In addition, to consider the effect of the environment on the electronic structure of the ground and the excited state as well as on the geometries, Polarizable Continuum Model (PCM),[202] and Conductor-like Screening Model (COSMO)[203] implicit solvent models with water as a solvent was employed. The DFT and TD-DFT level of the theory with BP86 functional has been previously successfully applied for investigating the ground and excited-state properties of Cbls.[122, 128-130, 137, 158, 173, 204]

4.3. Results and discussion

4.3.1 Photoreaction of MeCbl in the presence of the molecular oxygen

As outlined in the Introduction, the complete mechanistic details of the insertion of O_2 in the Co-C bond remain largely unknown. However, the previously reported[197] photochemical data strongly points out that the role of light is only to activate the Co-C bond of the MeCbl cofactor by inducing its partial or complete cleavage from the LF excited state. This LF electronic state then leads to the formation of Co(II)/CH$_3$ RP. It has also been suggested that after the formation of the photoinduced RP, the molecular oxygen intercepts the methyl radical and forms the methyl peroxy radical ($^•$OOCH$_3$ radical), which then reacts with Co(II).[94, 196] However, a reaction of Co(II) with $^•$OO-CH$_3$ radical in the excited state seems not feasible due to the changes in the electronic configuration of ([(Co^{II}(corrin)]$^{•+}$) sub-system. The electronic configuration of ([Co^{II}(corrin)]$^{•+}$) moiety in the LF excited state is unsuitable for forming a bond between the Co(II) center and the $^•$OO-CH$_3$ radical. This is because the electronic excitation to the LF state involves the transfer of a delocalized electron of corrin macrocycle to Co d_z^2 orbital, and this doubly occupied d_z^2 orbital of Co makes it unlikely to form a stable bond between the $^•$OO-CH$_3$ radical and ([Co^{II}(corrin)]$^{•+}$) fragment in the LF state. Thus, based on DFT/TD-DFT calculations, it was concluded that the insertion of oxygen should occur in the ground state regardless of possible mechanistic details. So, the most pertinent question here is, how does the insertion of oxygen occur with the partially or fully dissociated Co-C bond during the aerobic photolysis of MeCbl.

Based on existing photochemical data, four possible mechanistic pathways for the insertion of O_2 in the photolytically activated Co-C bond can be envisioned as it is depicted in Scheme 4.2. The first two mechanistic pathways (Scheme 4.2, paths a, b) can be

associated with a partially cleaved Co-C bond, where the de-excitation to the ground state by transferring an electron from d_z^2 orbital to metal d_{yz} orbital takes place prior to reaction with molecular oxygen. So, after the de-excitation to the ground state (Scheme 4.2, I), two different possible scenarios can be described as follows: (a) the oxygen first combine with Co(II) and the Co-OO subsequently reacts with the CH_3 or, (b) the triplet oxygen first reacts with the activated CH_3, and then the resulting $OO-CH_3$ radical forms the bond with the Co(II). Based on the present calculation, it has been found that the energetics difference
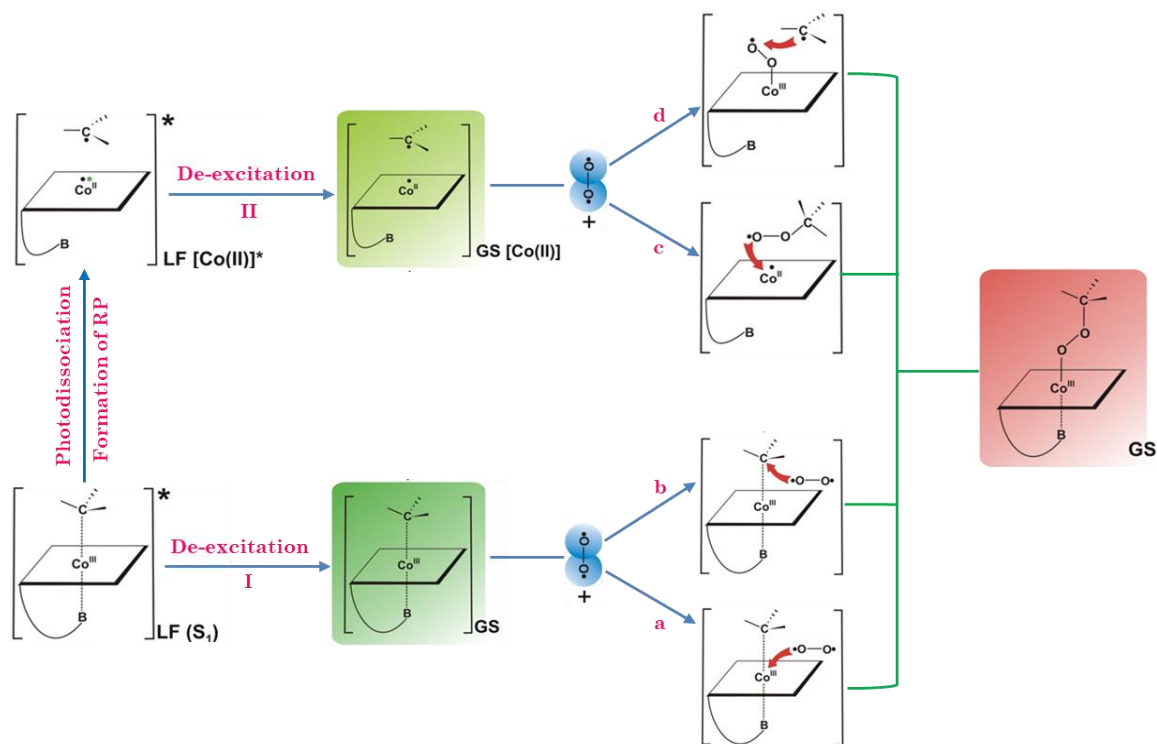
Scheme 4.2. General scheme of the photolysis of MeCbl in aerobic condition showing different pathways of oxygen insertion.

between the substrate ($[Im-[Co^{III}(corrin)]-Me] + O_2$) and associated intermediates in Path, a and b are 19 kcal/mol and 5 kcal/mol, respectively. Thus, the partial product $[Im+[Co^{II}(corrin)]^+]---OO-CH_3$) generating in path b is energetically more feasible than path a (Figure A6). This indicates that path b is the energetically more favorable route for

76

the insertion of oxygen in the Co-C bond. In addition, we can also have a dissociative process (Scheme 4.2, Paths c, and d), where after the formation of RP from the LF excited state, the RP is first deactivated to the ground state and then react with the molecular oxygen. The triplet oxygen can either be coupled with the doublet $CH_3^{\bullet}$ to generate $^{\bullet}OO$-CH_3 radical (Scheme 4.2, path c), or it can combine with the de-excited Co(II) center followed by the formation of Co-OOCH$_3$ intermediate (Scheme 4.2, Path d). However, existing photochemical and computational studies indicate that a dissociative reaction pathway seems less plausible for a few reasons. First, the high quantum yield (QY) of cage escape and the high diffusive mobility of the CH_3 radical. It should be noted that the photolysis of MeCbl excitation results in the rapid formation of a radical pair with a yield (ca. 15% in water). The photolysis yield of MeCbl may not seem a relatively low photolysis yield. However, it is worth mentioning that the methyl radical behaves somewhat atypically compared to the other alkyl products of photolysis. It has been reported that this is due to the high diffusive mobility of the CH_3 radical.[123, 205] The rate constant for the diffusive escape of the methyl radical is much larger than that for any other alkyl radicals, which can be anticipated based on hydrodynamic arguments and the size of the radical. An ultrafast cage escape (<100 ps) was observed for the methyl radical where the radical pair is produced through excitation to a directly dissociative electronic state.[205] Moreover, simultaneous competition between cage escape and geminate recombination accounts for the ultimate photochemical yield for producing solvent-separated radical pairs. Nevertheless, it is important to note that the direct photodissociation of methyl radical may accelerate the cage escape by producing radical pairs with excess kinetic energy in the recoil. Therefore, considering the competition between the rate of recombination and the

rate of escape from the solvent cage and high QY of cage escape, the radical-based dissociative mechanism seems less likely in the case of aerobic photolysis of MeCbl. Second, from both the thermodynamic and energetic points of view, a concerted pathway is more favorable than a dissociated process. Moreover, the dynamics of Cbl photolysis are dominated by the competition between geminate recombination and diffusive separation of the radical pair. While the rate of radical recombination is slightly dependent on the nature of the radical and the solvent, the competitive process of cage escape is more complicated and depends on many factors, such as the electronic and geometric structure of the radical, temperature, viscosity, and generally, the thermodynamic and hydrodynamic properties of the photoreaction.[205]

In the case of aerobic photolysis of MeCbl, the "cage" effect may play an important role in the mechanism of oxygen insertion into the photolyzing Co-C bond. The cage will act as a reactor at the molecular level by facilitating to keep the reactants close to each other. The solvent cage will be expanded as the Co-C distance increases, and at about 2.8 Å, the dissociating methyl group acquires a radical character. In this case, an attack of oxygen on the CH_3 radical from the opposite side of the dissociating Co-C bond in the direction from the solvent continuum to the edge of the cage is very likely. Efficient C-O bond formation requires appropriate spatial orientation between the CH_3 radical and O_2. The farther the oxygen atom is from the axis of the dissociating Co-CH_3 bond, the greater spatial reorientation of the CH_3 group must take place. This is somewhat more possible with longer Co-CH_3 distances. When the oxygen atom is near or on the axis of the dissociating Co-C bond, the reorientation of the methyl group is not required or is very small. However, after the formation of the H_3C-OO bond, spatial reorientation of the

78

resulting product is necessary to approach the radical oxygen to the deactivated Co(II) complex. Such spatial reorientations, especially in the case of the resulting H_3C-OO intermediate, may introduce some energy barrier to the formation of the Co-OO-CH$_3$. Moreover, it is challenging to determine finally whether the formation of a C-O bond at the border of the cage and the solvent continuum favors the formation of the Co-OO-CH$_3$ bond or it facilitates the closure of the solvent cage around the resulting H_3COO and Co(II) radicals. In this case, the influence of the "electronic" factor seems to be insignificant, while the thermodynamic and hydrodynamic properties will play a greater role here, as in the case of the escape of the methyl radical from the solvent cage. Similarly, we believe that due to the significant QY of the formation of the Co(II)/CH$_3$ radical pair compared to other Cbl alkyl derivatives, some of the generated free methyl radicals are attached to oxygen. Then the intermediate product is re-diffused into the vicinity of the Co(II) system and forms a Co(II)-OO-CH$_3$ bond. It should be noted that formally from an electronic point of view, the mechanistic aspect of a concerted pathway and the dissociated process are very similar. Rather, the main difference lies in the dynamics of the diffusion processes, which will play a fundamental role in the case of the dissociative process. As the work focuses mainly on the electronic processes of the mechanism under study, the issues of dynamics of possible diffusion and re-diffusion processes are not discussed in the paper. Thus, it should be further pointed out that the exactness of these calculations should be taken with caution, and the possibility of a complete dissociative process, where the photoinduced RP separates in solution and reacts with molecular oxygen, could not be completely ruled out.

Therefore, based on existing photochemical data and computations, we can propose that a process involving elongated Co---C bond, specifically Path b in Scheme 4.2, is the

most feasible pathway for the insertion of molecular oxygen. Hence, the following sections will discuss specific steps associated with the formation of the OO-CH3 bond followed by the reaction with the de-excited Co(II) center.

4.3.2 Co-CH₃ bond dissociation and the formation of OO-CH₃ bond: a one-dimensional model

The chemical reactions involving transition metal are often spin-forbidden. The photoreaction of MeCbl in the presence of oxygen is also a spin-forbidden reaction, which displays the changes in the total spin of the system. Thus, to investigate the mechanism of oxygen insertion in the photolysis of MeCbl, three different electronic states were considered for different possible spin couplings, namely the triplet state (T) and two singlet states with broken symmetry wave function (S(BS1), S(BS2)). The distribution of spin in the reaction system schematically can be described as follows:

$\uparrow$*Co --- C*$\downarrow$$\cdots$$\uparrow$*O-O*$\uparrow$ *for T,* $\downarrow$*Co --- C*$\downarrow$$\cdots$$\uparrow$*O-O*$\uparrow$ *or* $\uparrow$*Co* $\cdots$ *C*$\uparrow$$\cdots$$\downarrow$*O-O*$\downarrow$ *for S(BS1),*

or $\uparrow$*Co --- C*$\downarrow$$\cdots$$\uparrow$*O-O*$\downarrow$ *for S(BS2).*
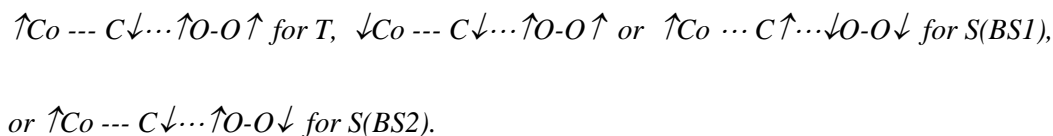
Previously based on a DFT/TD-DFT calculation, it has been suggested that in the aerobic photolysis of MeCbl, the photoreaction initiates through the activation of the Co-C bond and is followed by the interaction between the activated Co-C bond and the triplet oxygen.[197] The insertion of the oxygen with the elongated Co---C bond reportedly takes place at the ground state. Therefore, it is relevant to see how the formation of the C-O bond takes place during the dissociation of the Co-C bond. Toward this, the PECs along the reaction path (Im-[Co^{III}(corrin)]-CH$_3$)$^+$ + O$_2$ were computed for both base-on and base-off forms of MeCbl, based on a simple model in which the oxygen molecule was kept in an axial position at a fixed distance of 5.1 Å from the Co atom (Figure 4.2 and Figure A7).
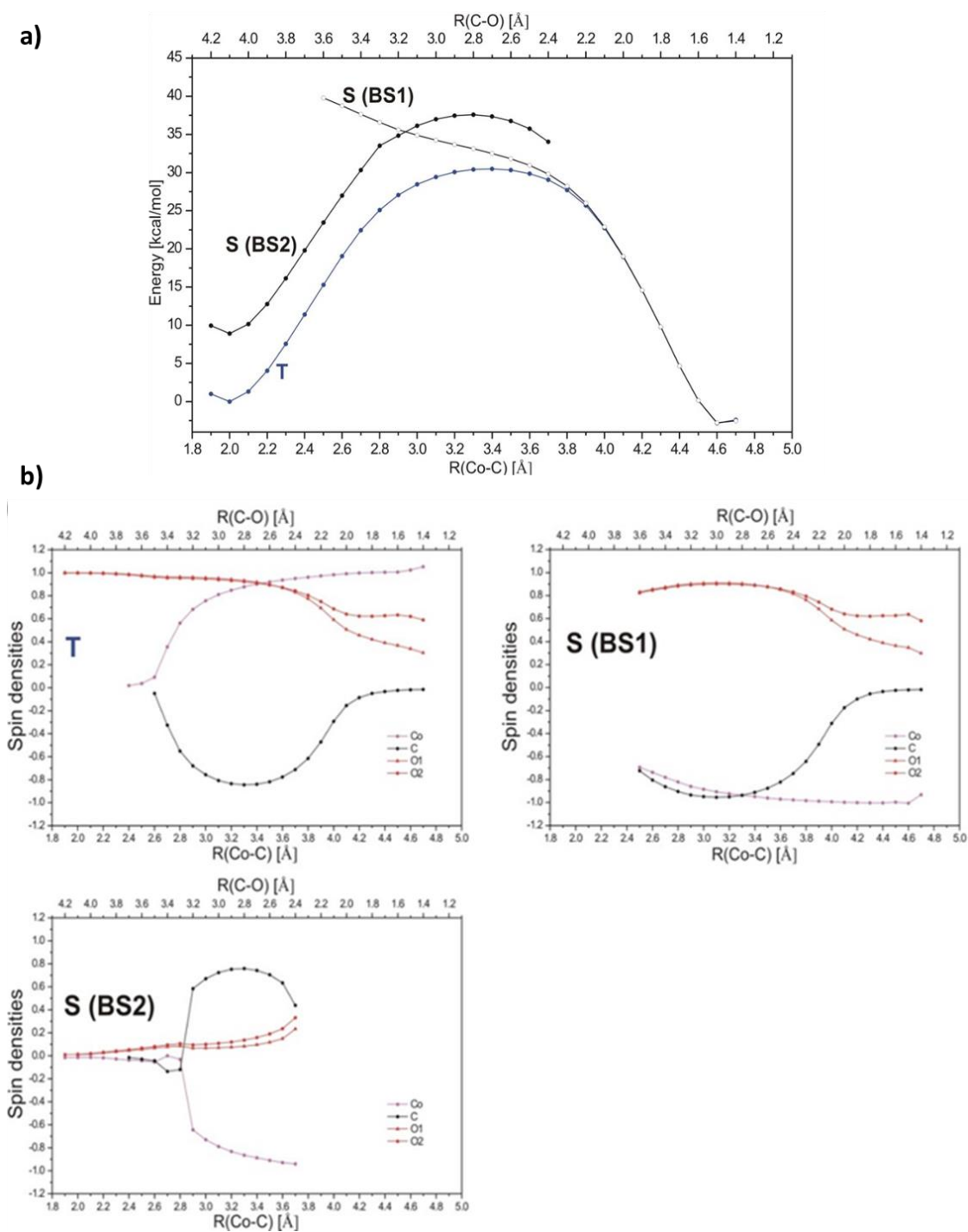
Figure 4.2. (a) Potential energy curves along reaction path for (Im-[Co^{III}(corrin)]- CH$_3$)$^+$ + O$_2$ → (Im-[Co^{II}(corrin)])$^{+\bullet}$ + $^\bullet$OO-CH$_3$ model reaction. Based on the UDFT/BP86 level of theory, the three electronic states were considered, namely the triplet state (T) and two singlet states with broken symmetry wave function (S(BS1), S(BS2)). The distribution of spin in the reaction system schematically can be presented as follows: ↑Co ⋯ C↓⋯↑O-O↑ for T, ↓Co ⋯ C↓⋯↑O-O↑ or ↑Co ⋯ C↑⋯↓O-O↓ for S(BS1), and ↑Co ⋯ C↓⋯↑O-O↓ for S(BS2). (b) Mülliken spin densities on cobalt, carbon, and oxygen atoms, directly involved in the reaction.

81

To compute the energy at each point of the PEC, the Co-C and C-O bond were systematically elongated and shortened, respectively, using a step size of 0.05 Å. A noticeable difference can be seen between the behavior of the triplet and singlet electronic state. For both T and S(BS2) electronic states, the spin density profile of Co and C around a Co-C bond distance of ~3.4 Å indicates a homolytic cleavage of the Co-C bond (Figure 4.2). It can also be seen from Figures 4.2 and Figure A7 that the spin polarization started developing at a Co-C distance greater than ~2.7 Å. As depicted in Figures 4.2 and A7, the energy proximity between the PECs associated with S(BS1) and T state can be observed at Co-C and C-O bond distances close to 3.7 Å and 2.4 Å, respectively. This indicates that during the formation of the C-O bond (i.e., formation of OO-CH$_3$ species), the S(BS1) and T states are practically near-degenerate over a wide range of C-O distances between 2.4-1.6 Å (Figure 4.2 and Figure A7). This T/S(BS1) crossing point at a C-O distance around 2.4-2.5 Å corresponds to a structure having a CH$_3$-O$_2$ bond. For the C-O distance around 2.4-2.3 Å, the spin densities on C and O atoms are almost zero, which indicates the formation of the C-O bond and OO-CH$_3$ species. After crossing the energy barrier associated with the formation of the C-O bond, the energies of the T and S(BS1) states decrease rapidly. This implies that the reaction of the methyl group with the molecular oxygen followed by the formation of the OO-CH$_3$ species stabilizes the system. Similar energetic behavior also has been observed in the case of base-off conformation.

4.3.3 Co-CH$_3$ bond dissociation and the formation of OO-CH$_3$ bond: a two-dimensional model

To further explore the mechanism of the oxygen insertion in the activated Co-C bond, a two-dimensional relaxed PES was constructed as a function of Co-C and C-O

bonds (Figure 4.3). As the photoinduced dissociation of the Co-C bond formally occurs from the LF excited state, where the structure of Cbl has either partially or entirely detached axial base, the PESs for the T and S(BS1) states were constructed considering the base-off form. To compute the PESs, the Co-C and C-O distances were systematically varied, using a step size of 0.05 Å in a range from 1.90 - 4.00 Å and 1.40 - 4.00 Å, respectively.
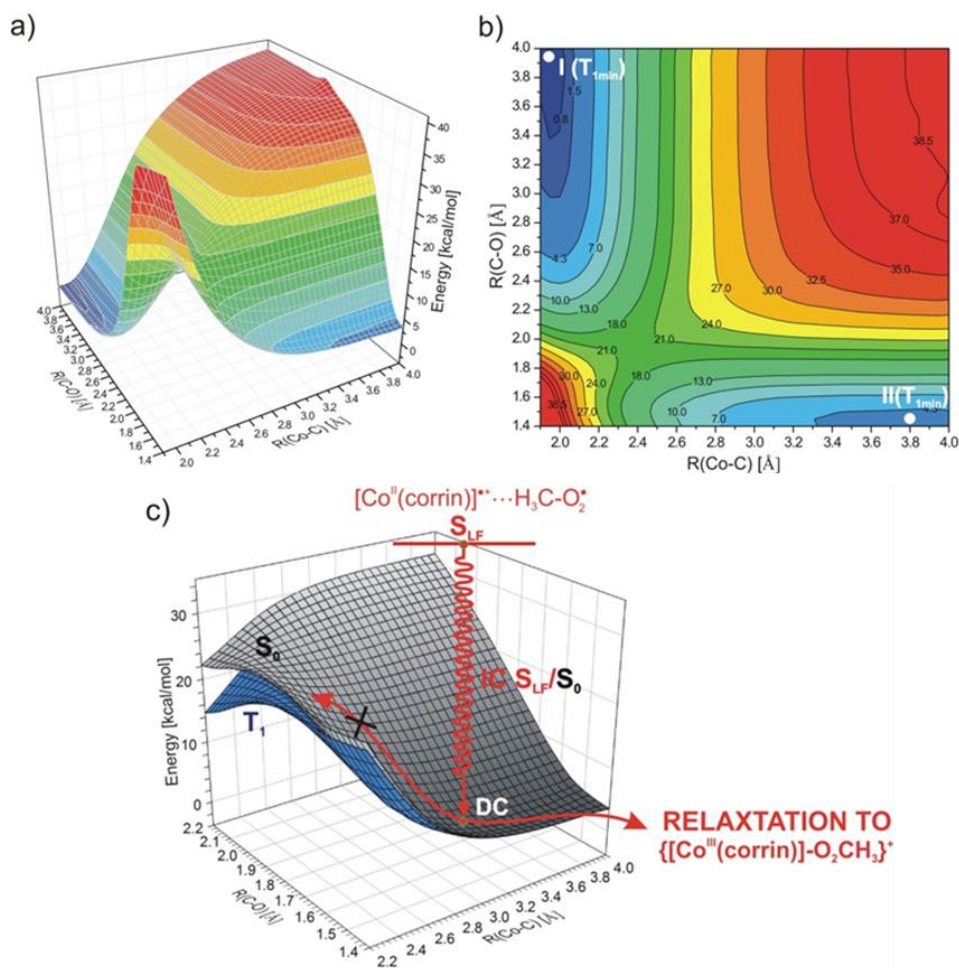
Figure 4.3 PES (a) together with its vertical projection (b) plotted as a function of Co-C and C-O distances for the triplet electronic configuration (T_1) of the reacting system in ($[Co^{III}(corrin)]$-Me)$^+$ + $O_2 \rightarrow$ ($[Co^{II}(corrin)]$)$^{+\bullet}$ + $^\bullet$O-O-CH$_3$ model reaction. (c) Fragment of PES of triplet state for shorter C-O distances and PES for S(BS1) and scheme of the deactivation process from the LF excited electronic state.

Figures 4.3a and 4.3b depict the PES of the triplet electronic state of MeCbl in aerobic conditions. The topology of the PES (Figures 4.3a and 4.3b) reveals two energy minima, namely I (T_{1min}) and II (T_{1min}). While the I (T_{1min}) is associated with the shorter Co-C and longer C-O bond distance, the II (T_{1min}) at a longer Co-C and shorter C-O bond length, corresponds to the product ($[Co^{II}(corrin)]^+$)---OO-CH$_3$, with the electronic configuration ↑Co ---↑O-OCH$_3$ (Figure A8). At a longer Co-C bond distance (about 3.8-4.0 Å), the S$_1$ LF state and S$_0$ states come in close enough proximity for internal conversion (IC) (Figure 4.4). The computed energy difference between the S$_1$ LF state and S$_0$ states at a longer Co-C bond distance is less than 8 kcal/mol (Figure 4.4), which is small enough for [Co^{II}(corrin)] to undergo nonradiative deactivation. Thus, the topology of the PESs near the II (T_{1min}) corresponds to the region where the deactivation of the excited state and formation of a bond between methyl and oxygen molecules occurs (Figure 4.3c). Therefore, from the photochemical point of view, the aforementioned part is the most interesting portion of PESs, which corresponds to the shorter C-O distances and longer Co-C bond distances. After reaching the LF electronic state, the photolysis of the Co-C bond prompts the formation of the Co(II)/CH$_3$ RP. In such a scenario, the reaction of activated CH$_3$ with the molecular oxygen present nearby is entirely plausible. Therefore, formally, the first stage of aerobic photoreaction is the activation of the Co-C bond and the formation of the LF state (through the elongation of axial bonds) on the S$_1$ PES. The second step is the insertion of oxygen in the activated Co-C bond and the formation of the (Im-[Co^{III}(corrin)]-OO-CH$_3$)$^+$ complex.
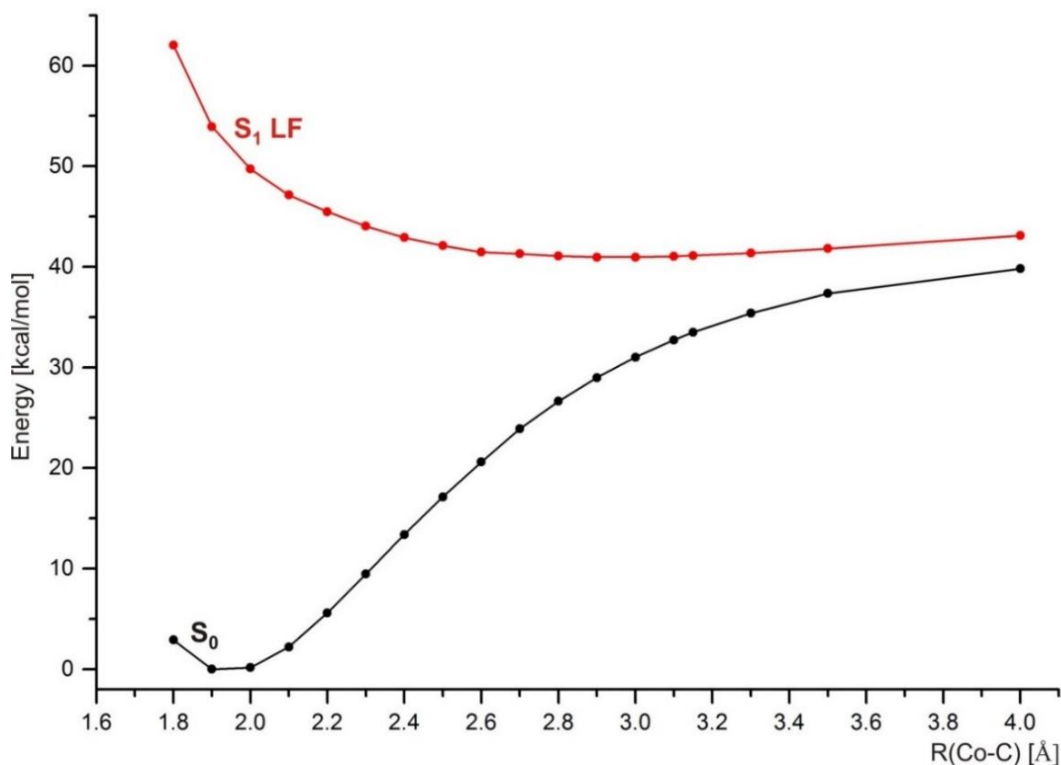
Figure 4.4. Potential energy curves of S_0 ground state and S_1 singlet state for ([Co^{III}(corrin)]–CH$_3$)$^+$ model complex as function Co-C axial bond length, obtained on the basis of calculation results using the MS CAS/CASPT2 method. The CAS active space used in this calculation contains occupied d orbitals of cobalt: $3d_{xz}$, $3d_{yz}$, $3d_{x2-y2}$, $3d_{xy}$ + n, a pair of sigma, sigma * orbitals of Co-C bond, and five unoccupied orbitals: $3d_{xy}$-n, $4d_{xz}$, $4d_{yz}$, $4d_{x2-y2}$, $4d_z^2$.

The formation of the Co---O bond has been explored by computing the S_0 and S_1 PESs for (Im-[Co^{III}(corrin)]-OO-CH$_3$)$^+$ complex as a function of axial bond lengths (Figure 4.5). The S_1 PES for (Im-[Co^{III}(corrin)]-OO-CH$_3$)$^+$ complex was constructed at TD-DFT/BP86 level of theory by calculating the vertical excitation for each optimized geometry of ground state S_0 PES. The topology of the S_1 PES for (Im-[Co^{III}(corrin)]-OO-CH$_3$)$^+$ complex depicts two energy minima regions (Figure 4.5c). These are denoted as I (S_{1min}) and II (S_{1min}) in Figure 4.5c.
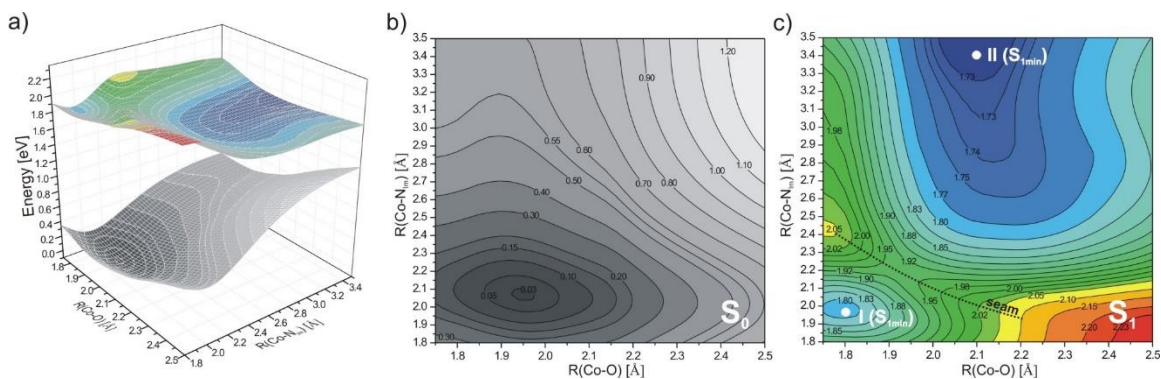
Figure 4.5. (a) Potential energy surfaces of ground state S_0 and first, vertical singlet excited state S_1 for (Im–[Co^{III}(corrin)]–O–O–CH$_3$)$^+$ model complex as a function of axial bond lengths, together with the vertical projection of PES for S_0 (b) and S_1 (c).

The Kohn-Sham (KS) orbitals involved in the electronic transition of these two minima are shown in Figure 6. The I (S_{1min}) arises from the p_o - $d_{yz} \rightarrow \pi^*$ type electronic excitation (Figure 4.6). While the II (S_1 min) minima region has an LF character which can be characterized as π + d_{yz}-$p_o \rightarrow \sigma^*(d_z^2)$+ p_o type electronic transition (Figure 4.6). The energetics of the II (S_1 min) indicates whether the ([Co^{II}(corrin)]-OO-CH$_3$)$^+$is photolitically stable. The shallow energy minima associated with this region and the ambient topology of II (S_1 min) minimum on S_1 PES (Figure 4.5c) suggests that an easy photodissociation of ([Co^{II}(corrin)]-OO-CH$_3$)$^+$ would be possible. This indicates that the formation of a stable Co-O bond (i.e., the formation of the ([Co^{II}(corrin)]-OO-CH$_3$)$^+$ occurs on the ground state. Moreover, the reaction of the OO-CH$_3$ group with the Co(II) in the excited state is also not feasible because, in the LF state, the Co ion has a doubly occupied d_z^2 orbital, which makes it unlikely to form a stable Co-O bond. Therefore, after the formation of LF state, three processes can occur, (i) de-excitation of [Co^{II}(corrin)] species from the LF region (ii) the reaction of CH$_3$ with molecular oxygen, (iii) the formation of (Im---[Co^{III}(corrin)]-OO-CH$_3$)$^+$ via the recombination of OO-CH$_3$ with the de-excited [Co^{II}(corrin)] fragment.
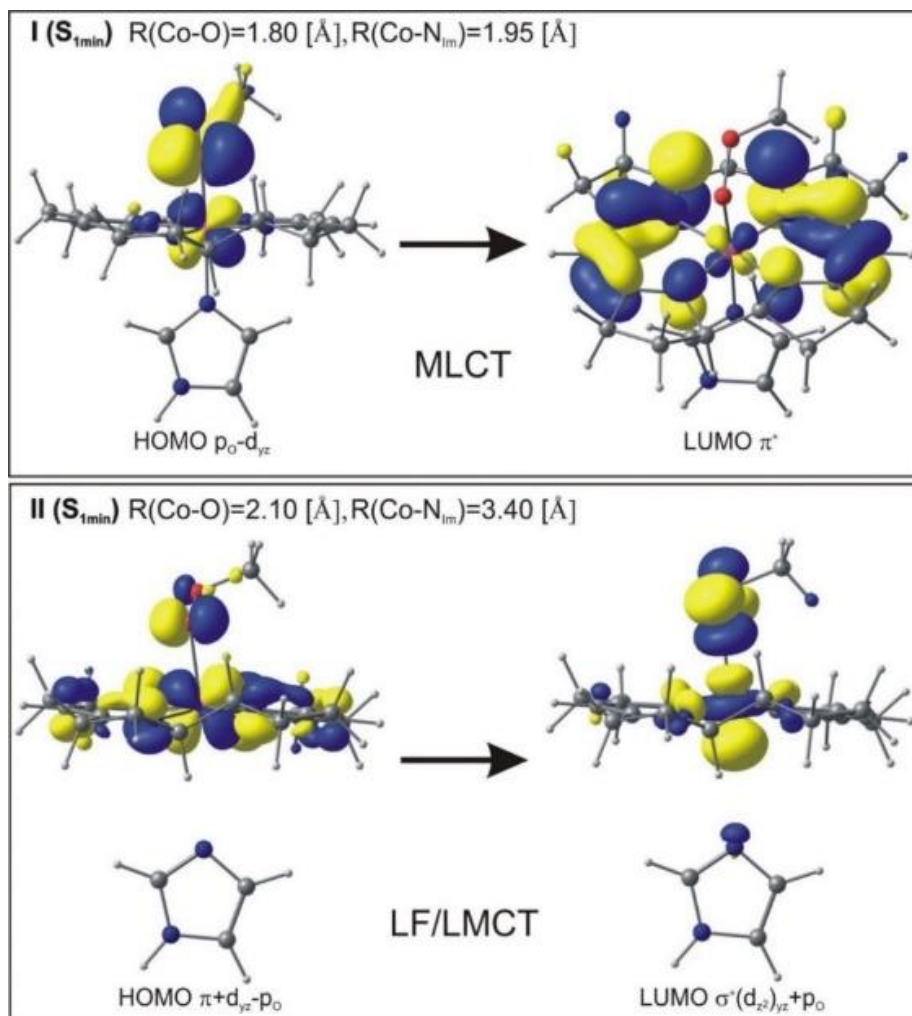
Figure 4.6. Kohn - Sham orbitals are involved in electronic excitation at two characteristic points on PES, I(S_{1min}) and II(S_{1min}), shown in Figure 4.5.

4.4 Conclusion: Mechanism of the photoreaction in the aerobic photolysis of methylcobalamin

The purpose of the present computational study was to unravel the mechanism of oxygen insertion in the aerobic photolysis of MeCbl. The mechanism of the photoreaction can be understood by analyzing the PEC and S_0 PES of $(Im-[Co^{III}(corrin)]-CH_3)^+ + O_2 \rightarrow (Im-[Co^{II}(corrin)])^{+\bullet} + {}^\bullet OO-CH_3$ reaction, as well as the S_1 PES for $(Im-[Co^{III}(corrin)]-OO-CH_3)^+$. A full schematic diagram of the mechanism of aerobic photolysis has been depicted

in Figure 4.7. Upon photoexcitation, the $(Im-[Co^{III}(corrin)]-CH_3^+)^+ + O_2$ system leads to the formation of MLCT electronic state and then goes to the LF electronic state (Step Ia, Figure 4.7). Once the photoreaction reaches the LF excited state, three processes can occur. First, the formation of OO-CH$_3$ through the reaction of CH$_3$ with molecular oxygen. Second, the de-activation of $(Im\cdots[Co^{II}(corrin)]\cdots CH_3)^+$ sub-system from the LF electronic state through changing the electronic configuration from $(d_{yz})^1(d_z^2)^2$ to $(d_{yz})^2(d_z^2)^1$. Finally, the formation of the deactivation complex (DC) complex via the recombination of OO-CH$_3$ species with the de-excited $[Co^{II}(corrin)]$ system.
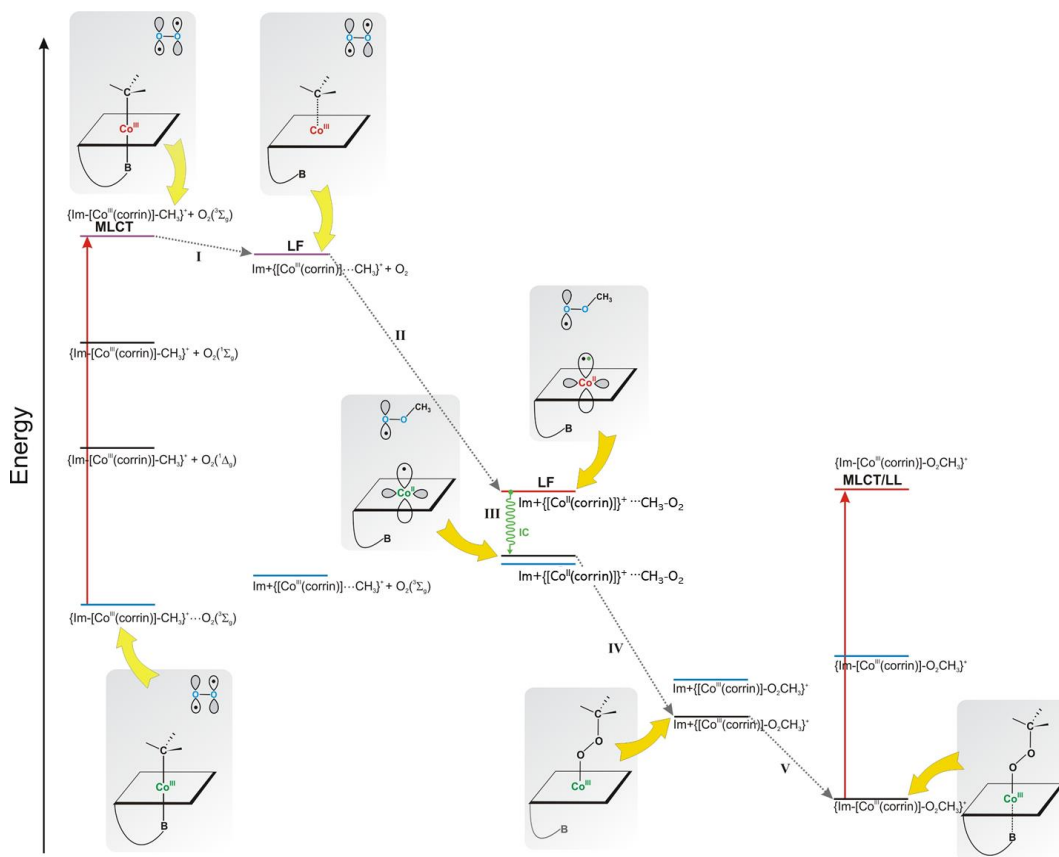
Figure 4.7. Energy diagram showing the involvement of excited states in MeCbl photoreaction in the presence of oxygen and the formation of a complex with Co-OOCH$_3$ bond. The blue lines correspond to triplet states. Black lines depicted singlet states, and violet lines can be ascribed to electronic, excited states in which formally singlet excited state of MeCbl interact with a triplet ground state of the oxygen molecule. The red lines correspond to singlet, excited states of the MeOOCbl system.

Based on the present DFT/TD-DFT calculation, it is evident that the IC from the LF state and the formation of the DC via the recombination of OO-CH$_3$ species with the de-excited [Co^{II}(corrin)] moiety (DC, Figure 4.3c) takes place in the region close to the II (T$_{1min}$) of Figure 4.3b. Thus, in the proposed mechanism, the deactivation of [Co^{II}(corrin)] subsystem may coexist with the formation of OO-CH$_3$, followed by immediate relaxation of the subsystems in the ground state. Moreover, the formation of the OO-CH$_3$ species followed by the formation of ([Co^{III}(corrin)]-OO-CH$_3$)$^+$ complex stabilizes the system compared to the reactant complex (Figure 4.7, stage IV). Furthermore, during the formation of Co-O bond, at the longer, Co-O and Co-N$_{Im}$ distances, mainly in the area of PES where the formation of ([Co^{III}(corrin)]-OO-CH$_3$)$^+$ complex occurs, the lowest triplet state (T) and singlet ground state (S$_0$) is near degenerate (Figure 4.8). Finally, this process concludes with the relaxation to the ground state minimum and the formation of axial bonds, resulting in a stable (Im-[Co^{III}(corrin)]-OO-CH$_3$)$^+$ (Step V, Figure 7 and Figure 4.8).
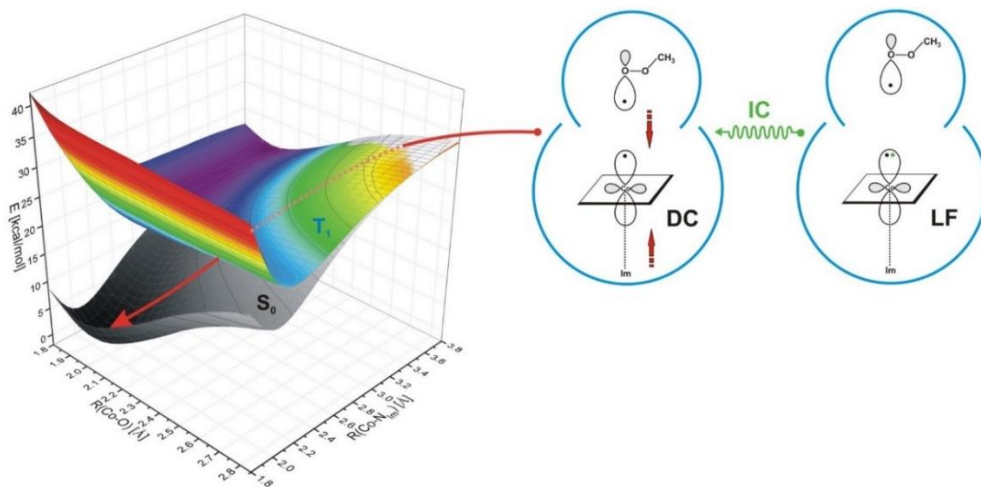
Figure 4.8. Potential energy surface of S$_0$ and T$_1$ state for (Im–[Co^{III}(corrin)]–O–O–CH$_3$)$^+$ model complex as function Co-O and Co-N$_{Im}$ axial bond lengths with a depicted estimate of relaxation path form LF electronic state.

CHAPTER V

THEORETICAL INVESTIGATION OF THE Co-C BOND CLEAVAGE DURING THE NATIVE CATALYSIS OF THE ADOCBL-DEPENDENT ITACONYL-CoA DEPENDENT MATHYLMALONYL-CoA MUTASE: WHAT TRIGGERS THE UNUSUAL ACTIVATION OF THE Co-C BOND

5.1 Background

[3]AdoCbl-dependent MCM, a B_{12}-dependent isomerase, is found in both bacteria and mammals. MCM reversibly converts M-CoA to succinyl-CoA (Scheme 5.1) via a radical-based 1,2 rearrangement.[13-14, 44, 67, 86, 92, 120, 206] However, a fascinating aspect of these AdoCbl-dependent enzymatic reactions is the trillion-fold rate enhancement of Co-$C_{5'}$ bond homolysis compared to the thermal homolysis in the solution.[45, 69, 207] To understand the origin of this large catalytic effect inside the enzyme, it is essential to elucidate the complete mechanism of the Co-$C_{5'}$ bond activation at the molecular level.

The Co-$C_{5'}$ bond in substrate-free AdoCbl-dependent MCM remains intact, and it is only after substrate binding that the cleavage process is initiated, as can be inferred from EPR or resonance Raman (RR) spectroscopic investigations.[208-209] Based on experimental and computational studies, several mechanistic proposals regarding the activation of the Co-$C_{5'}$ bond have been put forward. An early study suggested that corrin ring distortion by

---

[3] The discussion in this chapter is based on the publication *"Ghosh, A P.; Toda, M. J.; Kozlowski P.M (2021). What triggers the cleavage of the Co-$C_{5'}$ bond in coenzyme B_{12}-dependent itaconyl-CoA methylmalonyl-CoA mutase?* ACS Catal. 2021, 11, 7943–7955"

compression of the Co-N$_{axial}$ bond could lead to the destabilization of the Co-C$_{5'}$ bond.[73-74, 82] In the case of the MCM enzyme, it was postulated that the activation mechanism was related to the conformational switch as revealed by x-ray crystallographic data, and it was further proposed that the presence of the substrate could trigger the formation of Ado$^•$ by inducing the destabilization of the Co-C$_{5'}$ bond as a result of the tight adenine binding.[75-76]
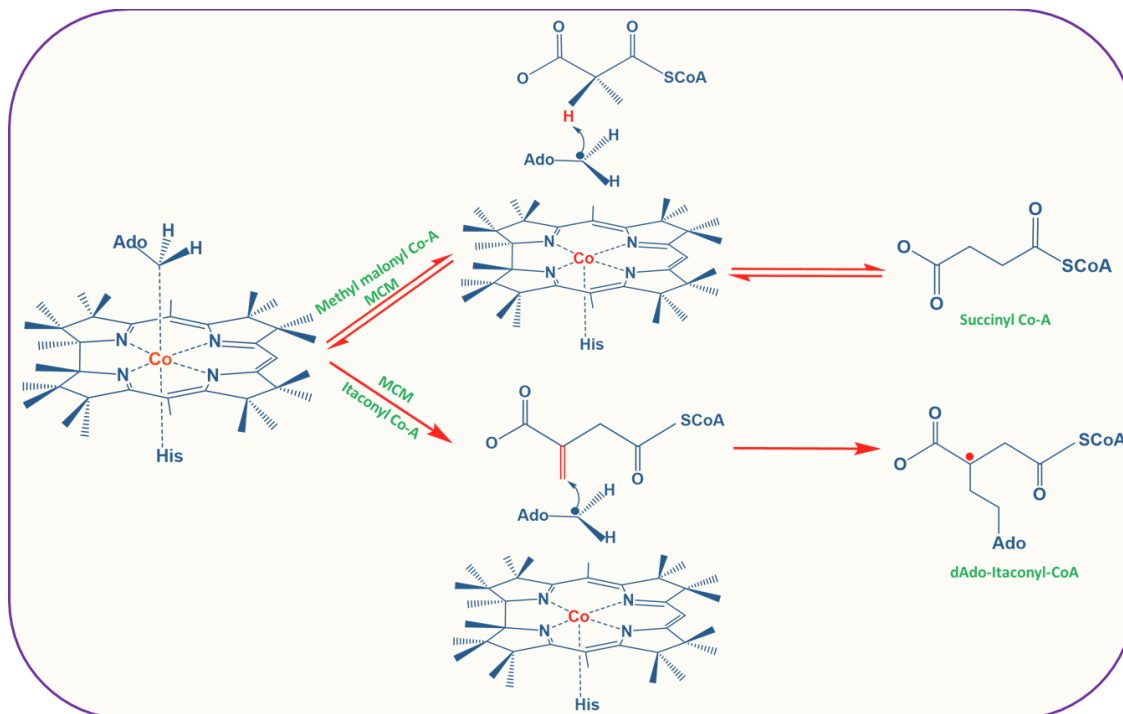
Scheme 5.1 Reactions catalyzed by MCM (upper panel) and MCM-[I-CoA] (lower panel).

The catalytic power in the AdoCbl-dependent MCM enzyme was also associated with the electrostatic interaction between the ribose of the Ado group and the amino acid residues of the enzyme active sit.[71, 210]. In addition to these, it has also been suggested that the catalytic power originates from binding the substrate molecule to the apoenzyme. It has further been postulated that the binding of the substrate triggers the radical formation by inducing the destabilization of the Co-C$_{5'}$ bond.[33, 75-76, 84] However, no consensus was

reached based on this mechanism. Moreover, a study based on the AdoCbl-dependent DDH suggests that a major conformational change can also be witnessed in the substrate-free enzyme upon the binding of AdoCbl cofactor with the apoenzyme, which leads to the labilization of the Co-C$_{5'}$ bond.[84] Thus, one cannot draw any logical conclusion into how the conformational change induced by substrate binding affects the catalytic activity and the unique labilization of the Co-C$_{5'}$ bond of AdoCbl-dependent enzymes.

More recently, a hypothesis related to the involvement of a Tyr residue present in the vicinity of the AdoCbl cofactor was put forward for understanding the catalytic origin of AdoCbl-dependent enzymes.[77, 79-81] The substrate-binding creates an H-bond network involving the -OH group of Tyr moiety that can play a critical role in displacing the hydroxyl proton of the Tyr residue (Tyr89 in the case of MCM enzyme). This will facilitate the electron transfer (ET), making the activation process a proton-coupled electron transfer PCET.[79] While these proposals shed light on the AdoCbl-dependent catalysis, none of these can explain the trillion-fold rate acceleration observed for cleavage of the Co-C$_{5'}$ bond in the enzyme compared to AdoCbl in solution.

However, the situation has recently changed because two new high-resolution crystal structures of the MCM enzyme were reported.[211] These have allowed for re-investigation of how the Co-C$_{5'}$ bond is activated. One crystal structure is substrate-free (PDB ID: 6OXC), and the other contains an inhibitor, namely itaconyl-CoA (I-CoA), instead of the native substrate M-CoA (PDB ID: 6OXD). I-CoA inhibits MCM by a radical suicide inactivation mechanism and is the chemical analog of the native substrate (M-CoA). Cleavage of the Co-C$_{5'}$ bond in the inhibited enzyme initially results in Co(II)/Ado RP formation. In native enzymatic catalysis, after RP formation, the primary Ado$^\bullet$ abstracts

hydrogen from M-CoA, which forms a substrate-centered radical prepped for rearrangement (Scheme 5.1).[208, 212] In the inhibitor-bound MCM, the Ado$^\bullet$ adds to the double bond in I-CoA, resulting in a stable tertiary carbon radical (Scheme 5.1).

The significant breakthrough in the newly reported MCM crystal structures is capturing the air-stable diradical formed after Co-C$_{5'}$ bond cleavage. An additional complication related to the investigation and understanding of the activation of the Co-C$_{5'}$ bond is its coupling with the subsequent H-atom abstraction step.[67] This hurdle has been removed for the present study because the MCM-[I-CoA] crystal structure captures the stage in the mechanism just after bond cleavage. Thus it decouples the H-atom abstraction step from the cleavage of the Co-C$_{5'}$ bond and the Ado· forms a stable C-C bond with the inhibitor. Therefore, the new crystallographic structures provided a new perspective for investigating and understanding the origin of the activation of the Co-C$_{5'}$ bond without the subsequent coupling with H-atom abstraction.

With the new crystal structures in hand, the origin of the catalytic power of AdoCbl-dependent MCM enzymes is explored by employing a QM/MM approach. Thus, to understand the activation of the Co-C$_{5'}$ bond inside the AdoCbl-dependent MCM-[I-CoA], the corresponding PECs associated with the cleavage of the Co-C$_{5'}$ bond in MCM-[I-CoA] and substrate-free MCM were constructed, PDB ID: 6OXD and 6OXC,[211] respectively. Both crystal structures contain a well-resolved structure for the Ado group. A comparison to the bond dissociation energy (BDE) of AdoCbl in solution is also provided. In addition, the role of a Tyr residue was also investigated to probe the involvement of a PCET mechanism.

5.2. Computational Method

93

5.2.1 Model building and system preparation

5.2.1.1 MCM-[I-CoA] model

To prepare a reliable model for QM/MM calculations, the recent crystal structure of MCM bound to inhibitor I-CoA was obtained from the PDB. The inhibitor bound MCM was crystallized at a 2.0 Å resolution (PDB ID = 6OXD).[211] The 6OXD crystal structure corresponds to the reactive and closed conformation of the enzyme. In MCM, the DBI base of AdoCbl is displaced, and a His residue from the protein takes its place as the lower axial ligand. Specifically, for 6OXD, the His629 (i.e., H629) is the lower ligand, and the delta nitrogen of the Im portion is bound to the Co. The crystal structure contains two independent chains, namely Chain A and B, but only chain A was used to construct the model for present calculations. Chain A contains the protein residues, AdoCbl cofactor, and the I-CoA inhibitor molecule, respectively. The Chimera software was used to generate the initial model, and then the structure was protonated. The protonation states of titratable residues at pH 7.0 were determined using the PropKa 3.0 software[144] via the PDB2PQR webserver. The TAO toolkit[213] was employed to modify input files, prepare inputs from previous calculations, and analyze results from the QM/MM calculations.

5.2.1.2 MCM substrate-free model

The structural model for the substrate-free MCM was obtained from the crystal structure of MCM (PDB ID: 6OXC at 1.9 Å resolution), which is associated with an unreactive and open configuration of MCM where the Co-$C_{5'}$ bond is intact. The crystal structure of substrate-free MCM is comprised of two different subunits, a B_{12} coenzyme binding α-subunit, and an inactive β-subunit. Similar to the MCM-[I-CoA] enzyme, the H629 of substrate-free MCM acts as the lower axial ligand of the AdoCbl cofactor, thus

adopting a base-off/His-on configuration. Again, using PropKa, the hydrogen atoms were added to the MCM substrate-free model, assuming a protonation state of titratable residues at pH 7.0. After the protonation, the crystal structure was minimized by the MM level of theory using the Amber force field. Finally, this minimized structure was used to generate the input for QM/MM calculations.

5.2.2 QM(DFT)/MM calculations

Due to the large size, a combined QM/MM method was employed. The chemically important sites of the MCM enzyme, including the active site, were treated at the QM level of theory while the rest of the protein with MM. Specifically, we have employed the QM/MM framework to investigate the activation and cleavage of the Co-C$_{5'}$ bond using both the inhibitor-bound MCM and substrate-free MCM crystal structures.

The set-up for the QM/MM calculations in this study is based on previously established methodologies for B$_{12}$-dependent systems, including EAL, GLM, MetH, and CarH.[162, 164-165, 179, 214] One of the benefits of the MCM crystal structures that are the basis for this study is that the cofactor's Ado group is well-resolved compared to EAL and GLM. In a previous QM/MM study of EAL, the Ado ligand had to be constructed manually as the AdoCbl analog, adeninylpentylcobalamin, was used in the crystal structure.[164] For GLM, both the 2′-endo and 3′-endo conformation of the ribose portion of the Ado ligand was included in the crystal structure, which added an additional challenge to the QM/MM set-up. Considering this, the QM/MM set-up from the 6OXC and 6OXD crystal structures was significantly more straightforward than for these previous systems due to the well-resolved cofactor.

Nevertheless, the QM/MM protocol for both inhibitor-bound and substrate-free MCM is consistent with the previously established protocols, which can be summarized as follows. First, the relevant chain is extracted from the crystal structure and minimized using the AMBER force field in Chimera. This is followed by protonation in the PropKa program. From here, the system is partitioned into the QM and MM layers. The partitioning of the MCM models is described in sections 5.2.2.1 MCM-[I-CoA] model and 5.2.2.2 MCM substrate-free model.

Again consistent with previous QM/MM studies, the high layer (QM) was treated with DFT at the DFT/BP86 level of theory,[131, 147], and the low layer was treated with MM. All QM/MM calculations reported here were performed using the ONIOM-ME[215] protocol as implemented in Gaussian 09 software.[145] The interface between the partitioned layers was treated by the hydrogen link atom approach. To be consistent with our previous studies, the DFT calculations were carried out using the GGA-type BP86 functional and TZVPP basis set for C, N, O, S, and Co and the TZVP basis set for H atoms.[155] Previous benchmark studies reported that the BP86 functional produces a reliable description of BDE and geometrical parameters compared with hybrid functionals. The results produced with BP86 functional are in agreement with the experiment as well as wave-function-based calculations.[148] The MM part of the low layer was treated with the AMBER force field (FF99SB).[216] The AMBER parameters of the B_{12} cofactor were obtained from calculations reported by Marques *et al*.,[167] while the parameters of the I-CoA inhibitor were obtained from the literature.[217] All atoms within a radius of 20 Å of the Co center were kept unfrozen and allowed to move during the geometry optimization, whereas atoms beyond 20 Å were kept frozen throughout our investigation.

5.2.2.1 MCM-[I-CoA] model

In the case of the inhibitor-bound MCM-[I-CoA] model, two layers were used. Specifically, the high layer included the truncated AdoCbl cofactor (Figure 5.1) which is in line with our previous studies of coenzyme B_{12}-dependent enzymes where the side chains of the corrin macrocycle, the nucleotide loop, and the DBI group was not included in the high layer but was -included in the low layer. In addition to the truncated cofactor, the QM layer contained a truncated portion of the I-CoA inhibitor, the Im part of the H629 residue, Arg223, and the Tyr105 amino acid residue. In addition to the side chains, nucleotide loop, and DBI of the cofactor, the low layer contained a portion of the inhibitor and the protein backbone.
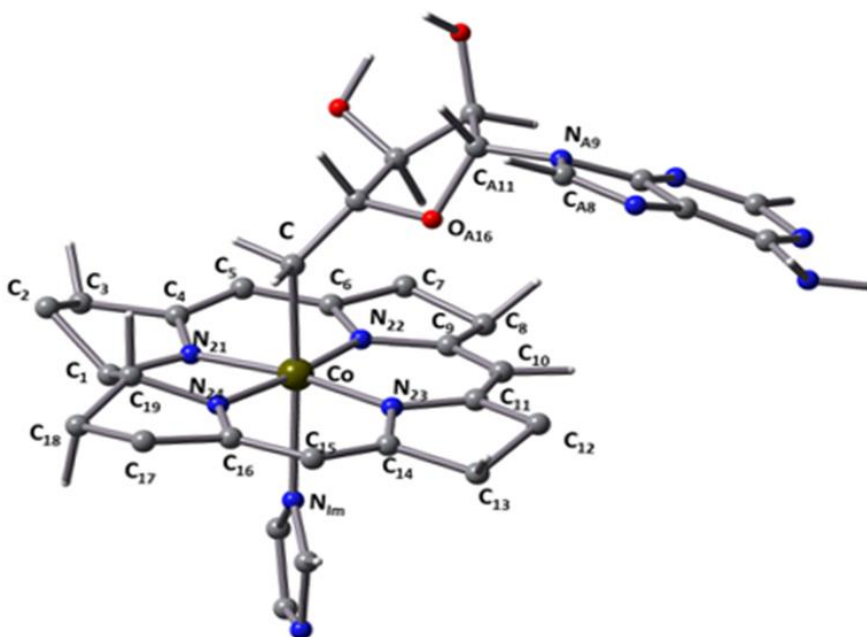
Figure 5.1. Truncated structure of AdoCbl cofactor containing atom numbers, which was used in the QM region (high layer).

5.2.2.2 MCM substrate-free model

The substrate-free model was partitioned in a similar fashion for the ONIOM calculations. The high layer contained the truncated AdoCbl cofactor and the Im group of H629 residue. The middle layer contained the side chains, which contained the corrin macrocycle, the nucleotide loop, and the DBI. The protein backbone was also placed into the low layer. There is a wealth of structural information available for the isolated AdoCbl and AdoCbl inside enzymes. As a result, a comparison of the key structural parameters of the AdoCbl cofactor has been completed with the data reported in the literature (Table 5.1) to ensure that the model systems were reliable.

Parameter	MCM substrate-free		MCM-[I-CoA]				
	Crystal Structure[a]	QM/MM[b]	Crystal Structure[c]	QM/MM[d]	QM/MM[d]	QM/MM[e]	QM/MM[f]
Multiplicity	Singlet	Singlet	Triplet	Triplet	Singlet	Singlet	Singlet
Axial Bonds (Å)							
$Co-C_{5'}$	2.53	2.06	4.11	4.88	4.89	3.77	2.02
$Co-N_{Im}$	2.27	2.26	2.38	2.15	2.15	2.16	2.27
Endocyclic Angles (°)							
θ_0	-37.33	-36.51	39.63	42.38	42.35	47.38	-20.33
θ_1	38.10	21.93	-32.03	-42.33	-42.31	-46.74	-10.28
θ_2	-20.81	2.88	8.04	26.26	26.26	26.85	39.55
θ_3	-0.45	-27.00	14.82	1.34	1.32	3.53	-52.49
θ_4	25.33	39.58	-35.72	-28.30	-28.27	-32.63	44.19
Pseudorotation Phase	196.09	157.07	355.09	16.63	16.65	14.40	113.13
Ribose Conformation	2'-endo	2'-endo	3'-endo	3'-endo	3'-endo	3'-endo	2'-endo
Exocyclic Angles (°)							
Glycosyl rotation (χCN)	-102.90	87.09	41.89	34.61	34.62	13.86	132.30
ϕ_2	59.76	158.08	115.22	85.76	85.45	130.88	138.11
ϕ_3	51.25	51.55	7.99	-58.87	-58.88	-45.26	70.45

Table 5.1 Structural parameters for substrate-free MCM and inhibitor bound, MCM-[I-CoA], crystal structures, and QM/MM optimized models.

(a) Substrate-free MCM PDB ID: 6OXC (b) QM/MM optimization of substrate-free MCM, where active site corresponds to Im-[Co^{III}(corr)]-Ado$^+$, (c) Crystal structure of MCM-[I-CoA] PDB ID: 6OXD,(d) QM/MM optimization where active site corresponds to Im-[Co^{II}(corr)]$^+$, Ado-[I-CoA], and Y105, (e) QM/MM optimization of Co/C$_{5'}$ diradical, where active site corresponds to Im-[Co^{II}(corr)]$^+$, Ado, truncated inhibitor, and Y105, (f) QM/MM optimization of 2′-endo conformation, where active site corresponds to Im-[Co^{III}(corr)]-Ado$^+$, truncated inhibitor, and Y105

5.3. Result and Discussions

5.3.1 Analysis of MCM-[I-CoA] triplet intermediate: Comparison with EPR studies

In the native reaction, MCM catalyzes the reversible isomerization of M-CoA to succinyl-CoA through the formation of Co(II)/Ado$^\bullet$ RP followed by the H-atom abstraction from the substrate M-CoA by Ado$^\bullet$ (Scheme 5.1). However, in I-CoA bound MCM, upon the initial formation of RP, the Ado radical forms a covalent bond ($C_{5'}$-C_M) with the I-CoA and terminates the catalytic cycle by forming a stable Ado-[I-CoA] radical (Scheme 5.1). The crystal structure of 6OXD captured this radical, which contains the AdoCbl cofactor with a dissociated Co-$C_{5'}$ bond and the Ado adduct I-CoA (Ado-[I-CoA]). EPR studies have revealed coupling between low spin Co(II) and the Ado-[I-CoA]$^\bullet$ radical, comparable with the EPR spectra of catalytic intermediate trapped during the MCM mediated transformation of M-CoA to succinyl-CoA.[211] The EPR spectra and associated hyperfine multiplicity further indicated that the diradical component had the signature of a triplet system.
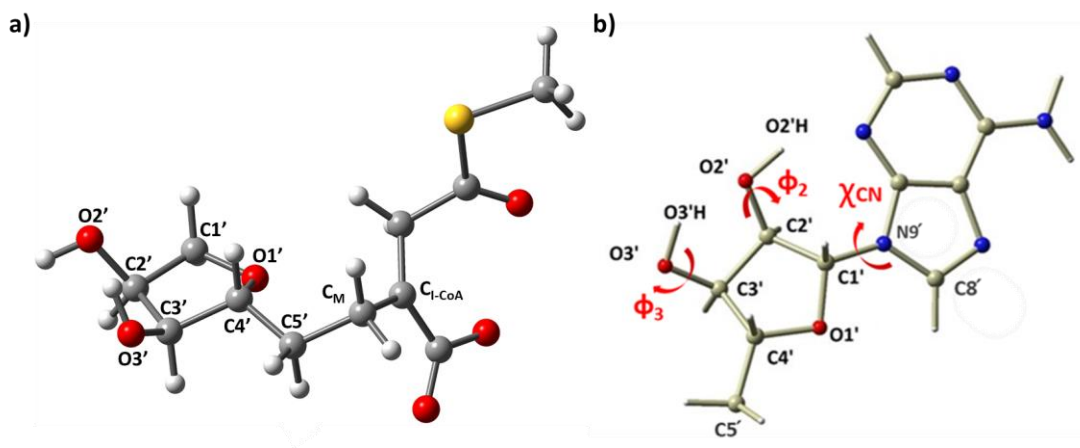
Figure 5.2 Atom numbering of (a) Ado-I-CoA and (b) Ado group used in this study. Geometric parameters related to ribose conformation of the Ado ligand for QM/MM optimized AdoCbl structure bound to MCM at different Co-C5' distances. Inset: Structure of Ado ligand with glycosyl rotation angle χ_{CN}=O1'-C1'-N1'-C5', exocyclic ribose angle Φ_2=C1'-C2'-O2'-O2'H, and exocyclic ribose angle Φ_3=C2'-C3'-O3'-O3'H. (b) Definition of psuedorotation phase (P), psuedorotation amplitude (Θ_m), and endocyclic ribose angles (Θ0-4). *If $\Theta0 > 0$ and $\Theta2+\Theta4-\Theta1-\Theta3 > 0$, X=0°. If $\Theta0 > 0$ and $\Theta2+\Theta4-\Theta1-\Theta3 < 0$, then X=360°. If $\Theta0 < 0$ then X =180°.* P values between −90° and 90° correspond to the 3'-endo conformation whereas *P values between 90° and 270° correspond to the 2'-endo conformation*.

To explore the nature of Co(II)/C_{I-CoA} diradical (C_{I-CoA} = the tertiary carbon of Ado-[I-CoA] moiety, Figure 5.3), the QM/MM geometry optimization was carried out for MCM-[I-CoA] structure considering a triplet electronic state. A frequency calculation was conducted to verify whether the geometry of the diradical with triplet multiplicity
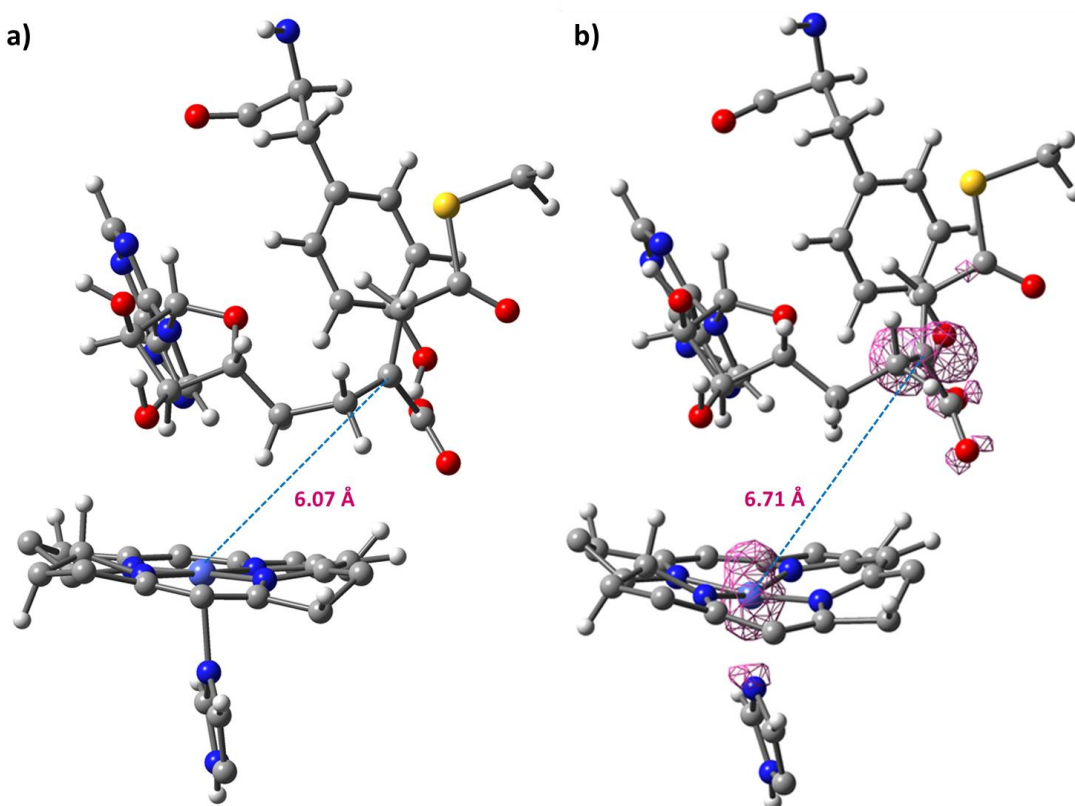
Figure 5.3. (a) MCM–[I-CoA] active site in the crystal structure. (b) QM/MM optimized structure of MCM-[I-CoA] active site. The spin density of the QM/MM optimized structure of MCM-[I-CoA] was calculated with triplet multiplicity.

corresponds to a stationary point. The absence of an imaginary frequency confirmed that the optimized geometry indeed corresponds to a stationary point. The $<S^2>$ value of the wave-function ($<S^2> = 2.002$) confirmed that the optimized structure has a signature of a triplet state. The tertiary C_{I-CoA} radical has a planner geometry and is 6.7 Å away from the metal center radical, the Co atom. This is consistent with the recently reported EPR

investigation, where the interspin distance is 6 Å (Figure 5.3). It can also be seen from Figure 5.3 that the Co(II) and $C_{\text{I-CoA}}$ centers are ferromagnetically coupled and the spin density was equally distributed between the Co(II) and $C_{\text{I-CoA}}$ (Figure 5.3b), in good agreement with the EPR study.[211] The $C_{5'}$-C_M bond length in the optimized MCM-[I-CoA] structure was found 1.52 Å, whereas in the crystal structure the $C_{5'}$ of Ado group is 1.5 Å away from the methylene C_M of the I-CoA moiety. A detailed comparison of all the important structural parameters of the QM/MM optimized model structures and the crystal structure of MCM-[I-CoA] is summarized in Table 5.1. A noticeable difference can be seen in the distance between the Co and $C_{5'}$ atom of the Ado group. The optimized distance between Co and $C_{5'}$ of 4.88 Å, which is a bit longer than the crystal structure (Table 5.1).

The various conformations of the Ado group in different crystal structures of MCM are of great importance in studying the native catalytic mechanism of AdoCbl-dependent MCM. The orientation of the Ado in MCM, or any Ado-dependent enzyme, depends on whether the Ado group is intact, dissociated, or displaced. A large-scale conformational change was observed upon binding the substrate.[75] Similarly, in the MCM-I-CoA, the binding of I-CoA with MCM induces a large conformational change to the enzyme active site when compared to native MCM. This change is more pronounced in the AdoCbl-binding region of MCM-[I-CoA]. The Ado group and the corrin ring of the I-CoA bound MCM are shifted by 2.1 Å in comparison to the substrate-free MCM. This also induces a significant change in the conformation of the adenine of the Ado group. While in the native MCM, the adenine of the Ado group is almost coplanar to the corrin ring, in the MCM-[I-CoA] complex, the adenine is positioned almost perpendicularly oriented with respect to the corrin ring, and the ribose portion of Ado adopts a 3′-endo conformation. A similar

orientation of Ado has also been observed in several other AdoCbl-dependent enzymes, such as GLM, D-ornithine aminomutase (OAM), or photoreceptor CarH.[218]

5.3.2 Cleavage of the $C_{5'}-C_M$ bond in the MCM−[I-CoA] complex

To explore the activation of the Co-$C_{5'}$ bond, an analysis of the PEC associated with Co-$C_{5'}$ dissociation and the formation of Co(II)/$C_{5'}$ diradical has to be performed. As previously discussed, in the crystal structure of MCM-[I-CoA], the Ado group is displaced toward the inhibitor and forms a covalent bond with the I-CoA methylene group. Hence, to explore the activation of the Co-$C_{5'}$ bond, corresponding reverse reactions were studied, namely cleavage of the $C_{5'}-C_M$ bond (for generating the Co(II)/$C_{5'}$ diradical intermediate) followed by the formation of the Co-$C_{5'}$ bond. Toward this, we have first studied the cleavage of the $C_{5'}-C_M$ bond by computing a relaxed PEC (Figure 5.4a). To generate corresponding PEC, the $C_{5'}-C_M$ bond was systematically elongated from 1.5 Å to 2.9 Å
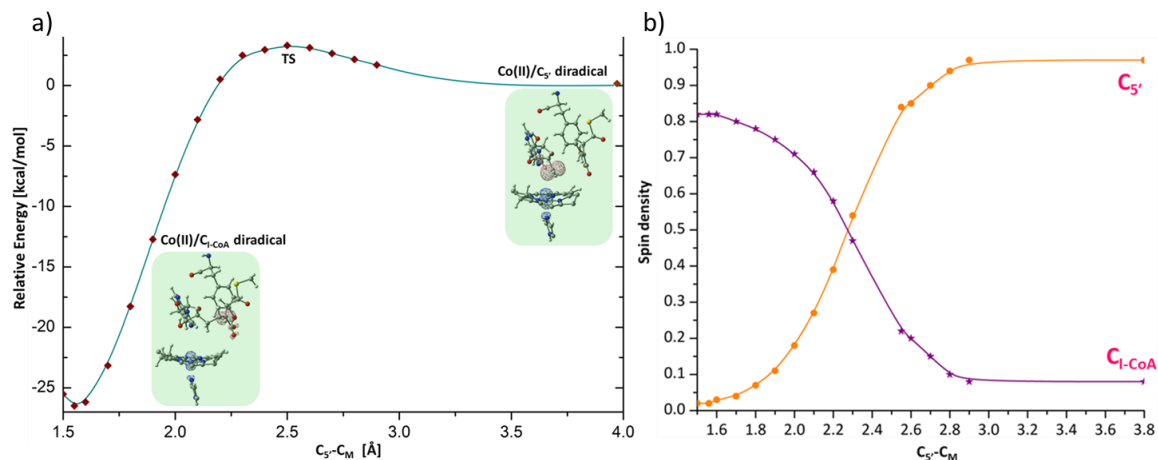
Figure 5.4 (a) Potential energy curve obtained by relaxed scans along the $C_{5'}-C_M$ bond **(b)** Spin density distribution of the $C_{5'}$ -C_M bond throughout the cleavage in MCM-[I-CoA] enzyme.

using a step size of 0.1 Å, assuming an open-shell unrestricted singlet. The spin density values indicate that with increasing $C_{5'}-C_M$ bond distance, the spin density of the tertiary

$C_{I\text{-CoA}}$ atom shifts to the $C_{5'}$ of the Ado group, while the spin densities of the Co (-0.99) and C_M atoms remain unchanged (Figure 5.4b). For a $C_{5'}$-C_M bond distance of 2.9 Å, the spin densities on $C_{I\text{-CoA}}$ and $C_{5'}$ are almost zero and +1.0, respectively. This indicates the successful formation of the Co(II)/$C_{5'}$ diradical. Using the geometry associated with this point, the unconstrained optimization of the MCM-[I-CoA] structure was performed. The optimized geometry has a $C_{5'}$--C_M distance of 4.0 Å, which indicates the complete cleavage of the $C_{5'}$-C_M bond. The analysis of the spin density distribution reveals that the spin density is evenly distributed between the Co and $C_{5'}$ of the Ado group, and distribution further verifies the formation of Co(II)/$C_{5'}$ diradical (Figure A9). Upon the formation of Co(II)/$C_{5'}$ diradical, the $C_{5'}$ atom was slightly directed toward the Co atom without any significant change in the conformation of the Ado group.

The points near the maximum energy on the $C_{5'}$-C_M PEC (Figure 5.4a) were used as the initial guesses for locating the transition state (TS) associated with the reverse reaction described above, i.e., the cleavage of the $C_{5'}$-C_M bond. Although the PEC was explored from the product to the reactant, consistent with the available x-ray structure, in enzymatic reaction, this TS can be associated with the formation of the $C_{5'}$-C_M bond between Ado radical and inhibitor. The TS corresponds to the geometry where the $C_{5'}$-C_M bond length is 2.49 Å, and its validity was verified by the frequency calculation. The presence of a single imaginary vibrational frequency, $557i$ cm^{-1}, confirmed the nature of the TS. The transition vectors, as depicted in Figure 5.5, clearly indicate that the imaginary frequency of $557i$ cm^{-1} is associated with $C_{5'}$-C_M bond displacement. It is also apparent from Figure 5.5 that the TS state connects the reactant and the product.
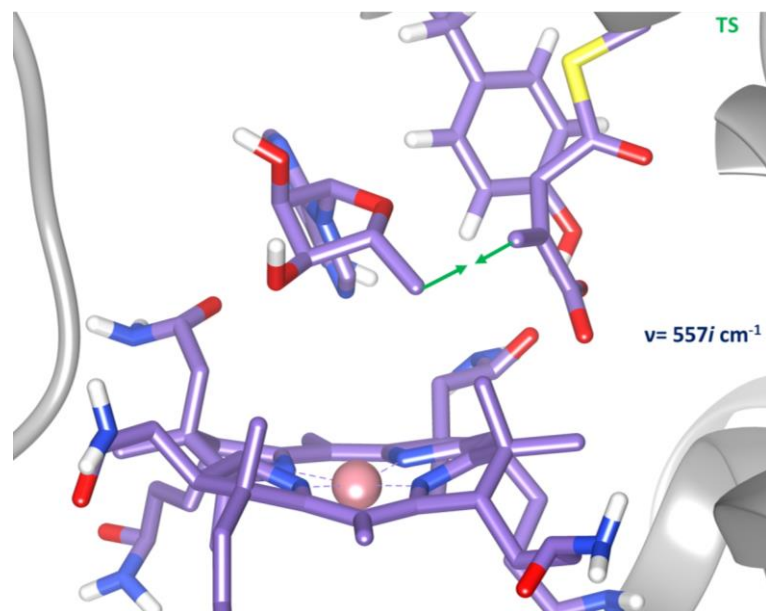
Figure 5.5 Transition state (TS) structure and corresponding transition vector (in green). The imaginary frequency value (557i cm^{-1}) for TS is reported

5.3.3 Formation of Co-C$_{5'}$ bond in MCM-[I-CoA] complex

The formation of the Co(II)/C$_{5'}$ diradical was followed by an investigation into the formation of the Co- C$_{5'}$ bond. The conformation of the Ado moiety has previously been shown to influence the energetics and dissociation of the Co- C$_{5'}$ bond. Thus, PECs were built with two different conformations of the Ado group in mind, namely the 2-endo and 3-endo conformations (Figure 5.6), and superimposed to determine when the ribose group undergoes a conformational change during Co- C$_{5'}$ bond activation. In the crystal structure of the MCM-[I-CoA] model (the initial Co(II)/C$_{I-CoA}$ diradical form), as well as in the Co(II)/C$_{5'}$ diradical intermediate, the ribose ring of Ado moiety is in the 3′-endo conformation (denoted as D3′ in Figure 5.6). Using the structure 3′-endo Co(II)/C$_{5'}$ diradical intermediate, the 2′-endo Co(II)/C$_{5'}$ diradical (denoted as D2′ in Figure 5.6) was prepared by adjusting a few selected conformational parameters, such as endocyclic angles θ and exocyclic angle χ$_{CN}$ of the Ado group. (Visualization of these parameters is given in

Figure 5.2). The computation of the PECs was started from the Co(II)/C$_{5'}$ diradical state of MCM-[I-CoA] by systematically contracting the Co-C$_{5'}$ bond length with a step size of 0.1 Å. For both the PECs (green curve, 2′-endo, and orange curve, 3′-endo), the spin density value associated with the Co and C$_{5'}$ atom indicate a homolytic cleavage of the Co-C$_{5'}$ bond (Figure A10). While the spin density profiles for the two curves are similar, noticeable differences can be seen in the energetics of these PECs.
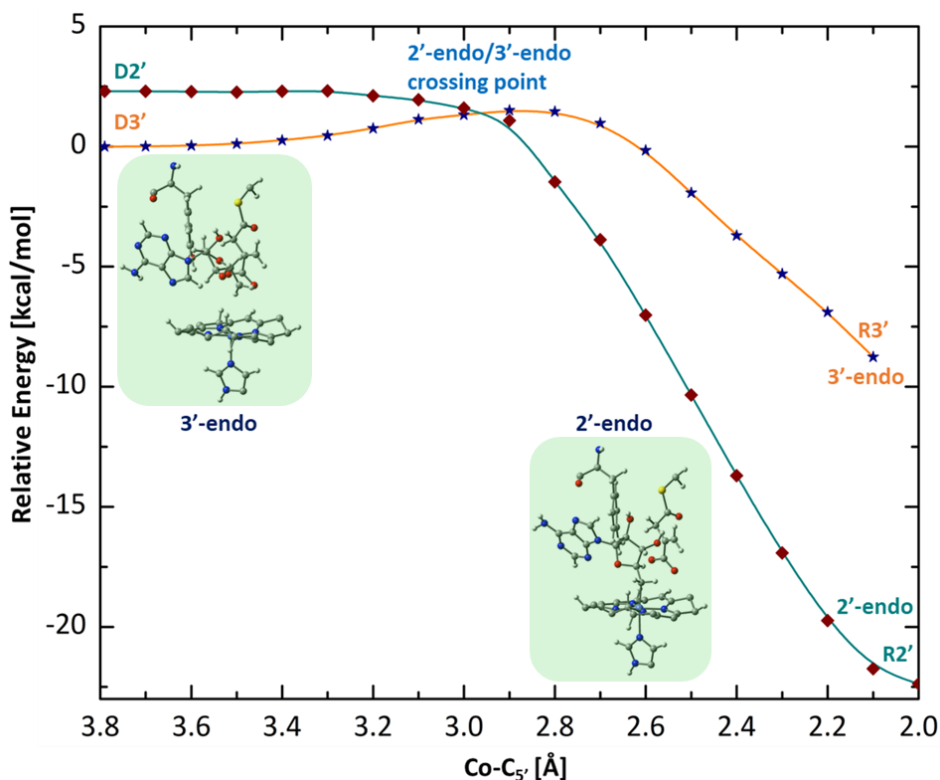
Figure 5.6 Potential energy curves obtained by relaxed scans along the Co- C$_{5'}$ bond in MCM-[I-CoA] complex.

At the dissociated state (for longer Co-C$_{5'}$ bond length), the D3′ (C3′-endo) is energetically lower than the D2′ (Figure 5.6). The energy of the 3′-endo conformation remains lower than its 2′-endo counterparts until the two PECs cross at a Co-C$_{5'}$ bond distance of ~3.0 Å (Figure 5.6). After crossing two curves, the energy falls quite rapidly,

and the 2′-endo conformation becomes energetically lower than the 3′-endo conformation. Moreover, at a Co- $C_{5'}$ bond length of 2.1 Å, the 2′-endo conformation (R2′) is almost 11.3 kcal/mole lower in energy than the 3′-endo conformation (R3′ in Figure 5.6). This destabilization of R3′ in the bound state can be explained by the proximity of the OH group of C3′ atom (C3′-OH) of the ribose to the corrin ring, specifically toward the H atom associated with the C19 of the corrin ring (Figure 5.7). Figure 5.7 shows that as the Co-C bond decreases, it increases the proximity between the OH group of C3′ atom of the ribose and the H atom of C19 of the corrin macrocycle, which impedes the formation of the Co-$C_{5'}$ bond in the R3′ state and causes distortion in the corrin ring. Thus, reversibly it can be
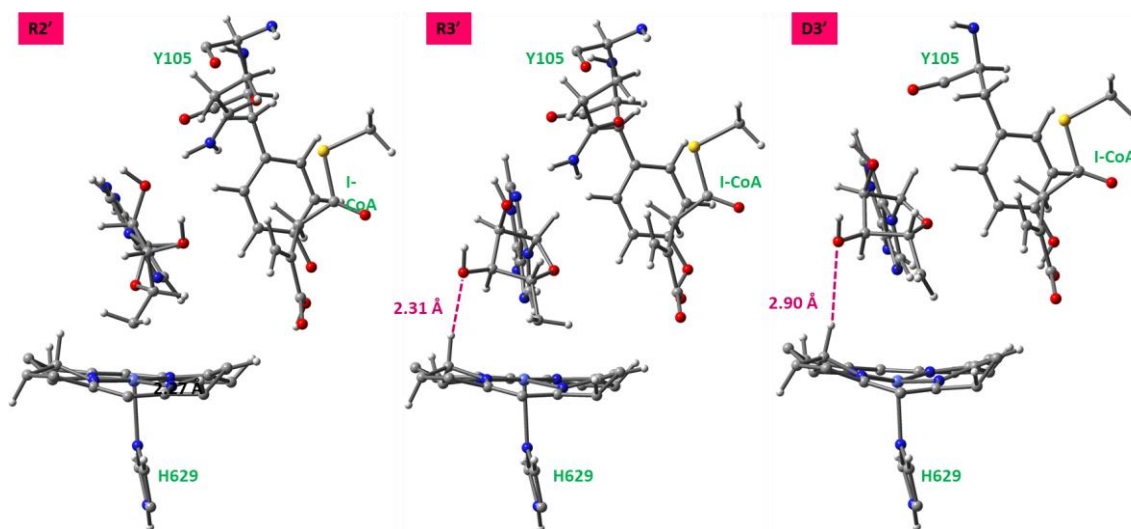
Figure 5.7 QM/MM optimized AdoCbl bound to MCM-[I-CoA] in the (a) 2′-endo (R2') (b) 3′-endo conformation (R3') at the bound state and (c) 3′-endo conformation (D3') at the dissociated state.

seen that during the activation of the Co-$C_{5'}$ bond, the Ado undergoes a conformational change in the MCM-[I-CoA] model, which is consistent with other AdoCbl-dependent enzymes as well as with crystallographic data available for GLM enzyme.[218-219] While in

the dissociated state, the ribose is in the 3′-endo conformation, it adopts the 2′-endo conformation in the bound state (R2′) (Figure 5.7).

Taking the above into consideration, based on Figure 5.6, the Co-C$_{5′}$ bond dissociation inside MCM enzyme can be explained as follows: the activation of the Co-C$_{5′}$ bond starts from the R2′ conformation at Co-C$_{5′}$ bond 2.0 Å, where the spin density on the Ado moiety and Co atom is zero and proceeds through the 2′-endo until it crosses the 3′-endo curve at a 3.0 Å as evident from PECs. After the crossing point, the ribose adopts the 3′-endo conformation as evident from changes associated with the psuedorotation phase (from 113.13 to 14.40 in the 3′-endo). Then it progresses through the 3′-endo for the complete dissociation of the Co-C$_{5′}$ bond. At the Co-C$_{5′}$ bond 3.8 Å, the spin density of Ado is 0.99 and on Co atom is -1.0, which suggests the completion of the homolytic cleavage. The calculated Co-C$_{5′}$ BDE based on the energy difference between the R2′ and D3′ state is 22.7 kcal/mol. At the dissociated limit, the D3′ is energetically more stabilized than the D2′ by almost 2.5 kcal/mol. Most likely, the hydrogen bonding (H-bonding) of the C2′-OH of ribose moiety with the Gln346 (NH$_{Gln346}$····O2′) and the interaction between NH$_2$ of the adenine group with the Gly107 through H-bonding network stabilizes the D3′ structure. These interactions also orient the Ado$^{•}$ towards the I-CoA (or M-CoA in native MCM) for the subsequent step in the catalytic cycle. A similar conformational change of the Ado moiety was also observed in the AdoCbl-dependent GLM.[218] While in AdoCbl-dependent mutases, the ribose group undergoes a conformation change during the catalytic activation of the Co-C$_{5′}$ bond, in other AdoCbl-dependent eliminase, such as the EAL, it is the changes in χ_{CN} angle (i.e., adenine plane relative to the ribose).[220] Such rotation facilities the migration of Ado radical while preserving the ribose conformation.

5.3.4 QM/MM structures of MCM without substrate

The substrate-free MCM (6OXC) crystal structure captures some stage of the homolytic cleavage of the Co-C5′ bond of AdoCbl and, accordingly, the Co-C$_{5'}$ bond length in the substrate-free MCM was found to be 2.53 Å. Several attempts were made to optimize this structure to obtain a dissociation limit without constraints imposed on bond length. Still, these calculations were unsuccessful, and optimization of the model system led to the reformation of the Co-C$_{5'}$ bond. The reformed Co-C$_{5'}$ bond in the QM/MM model was 2.06 Å (Figure 5.8), which agrees well with previous QM/MM studies involving intact AdoCbl. The parameters for the 6OXC crystal structure listed in Table 5.1 correspond to the point in the catalytic cycle when the Co-C$_{5'}$ are partially cleaved. In contrast, the structural parameters for the QM/MM model listed in Table 5.1 of substrate-free MCM represent the resting state of the enzyme where the Co-C$_{5'}$ bond of AdoCbl is intact. Other vital structural parameters are listed in Table 5.1 and include the endocyclic and exocyclic angles of ribose.
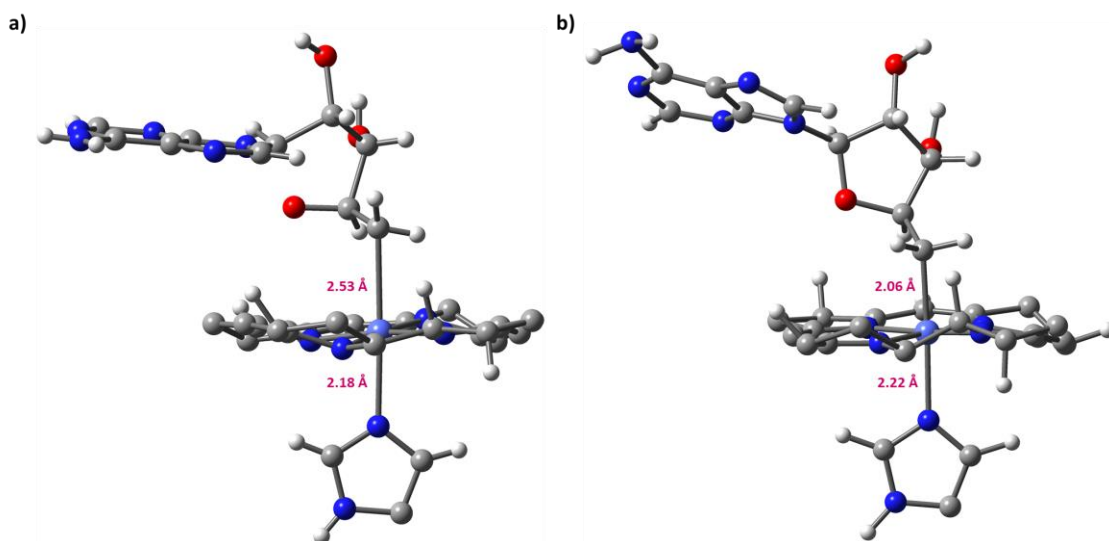
Figure 5.8. MCM (a) crystal structure (PDB ID: 6OXC) and (b) QM/MM optimized AdoCbl bound to MCM from PDB ID: 6OXC. Ribose is in the 2′-endo conformation. Co-C$_{5'}$ and Co-N$_{Im}$ bond distances are indicated.

While the Co-C$_{5'}$ bonds from the crystal structure indicate two different events in the catalytic cycle, the Co-N$_{Im}$ bond was nearly identical between the crystal structure and the optimized model, namely 2.26 Å and 2.27 Å, respectively. Interestingly, despite the elongated Co-C$_{5'}$ bond, the ribose portion of the Ado group retains the 2'-endo conformation consistent with the crystal structure.

5.3.5 Cleavage of the Co−C$_{5'}$ bond in the substrate-free MCM: Comparison of Co−C5′ bond cleavage with the isolated cofactor and with the MCM−[I-CoA] complex

The primary objective in studying the substrate-free model of MCM was to compare the Co-C$_{5'}$ BDE energy to that of isolated AdoCbl cofactor and I-CoA bound MCM to determine if the enzymatic environment and to what extend substrate-binding affected the BDE of AdoCbl. With this in mind, the cleavage of the Co-C$_{5'}$ bond in the substrate-free MCM was investigated by systematically elongating the Co-C$_{5'}$ bond from 2.0 Å to 3.8 Å with a step size of 0.1 Å. The computed PEC of the Co-C$_{5'}$ bond dissociation is depicted in Figure 5.9. The spin density values of the Co and C$_{5'}$ are indicative of homolytic cleavage of the Co-C$_{5'}$ bond (Figure A11). It was found that the spin polarization appears when the Co-C$_{5'}$ bond is stretched to 2.7 Å, which leads to the formation of RP at the dissociation limit. Around 3.8 Å, the homolytic cleavage is essentially completed, and the spin density on the Co and C$_{5'}$ atoms are nearly +1.0 and -1.0, respectively (Figure A11). The computed energy barrier associated with the homolytic cleavage of the Co-C$_{5'}$ bond is 22.2 kcal/mol (Figure 5.9). This is nearly identical to the energy barrier based on the PEC of MCM-[I-CoA] (Figure 5.9). While the BDE for substrate-free MCM and MCM-[I-CoA] are almost identical (22.2 kcal/mol vs. 22.7 kcal/mol, respectively), the confirmation of the Ado group is different between the two models. In the case of MCM-

[I-CoA], the ribose group undergoes a conformational change during the catalytic activation of the Co-C$_{5'}$ bond, whereas the conformation of ribose (2′-endo) does not
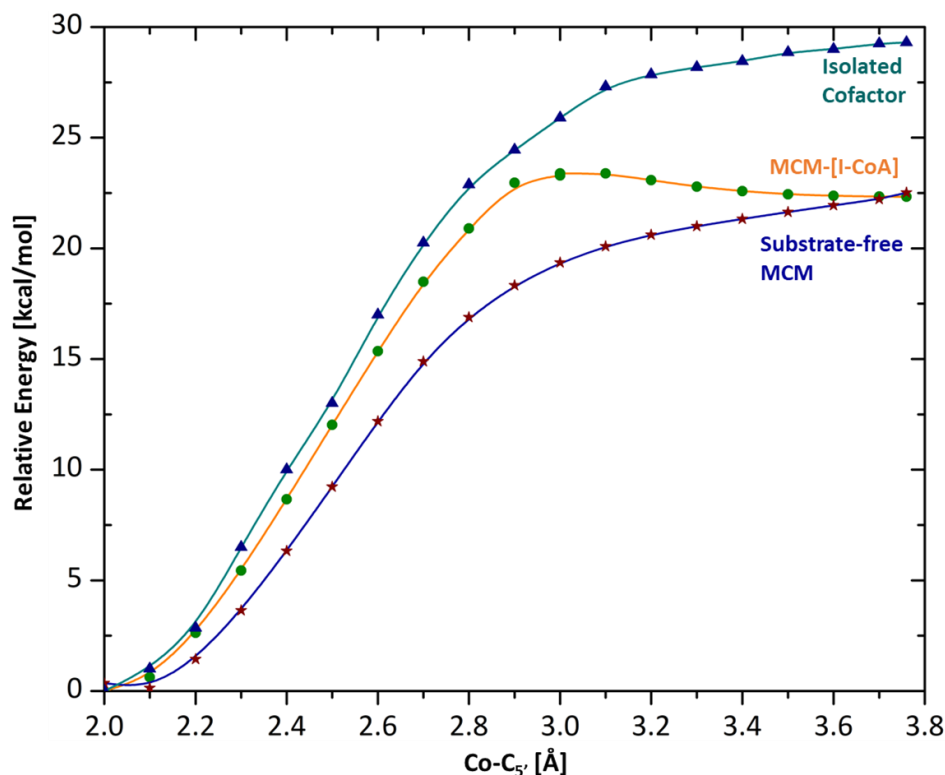
Figure 5.9. Relaxed scans obtained potential energy curves along with the Co-C$_{5'}$ bond in substrate-free MCM, MCM-[I-CoA], as well as in isolated AdoCbl cofactor.

change along with the PEC of substrate-free MCM (Figure 5.10). It has also been noticed from Figure 5.11 that for the AdoCbl-bound structure up to a Co-C$_{5'}$ distance of 3.0 Å, the changes in PEC are nearly identical. However, after 3.0 Å, the Ado group of MCM-[I-CoA] undergoes a conformational change and adopts the 3′-endo conformation based on changes associated with the psuedorotation phase. Figure 5.11 depicts the complete catalytic reaction profile for the MCM-[I-CoA], which can be explained as follows: the activation of the Co-C$_{5'}$ bond starts from the R2′ conformation at Co-C$_{5'}$ bond 2.0 Å and proceeds through the 2′-endo until it crosses the 3′-endo curve at a 3.0 Å as evident from PECs. After the crossing point, the ribose adopts the 3′-endo conformation. Then it

progresses through the 3′-endo for the complete dissociation of the Co-C$_{5'}$ bond. At the Co-C$_{5'}$ bond 3.8 Å, the spin density of Ado is 0.99 and on Co atom is -1.0, which suggests the completion of the homolytic cleavage. After the formation of the Ado$^{\bullet}$, it interacts with the inhibitor and forms a covalent bond (C$_{5'}$-C$_M$ bond) with the I-CoA methylene group. The formation of the C$_{5'}$-C$_M$ bond in the I-CoA inhibition of MCM (the corresponding TS of this bond formation is located at C$_{5'}$-C$_M$ bond 2.49 Å, see Figure 5.4) is represented by the teal curve in Figure 5.11. The most interesting outcome here is the identical energy barrier associated with the activation of the Co-C$_{5'}$ bond for both substrate-free MCM and MCM-[I-CoA]. This observation questions the previously suggested idea that a substrate-induced (I-CoA is a structural analog of the substrate M-CoA) conformational change reduces the BDE and triggers the cleavage of the Co-C$_{5'}$ bond.
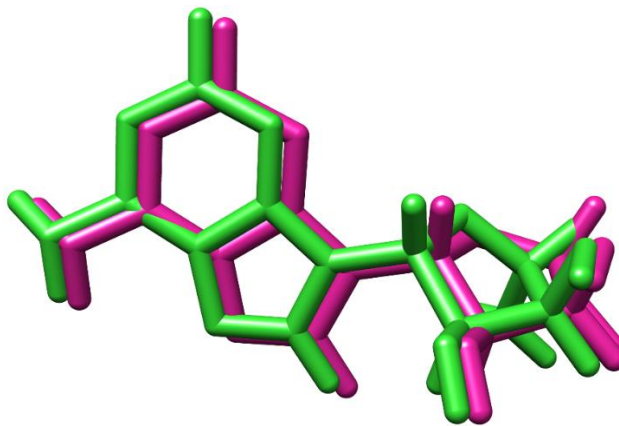
Figure 5.10. Conformations of Ado along the PEC of the Co-C$_{5'}$ dissociation for the substrate-free MCM (blue curve in Figure 5.9). Green structures correspond to initial PEC points, and the structures in pink correspond to endpoints of the PEC. Hydrogen atoms are omitted for clarity.

On the other hand, the calculated energy barrier of the homolytic cleavage of the Co-C$_{5'}$ bond in both substrate-free MCM and MCM-[I-CoA] is lower than the energy barrier associated with the PEC of isolated AdoCbl in a gas phase (Figure 5.9). The computed BDE for isolated AdoCbl cofactor in solution was found to be 29 kcal/mol,
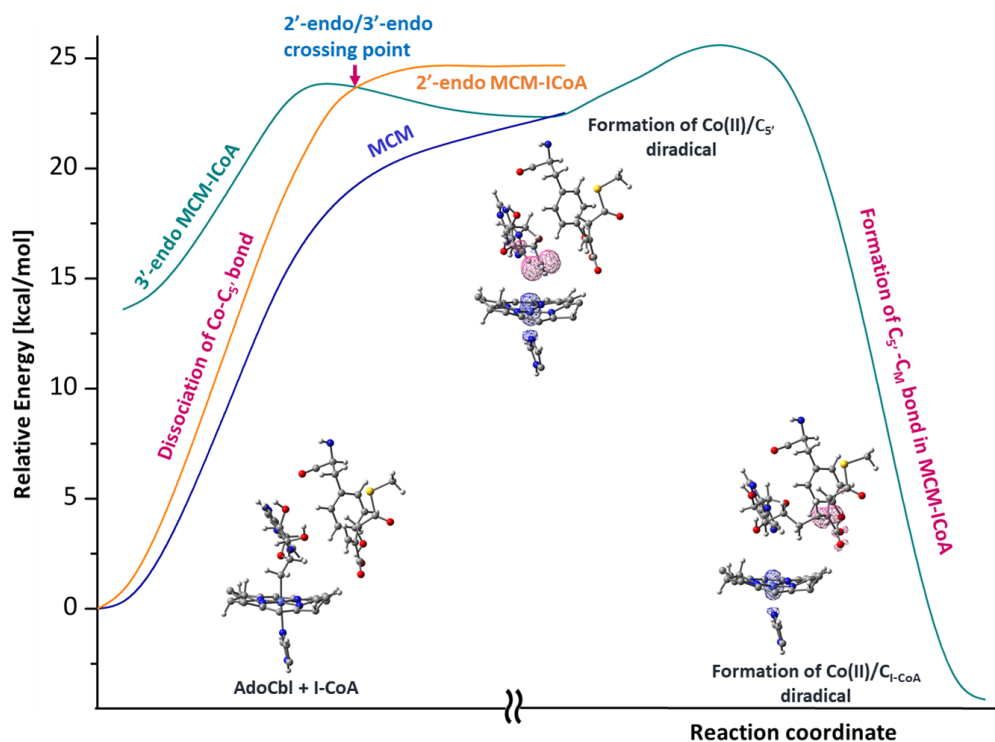
Figure 5.11: Potential energy profiles obtained by relaxed scans along the Co-C$_{5'}$ distance. The blue curve represents Co-C$_{5'}$ bond dissociation energy (BDE) for substrate-free MCM. The orange curve represents Co-C$_{5'}$ BDE from left to right and the formation of Co-C$_{5'}$ from right to left. Conformational change of ribose along Co-C$_{5'}$ scan is indicated in labeling. The teal curve represents the formation of the C$_{5'}$-C$_M$ bond in the I-CoA inhibition of MCM. The transition state (TS) associated with the C$_{5'}$-C$_M$ bond formation is also labeled (see Figures 5.4 and 5.5 for the structure of the TS).

which is in good agreement with the experiment (experimental BDE was 30.9±4.1 kcal/mol)[44, 221] as well as with previous computational studies.[220, 222] The difference in the energy barrier for Co-C$_{5'}$ bond cleavage between the substrate-free MCM and isolated AdoCbl most likely indicates an electronic and steric contribution of the protein environment. Upon binding with the enzyme, the AdoCbl participates in H-bonding with some active site residues. In particular, the ribose moiety is engaged in H-bonding interaction with the Gln346. In addition, the C2′-OH group of ribose also has an H-bonding network with the Arg223 and His260 residue. These interactions between the adenosyl

group and the protein environment influence the labilization of the Co-C$_{5'}$ bond and reduce

the barrier for the Co-C$_{5'}$ bond cleavage. A similar kind of interaction is also observed for

the MCM-[I-CoA] model where the C2′-OH of ribose and the NH$_2$ of the adenine group

has H-bonding interaction with the Gly107 and Gln346 (NH$_{Gln346}$····O2′), respectively. Due

to these interactions between the ribose and the amino acid residues, the Ado$^\bullet$ cannot fully

dissociate from the coenzyme.

While it is true that the protein environment, most likely the amino acid residues

surrounding the active site, influences the labilization of the Co-C$_{5'}$ bond in MCM, it only

reduces the Co-C$_{5'}$ bond barrier by a few kcal/mol. However, this slight reduction in the

energy barrier cannot explain the unusual activation of Co-C$_{5'}$ bond homolysis inside the

enzyme, as it is believed that the energy barrier should be reduced by a factor of two to

achieve the trillion-fold rate acceleration. So the question remains, "What triggers the Co-

C$_{5'}$ bond's unique activation in the presence of substrate?"

5.3.6. Role of the Tyr residue in the activation of Co-C bond: feasibility of a PCET mechanism

Crystal structures available for AdoCbl-dependent enzymes reveal that a Tyr

residue is situated in close proximity of the AdoCbl cofactor, at an average distance of 7.5

Å from the Co atom of the corrin ring.[29, 211] The analysis of crystallographic data indicates

that substrate binding to the MCM enzyme causes a displacement of this Tyr by directing

the phenoxyl group toward the cofactor or the substrate molecule. Furthermore, a site-

specific mutation of Tyr residue in MCM resulted in a drop in the catalytic activity by a

magnitude of ~10^3-10^4.[77] This prompted us to investigate the role of Tyr residue as a redox

center in the activation of the Co-C$_{5'}$ bond in the MCM-[I-CoA]. It needs to be pointed out

that the Tyr residue has precedence of behaving as a redox center in many biological

processes, such as in cytochrome c oxidase, photosystem I/II, or ribonucleotide reductase, to exemplify just a few of them.[87-91] Thus, in the case of AdoCbl-dependent enzymatic catalysis, if TyrOH serves as a redox center, it would induce an electron transfer (ET) to the AdoCbl. Specifically, the proton transfer (PT) from the TyrOH residue coupled with the ET process via a proton-coupled electron transfer (PCET) would form AdoCbl/Tyr diradical intermediate. The formation of TyrO$^\bullet$, namely TyrOH $\rightarrow$ TyrO$^-$ $\rightarrow$ TyrO$^\bullet$, through the deprotonation of the phenoxyl group by the substrate-binding will facilitate the transfer of an electron to the AdoCbl cofactor and form a corrin-ring-based radical anion ([AdoCbl]$^{\bullet-}$). Considering the high negative redox potential of coenzyme B$_{12}$, it would be interesting to see whether the deprotonation of TyrOH residue and the formation of [AdoCbl]$^{\bullet-}$ would be energetically feasible. Moreover, it was demonstrated that the electrochemical reduction of B$_{12}$ cofactors leads to a significant reduction in the BDE of Co-C$_{5'}$ bond dissociation.[223-225] Therefore, the energetics of the formation of the [AdoCbl]$^{\bullet-}$ / TyrO$^\bullet$ diradical formation was explored to analyze the feasibility of a PCET in conjunction with the activation of the Co-C$_{5'}$ bond in the MCM-[I-CoA]. Toward this, the ONIOM-based QM/MM calculations have been carried using the structure of MCM-[I-CoA] (R2$'$ conformation, where the Co-C$_{5'}$ bond has an equilibrium distance of 2.02 Å) assuming both the neutral tyrosine (AdoCbl / TyrOH complex) and a deprotonated Tyr105 residue (AdoCbl / TyrO$^-$).

In the MCM-[I-CoA] the Tyr105 is situated in the vicinity of the I-CoA, where the phenoxyl proton of the Tyr105 (Tyr105OH) is pointed toward the COO$^-$ group of the I-CoA, and the distance of Tyr105OH $\cdots$ $^-$OOC was found 2.73 Å (Figure 5.12). A closer inspection of this structure reveals a network of H-bonding around the Tyr105 residue,

which weakens the -OH of the Tyr105 and helps in facilitating the PT to the COO^- group of the I-CoA. On the other hand, in substrate-free MCM, the Tyr105OH is pointed in the opposite direction and situated far away from the Co center. In substrate-free MCM, the corresponding distance between the Tyr105OH and the Co atom is 16.48 Å, while in MCM-[I-CoA], the Tyr105OH ···· Co distance is 7.48 Å (Figure 5.12).
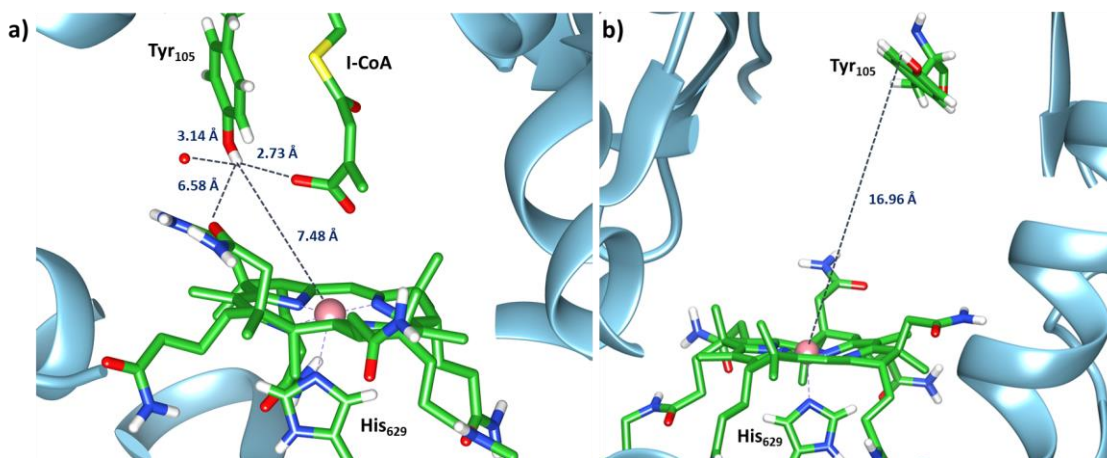
Figure 5.12. Close up of the active site showing the location of Tyr105 residue relative to the substrate and the corrin ring: (a) 6OXD-based crystal structure of MCM-[I-CoA] (b) 6OXC-based crystal structure of MCM substrate-free.

Nevertheless, to explore the feasibility of the formation of the $[AdoCbl]^{\cdot -}$ through the ET of the Tyr105, we optimized the deprotonated model or the anionic state AdoCbl / $TyrO^-$ assuming a triplet wave-function initially. No structural change has been observed in the deprotonated complex AdoCbl / $TyrO^-$ compared with the neutral AdoCbl/TyrOH complex. The triplet wave-function was then used to generate the initial guess for the $[AdoCbl]^{\cdot -}$ / $TyrO^{\cdot}$ diradical complex. Hence, a singlet state calculation has been performed using the triplet wave function on the AdoCbl / $TyrO^-$ complex assuming an unrestricted Kohn-sham formalism for allowing spin polarization inside the active site. The

analysis of the spin density distribution of the optimized structure and the associated $\langle S^2 \rangle$ value being equal to $\langle S^2 \rangle = 0.402$ indicated that the deprotonation of the Tyr residue induces the ET to the AdoCbl cofactor, consistent with the open-shell singlet electronic structure. An isosurface spin density profile was generated (Figure 5.13) to depict the spin density distribution in the diradical state. It shows that, while an unpaired electron is localized in the Tyr105 residue, the other electron is mainly delocalized in the corrin ring of the AdoCbl, which agrees with the previously reported results for the isolated model for the MCM-substrate complex.[80]
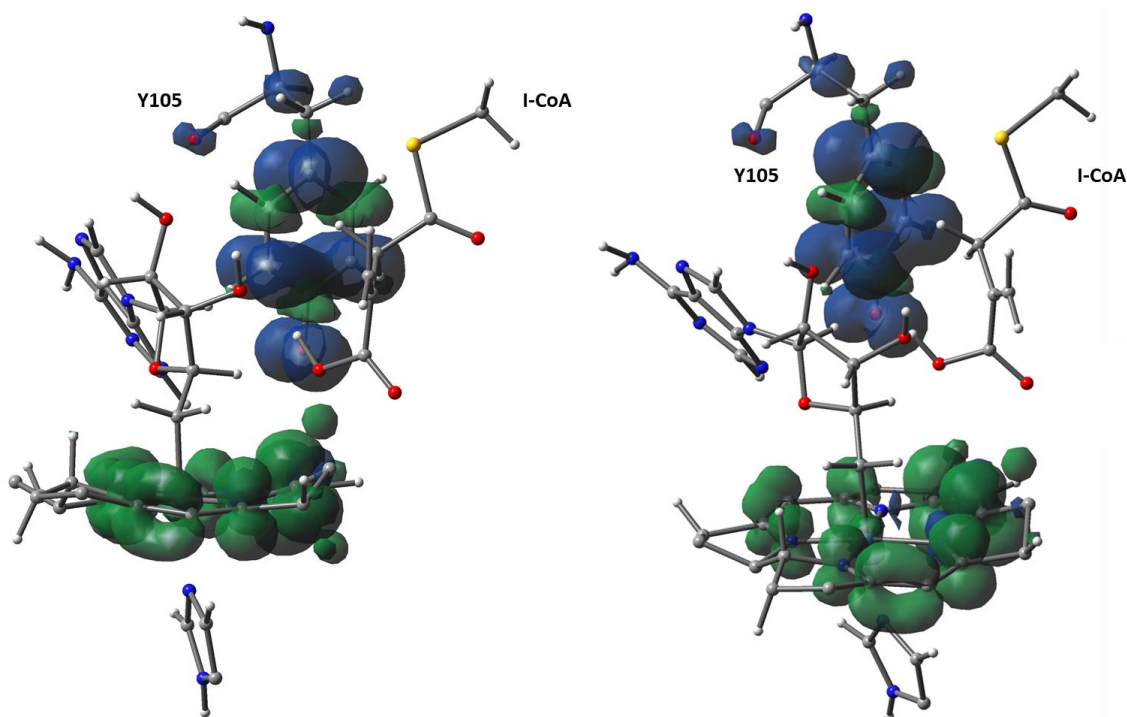
Figure 5.13. Spin density distribution in the active site models of MCM-[I-CoA] computed, where blue and green colors represent the alpha and beta spin density distributions, respectively. The spin densities have been shown from two different angles.

On the other hand, no spin-polarized solution was found for the neutral AdoCbl / TyrOH complex. Moreover, the diradical state is energetically lowered than its neutral counterpart, which indicates that the [AdoCbl]$^{\bullet -}$ / TyrO$^{\bullet}$ diradical state is the lowest

electronic state of the system. It has been demonstrated before that while the Tyr residue act as an electron-donating (nucleophilic) group, the electron-accepting (electrophilic) region is located on the corrin ring of the AdoCbl.[81] These observations indicate that the Tyr105 residue can play a crucial role in triggering the cleavage of the Co-C$_{5'}$ bond in the MCM-[I-CoA] by facilitating an ET to the AdoCbl cofactor via a PCET mechanism. According to the classical thermodynamic and Bell–Evans– Polanyi (BEP) principle,[226] there is a linear relationship between the activation energy (EA) and enthalpy of reaction (ΔH). Thus, an energetically more favorable product causes a lower reaction barrier and thus a faster reaction. However, many systems do not behave according to the BEP-like principle. It should be noted that the PCET mechanism prediction in this chapter is thermodynamic rather than kinetic. According to Marcus theory, reaction thermodynamics influence the reaction kinetics in an ET reaction. When ET reactions become very thermodynamically favorable, they slow down, resulting in a seemingly contradictory interaction of kinetics and thermodynamics.[227,228,229,230] In other words, while biological reactions involving PCET produce the most energy-efficient route, it could raise the kinetic barrier to the overall process. This is because if the free energy difference between ET and PT falls below the reorganization energy, the overall process becomes kinetically unfavorable. While this parabolic dependence has been observed for ET and PT, a more complicated relationship is observed for a concerted electron−proton transfer (EPT).[230] In EPT kinetics, the contribution of reorganization energy is more complex than for ET because it includes contributions from both transferring electron and proton. Nevertheless, while the exact mechanism of Co-C bond activation is currently under investigation, the proposed PCET is undoubtedly beneficial both from the thermodynamic and mechanistic

points of view to avoid high-energy intermediates. Thus, while the thermodynamic feasibility of the PCET process for MCM enzyme has been demonstrated in this chapter, the kinetic feasibility of the PCET driven Co-C bond activation is worth investigating and a kinetic theoretical framework needs to be established.

5.4. Conclusions

"What triggers the cleavage of the Co-$C_{5'}$ bond in AdoCbl-dependent enzymatic catalysis?" is one of the most fundamental questions in B_{12} chemistry. Using the ONIOM-based QM/MM approach, we explored the cleavage of the Co-$C_{5'}$ bond in the Ado-dependent MCM-[I-CoA] and substrate-free MCM to shed light on this long-standing conundrum. It should be mentioned that experimentally it has been shown that the activation of AdoCbl (specifically in AdoCbl-dependent mutases) is predominantly dependent on the enthalpic factor (91%) rather than the entropic factor. The most exciting outcome of our investigation was the similar BDE associated with the Co-$C_{5'}$ bond for both substrate-free MCM and MCM-[I-CoA]. This observation speaks against the previously postulated idea that a substrate-induced conformational change reduces the BDE and triggers the cleavage of the Co-$C_{5'}$ bond. While the BDE for substrate-free MCM and MCM-[I-CoA] are almost identical (22.2 kcal/mol vs. 22.7 kcal/mol, respectively), the conformation of the Ado group is different between the two models. While in MCM-[I-CoA], the ribose group undergoes a conformational change during the catalytic activation of the Co-$C_{5'}$ bond, the conformation of ribose (2′-endo) does not change along with the PEC of substrate-free MCM. The computed BDE of the homolytic cleavage of the Co-$C_{5'}$ bond in both substrate-free MCM and MCM-[I-CoA] is lower than the energy barrier associated with the PEC of isolated AdoCbl in a gas phase (29 kcal/mol) (Figure 5.9). The

reduction in BDE inside enzyme (both in the case of substrate-free MCM and MCM-[I-CoA]) indicates an electronic contribution of the protein environment on the cleavage of the Co-$C_{5'}$ bond. Upon binding with the enzyme, the AdoCbl participates in H-bonding with some active site residues. These interactions between the Ado group and the protein environment influence the labilization of the Co-$C_{5'}$ bond and reduce the barrier for the Co-$C_{5'}$ bond cleavage. However, the protein environment only reduces the barrier of the Co-$C_{5'}$ bond by a few kcal/mol. This slight reduction in the energy barrier cannot explain the trillion-fold rate acceleration of Co-$C_{5'}$ bond homolysis.

Nonetheless, in the quest for the underlying mechanism of the trillion-fold rate enhancement of Co-$C_{5'}$ bond homolysis, we have also explored the role of Tyr residue as a redox center and the feasibility of a PCET mechanism in the Co-$C_{5'}$ bond activation. It was found that the $[AdoCbl]^{\bullet-}$ / $TyrO^{\bullet}$ diradical state is the lowest electronic state of the system, which implies that the Tyr105 residue can play a crucial role in triggering the cleavage of the Co-$C_{5'}$ bond in the MCM-[I-CoA] by facilitating an ET to the AdoCbl cofactor via a PCET mechanism. Furthermore, it was demonstrated that the electrochemical reduction of B_{12} cofactors leads to a significant reduction in the BDE of the Co-$C_{5'}$ bond. Thus, based on our present calculations, it can be proposed that the Tyr105 residue present in the vicinity of the active site can act as a redox center and trigger the activation of the Co-$C_{5'}$ bond in the MCM-[I-CoA]. This hypothesis can be further explored by a site-specific mutation of the Tyr105 by phenylalanine (Phe). This kind of site-specific mutation (by replacing Tyr_{435} with a Phe) has been previously reported to demonstrate the role of Tyr in the catalytic activity of human monoamine oxidase. Thus, further

investigation to explore the crucial role of Tyr105 residue in facilitating the cleavage of the

Co-C$_{5'}$ bond would be worth pursuing.

CHAPTER VI

CONCLUSIONS AND FUTURE DIRECTIONS

Since the discovery of vitamin B_{12} almost 100 years ago, our understanding of the B_{12} cofactor and its derivatives has advanced tremendously. However, despite the advancements made over the last few decades about the structure and properties, many concerns about how B_{12}-dependent enzymes function at the molecular level remain unanswered. Moreover, with technological advancement, it is becoming evident that vitamin B_{12} and its derivatives can be used for various purposes, such as bio-fuel conversion, catalyst design, artificial enzyme design, to name a few.[49,114-115] AdoCbl-dependent enzymes, for example, use radical chemistry to catalyze chemically critical processes like alcohol to aldehyde conversion and glycerol dehydration, which has gained much importance in response to growing concerns about climate change and resulting in an oversupply of glycerol. In this situation, converting glycerol to one of its numerous viable precursors is critical. Therefore, the conversion of glycerol to 1,3-propanediol has garnered a lot of interest in recent years.[16, 114] For catalyzing this type of reaction, AdoCbl-dependent enzymes use radical-based chemistry. Hence, understanding the underlying mechanism of the B_{12}-dependent reaction is one of the most critical factors in applying to these disciplines.

The most crucial step in these catalytic reactions is to reduce the activation energy to a certain extent while significantly increasing the rate of reactions to enable the production of radical pairs. In the enzymatic context of radical pair production, exercise strict control over the radicals to catalyze these chemically significant processes. As a result, many enzymes could be employed as green catalysts that demand a thorough understanding of B_{12}-dependent processes. Furthermore, the B_{12}-dependent systems also possess complex photolytic properties through the light-sensitive Co-C bond. Studies have revealed that the light sensitivity of B_{12}-dependent systems can be used to develop phototherapeutic applications.[116-117] The phototherapeutic has a wide range of applications, from cancer therapy to tissue engineering; therefore, theoretical understanding of the photoactivation of the Co-C bond is crucial. Thus, the activation of the Co-C bond in B_{12}-dependent native catalytic and photolytic reactions has been investigated from a computational perspective.

A substantial portion of the work presented in this dissertation was devoted to investigating the activation of the Co-C bond in B_{12}-dependent enzymes and how the enzymatic environment influences the photolysis of the B_{12} cofactor, such as MeCbl. The photoactivation of the Co-C bond and the photolytic properties of MeCbl depend on the cofactor's environment, whether it is in solution or inside the enzymatic environment. The DFT/MM and TD-DFT/MM study has shown that the enzyme protects the MeCbl cofactor against photolysis. It proposed that the protein environment prevents the photodissociation of organometallic Co-C bonds by destabilizing the LF electronic state, which could plausibly affect the formation of $Co(II)/CH_3$ RP in the LF state and alter the photochemical yield of cob(II)alamin. The hydrophobic residues of the cap domain that surrounds the

upper face (or β face) of the MeCbl cofactor protect the photolysis of MeCbl by caging the methyl radical and inducing the geminate recombination of the Co(II)/CH$_3$ RP. We also explored that the mutation of this cap domain (F708A) can further alter the photolysis of enzyme-bound MeCbl in three possible ways: (1) changing the photochemical yield of Co(II)/CH$_3$ RP by increasing the energy difference between MLCT and LF minima. The energy difference between MLCT and LF minima for WT-MetH is almost three times higher than its mutant counterpart (F708-MetH). (2) The mutation of F708A also decreases the energy barrier for photoreaction. (3) The mutation decreases the rate of geminate recombination. For F708A-MetH, the deactivation rate constant is almost 20% lower than WT-MetH, indicating a higher photolysis rate. These observations are consistent with the experimental findings, which reported a significant rate enhancement of photolysis by ~ 62-fold for F708A-MetH. Considering all of these, we can conclude that mutation in the cap domain of the Cbl-binding module of MetH can influence the photoactivation of the Co-C bond in enzyme-bound MeCbl by altering the rate of photolysis. This theoretical insight can also be helpful to investigate further the effect of the mutation on the photolytic properties of vitamin B$_{12}$-dependent enzymes.

Apart from the nature of axial ligands and the cofactor's environment, the photochemical and photophysical properties of Cbls can also be modulated in the presence of molecular oxygen, i.e., in aerobic conditions. Whereas many experimental and computational investigations have been carried out to explore the inherent mechanism of the anaerobic photolysis of Cbls, the mechanism of the photodissociation of the Co-C bond in the presence of oxygen is still not well explored. Our DFT/TD-DFT calculations revealed that when the Im-[Co^{III}(corrin)]-CH$_3^+$ + O$_2$ system is photoexcited, the MLCT

electronic state is formed, followed by the LF electronic state. Three steps can occur from the LF excited state. The first step is the production of OO-CH$_3$ by reacting CH$_3$ with molecular oxygen. Second, by shifting the electronic configuration from $(d_{yz})^1(d_{z^2})^2$ to $(d_{yz})^2(d_{z^2})$, the Im[Co^{II}(corrin)]CH$_3^+$ sub-system is deactivated from the LF electronic state. Finally, the deactivation complex is formed via the recombination of OO-CH$_3$ species with the de-excited [Co^{II}(corrin)] system. The role of light, in this case, is to activate the Co-C bond.

A portion of this dissertation was also devoted to investigating the catalytic origin and unusual activation of the Co-C bond in the native catalysis of AdoCbl-dependent mutases. We investigated the cleavage of the Co-C5 bond in the Ado-dependent MCM-[I-CoA] and substrate-free MCM using the ONIOM-based QM/MM technique to shed light on this long-standing puzzle. The most intriguing finding of our research was that both substrate-free MCM and MCM-[I-CoA] have similar BDE linked with the Co-C5 bond.[231] This finding contradicts the previously held belief that a substrate-induced conformational change lowers the BDE and causes the Co-C$_5$ bond to be cleaved. The BDE for substrate-free MCM and MCM-[I-CoA] is nearly identical (22.2 kcal/mol vs. 22.7 kcal/mol, respectively),[231] although the Ado group structure differs between the two models. The computed BDE of the cleavage of the Co-C$_{5'}$ bond in both substrate-free MCM and MCM-[I-CoA] is lower than the energy barrier associated with the PEC of isolated AdoCbl in a gas phase (29 kcal/mol). This slight reduction in BDE can not explain the trillionfold rate enhancement of the Co-C bond. This observation puts into question previously reported hypotheses that substrate-induced conformational changes reduce the BDE and trigger the cleavage of the Co-C$_{5'}$ bond.[76, 84] Present QM/MM results also indicate that the energy

barrier for homolytic cleavage of the Co-C$_{5'}$ bond in both substrate-free MCM and MCM-[I-CoA] is lower than the energy barrier for the isolated cofactor. While the protein environment reduces the barrier for the Co-C$_{5'}$ bond cleavage, the reduction to the energy barrier is too small to fully explain the trillion-fold rate acceleration. So, we also explored the role of Tyr105 as a redox center and the feasibility of a PCET mechanism. It was found that the [AdoCbl]$^{\bullet-}$ / TyrO$^{\bullet}$ diradical state is the lowest electronic state implying that the Tyr105 residue can play a crucial role in triggering the cleavage of the Co-C$_{5'}$ bond in MCM-[I-CoA] by facilitating an electron transfer (ET) to the AdoCbl cofactor via a PCET mechanism.

REFERENCES

1.   Minot, G. R.; Murphy, W. P., Treatment of pernicious anemia by a special diet. **1926**. *Yale J. Biol. Med.* **2001,** *74* (5), 341-353.

2.   Dolphin, D., *B_{12}*. John Wiley & Sons: New York, **1982**.

3.   Rickes Edward, L.; Brink Norman, G.; Koniuszy Frank, R.; Wood Thomas, R.; Folkers, K., Crystalline Vitamin B_{12}. *Science* **1948,** *107* (2781), 396-397.

4.   Dorothy Crowfoot Hodgkin, F. R. S., June Lindsey, Maureen Mackay, K. N. Trueblood, The structure of vitamin B_{12}- IV. The X-ray analysis of air-dried crystals of B_{12}. *Proc. R. Soc. London, Ser. A* **1962,** *266* (1327), 475.

5.   Barker, H. A.; Smyth, R. D.; Weissbach, H.; Toohey, J. I.; Ladd, J. N.; Volcani, B. E., Isolation and properties of crystalline cobamide coenzymes containing benzimidazole or 5, 6-dimethylbenzimidazole. *J. Biol. Chem.* **1960,** *235*, 480-8.

6.   Hodgkin, D. C.; Kamper, J.; Mackay, M.; Pickworth, J.; Trueblood, K. N.; White, J. G., Structure of Vitamin B_{12}. *Nature* **1956,** *178* (4524), 64-66.

7.   Woodward, R. B., The total synthesis of vitamin B_{12}. *Pure Appl. Chem.* **1973,** *33* (1), 145-178.

8.   Krautler, B. A., D., Golding, B. T., *Vitamin B_{12} and B_{12}-Proteins*. Wiley-VCH: Weinheim, 1998.

9.   Rodionov, D. A.; Vitreschak, A. G.; Mironov, A. A.; Gelfand, M. S., Comparative genomics of the vitamin B_{12} metabolism and regulation in prokaryotes. *J. Biol. Chem.* **2003,** *278* (42), 41148-59.

10.   Geremia, S.; Randaccio, L.; Marzilli, L. G., 3.16 - B_{12} Enzymes, Function, and Small Molecules as Models. In *Comprehensive Inorganic Chemistry II (Second Edition)*, Reedijk, J.; Poeppelmeier, K., Eds. Elsevier: Amsterdam, **2013**; pp 423-453.

11.   Banerjee, R.; Gherasim, C.; Padovani, D., The tinker, tailor, soldier in intracellular B_{12} trafficking. *Curr. Opin. Chem. Biol.* **2009,** *13* (4), 484-491.

12.   Banerjee, R., *Chemistry and Biochemistry of B_{12}.* Wiley: New York, **1999**.

13.   Banerjee, R. P. a. R., Evidence from Electron Paramagnetic Resonance Spectroscopy of the Participation of Radical Intermediates in the Reaction Catalyzed by Methylmalonyl-coenzyme A Mutase. *J. Biol. Chem.* **1995,** *270*, 9295-9300.

14.   Banerjee, R., Radical Carbon Skeleton Rearrangements: Catalysis by Coenzyme B_{12}-Dependent Mutases. *Chem. Rev.* **2003,** *103* (6), 2083.

15.   Banerjee, R., Radical Peregrinations Catalyzed by Coenzyme B_{12}-Dependent Enzymes. *Biochemistry* **2001,** *40* (21), 6191-6198.

16.   Roth, J. R.; Lawrence, J. G.; Bobik, T. A., Cobalamin (coenzyme B_{12}): synthesis and biological significance. *Annu. Rev. Microbiol.* **1996,** *50*, 137-81.

17.   Banerjee, R. V.; Matthews, R. G., Cobalamin-dependent methionine synthase. *FASEB J.* **1990,** *4* (5), 1450-1459.

18. Goulding, C. W.; Postigo, D.; Matthews, R. G., Cobalamin-Dependent Methionine Synthase Is a Modular Protein with Distinct Regions for Binding Homocysteine, Methyltetrahydrofolate, Cobalamin, and Adenosylmethionine. *Biochemistry* **1997,** *36* (26), 8082-8091.

19. Degnan, P. H.; Taga, M. E.; Goodman, A. L., Vitamin B_{12} as a modulator of gut microbial ecology. *Cell. Metab.* **2014,** *20* (5), 769-778.

20. Hodgkin, D. C.; Pickworth, J.; Robertson, J. H.; Trueblood, K. N.; Prosen, R. J.; White, J. G., Structure of Vitamin B_{12} : The Crystal Structure of the Hexacarboxylic Acid derived from B_{12} and the Molecular Structure of the Vitamin. *Nature* **1955,** *176* (4477), 325-328.

21. Ouyang, L.; Rulis, P.; Ching, W.-Y.; Slouf, M.; Nardin, G.; Randaccio, L., Electronic structure and bonding in hydroxocobalamin. *Spectrochim. Acta, Part A* **2005,** *61* (7), 1647-1652.

22. Randaccio, L.; Geremia, S.; Nardin, G.; Wuerges, J., X-ray structural chemistry of cobalamins. *Coord. Chem. Rev.* **2006,** *250* (11), 1332-1350.

23. Randaccio, L.; Furlan, M.; Geremia, S.; Šlouf, M.; Srnova, I.; Toffoli, D., Similarities and Differences between Cobalamins and Cobaloximes. Accurate Structural Determination of Methylcobalamin and of LiCl- and KCl-Containing Cyanocobalamins by Synchrotron Radiation. *Inorg. Chem.* **2000,** *39* (15), 3403-3413.

24. Geno, M. K.; Halpern, J., Why does nature not use the porphyrin ligand in vitamin B_{12}? *J. Am. Chem. Soc.* **1987,** *109* (4), 1238-1240.

25.   Yoshizawa, K.; Nakayama, T.; Kamachi, T.; Kozlowski, P. M., Vibronic Interaction in Metalloporphyrin π-Anion Radicals. *J. Phys. Chem. A* **2007,** *111* (5), 852-857.

26.   Andruniow, T.; Kozlowski, P. M.; Zgierski, M. Z., Theoretical analysis of electronic absorption spectra of vitamin B_{12} models. *J. Chem. Phys.* **2001,** *115* (16), 7522-7533.

27.   Kurmaev, E. Z.; Moewes, A.; Ouyang, L.; Randaccio, L.; Rulis, P.; Ching, W. Y.; Bach, M.; Neumann, M., The electronic structure and chemical bonding of vitamin B_{12}. *Europhys. Lett.* **2003,** *62* (4), 582.

28.   Randaccio, L.; Geremia, S.; Demitri, N.; Wuerges, J., Vitamin B_{12}: Unique Metalorganic Compounds and the Most Complex Vitamins. *Molecules* **2010,** *15* (5), 3228-3259.

29.   Drennan, C. L.; Huang, S.; Drummond, J. T.; Matthews, R. G.; Lidwig, M. L., How a protein binds B_{12}: A 3.0 A X-ray structure of B_{12}-binding domains of methionine synthase. *Science* **1994,** *266* (5191), 1669-74.

30.   Eisenberg, A. S.; Likhtina, I. V.; Znamenskiy, V. S.; Birke, R. L., Electronic Spectroscopy and Computational Studies of Glutathionylco(III)balamin. *J. Phys. Chem. A* **2012,** *116* (25), 6851-6869.

31.   Kräutler, B., Chapter 20 - Biological Organometallic Chemistry of Vitamin B_{12}-Derivatives. In *Advances in Bioorganometallic Chemistry*, Hirao, T.; Moriuchi, T., Eds. Elsevier: 2019; pp 399-430.

32.   Kräutler, B., Vitamin B$_{12}$: chemistry and biochemistry. *Biochem. Soc. Trans.* **2005,** *33* (4), 806-810.

33.   Banerjee, R., The Yin-Yang of cobalamin biochemistry. *Chem. Biol.* **1997,** *4* (3), 175-186.

34.   Banerjee, R.; Ragsdale, S. W., The many faces of vitamin B12: catalysis by cobalamin-dependent enzymes. *Annu. Rev. Biochem.* **2003,** *72*, 209-47.

35.   Bhongir Aparna, V.; Srilatha, B.; Rajagopalan, V.; Kumar Sai, S., Folic acid, Vitamin B$_{12}$, and DNA methylation: an update. *Asian J. Pharm. Clin. Res.* **2018,** *11* (1).

36.   Bonnett, R., The Chemistry of the Vitamin B$_{12}$ Group. *Chem. Rev.* **1963,** *63* (6), 573-605.

37.   Brearley, A. E.; Gott, H.; Hill, H. A. O.; O'Riordan, M.; Pratt, J. M.; Williams, R. J. P., The chemistry of vitamin B$_{12}$. Part XIV. Reaction of vitamin B$_{12}$s with nitrobenzene and its reduction products. *J. Chem. Soc. A* **1971,** (0), 612-614.

38.   Bridwell-Rabb, J.; Drennan, C. L., Vitamin B$_{12}$ in the spotlight again. *Curr. Opin. Chem. Biol.* **2017,** *37*, 63-70.

39.   Brown, K. L., Chemistry and Enzymology of Vitamin B$_{12}$. *Chem. Rev.* **2005,** *105* (6), 2075-2150.

40.   Das, P. K.; Hill, H. A. O.; Pratt, J. M.; Williams, R. J. P., The chemistry of vitamin B$_{12}$. Part VIII. Controlled potential reduction of vitamin B12a. *J. Chem. Soc. A* **1968,** (0), 1261-1264.

41.   Dolphin, D., *B₁₂ Volume 1: Chemistry*. John Wiley & Sons, New York: 1982; Vol. 1.

42.   Giedyk, M.; Goliszewska, K.; Gryko, D., Vitamin B_{12} catalysed reactions. *Chem. Soc. Rev.* **2015,** *44* (11), 3391-404.

43.   Brooks, A. J.; Vlasie, M.; Banerjee, R.; Brunold, T. C., Co-C bond activation in methylmalonyl-CoA mutase by stabilization of the post-homolysis product Co^{2+} cobalamin. *J. Am. Chem. Soc.* **2005,** *127* (47), 16522-8.

44.   Fink, R. G., Coenzyme B_{12}-Based Chemical Precedent for Co-C Bond Homolysis and Other Key Elementary Steps. In *Vitamin B₁₂ and B₁₂-Proteins*, 1998; pp 383-402.

45.   Finke, R. G.; Martin, B. D., Coenzyme $AdoB_{12}$ vs $AdoB_{12}$-homolytic Co-C cleavage following electron transfer: a rate enhancement greater than or equal to $10^{(12)}$. *J. Inorg. Biochem.* **1990,** *40* (1), 19-22.

46.   Frey, P. A.; Reed, G. H., Radical mechanisms in adenosylmethionine- and adenosylcobalamin-dependent enzymatic reactions. *Arch. Biochem. Biophys.* **2000,** *382* (1), 6-14.

47.   Marsh, E. N.; Melendez, G. D., Adenosylcobalamin enzymes: theory and experiment begin to converge. *Biochim. Biophys. Acta* **2012,** *1824* (11), 1154-64.

48.   Marsh, E. N.; Patterson, D. P.; Li, L., Adenosyl radical: reagent and catalyst in enzyme reactions. *Chembiochem* **2010,** *11* (5), 604-21.

49.   Costentin, C.; Robert, M.; Savéant, J.-M., Does Catalysis of Reductive Dechlorination of Tetra- and Trichloroethylenes by Vitamin B_{12} and Corrinoid-Based Dehalogenases Follow an Electron Transfer Mechanism? *J. Am. Chem. Soc.* **2005,** *127* (35), 12154-12155.

50.   Liao, R.-Z.; Chen, S.-L.; Siegbahn, P. E. M., Unraveling the Mechanism and Regioselectivity of the B_{12}-Dependent Reductive Dehalogenase PceA. **2016,** *22* (35), 12391-12399.

51.   Matthews, R. G., Cobalamin- and Corrinoid-Dependent Enzymes. *Metal ions in life sciences* **2009,** *6*, 53-114.

52.   Krone, U. E.; Laufer, K.; Thauer, R. K.; Hogenkamp, H. P., Coenzyme F430 as a possible catalyst for the reductive dehalogenation of chlorinated C1 hydrocarbons in methanogenic bacteria. *Biochemistry* **1989,** *28* (26), 10061-5.

53.   Krone, U. E.; Thauer, R. K.; Hogenkamp, H. P. C., Reductive dehalogenation of chlorinated C1-hydrocarbons mediated by corrinoids. *Biochemistry* **1989,** *28* (11), 4908-4914.

54.   Banerjee, R., B_{12} Trafficking in Mammals: A Case for Coenzyme Escort Service. *ACS Chem. Biol.* **2006,** *1* (3), 149-159.

55.   Matthews, R. G., Cobalamin-Dependent Methyltransferases. *Acc. Chem. Res.* **2001,** *34* (8), 681-689.

56.   Matthews, R. G.; Koutmos, M.; Datta, S., Cobalamin-dependent and cobamide-dependent methyltransferases. *Curr. Opin. Struct. Biol.* **2008,** *18* (6), 658-666.

57.   Banerjee, R., Radical Carbon Skeleton Rearrangements: Catalysis by Coenzyme B$_{12}$-Dependent Mutases. *Chem. Rev.* **2003,** *103* (6), 2083-2094.

58.   Russell-Jones, G.; McTavish, K.; McEwan, J.; Rice, J.; Nowotnik, D., Vitamin-mediated targeting as a potential mechanism to increase drug uptake by tumours. *J. Inorg. Biochem.* **2004,** *98* (10), 1625-1633.

59.   Waibel, R.; Treichler, H.; Schaefer, N. G.; van Staveren, D. R.; Mundwiler, S.; Kunze, S.; Kuenzi, M.; Alberto, R.; Nuesch, J.; Knuth, A.; Moch, H.; Schibli, R.; Schubiger, P. A., New derivatives of vitamin B$_{12}$ show preferential targeting of tumors. *Cancer Res.* **2008,** *68* (8), 2904-11.

60.   Broderick, W. E.; Hoffman, B. M.; Broderick, J. B., Mechanism of Radical Initiation in the Radical S-Adenosyl-l-methionine Superfamily. *Acc. Chem. Res.* **2018,** *51* (11), 2611-2619.

61.   Reed, G. H., Radical mechanisms in adenosylcobalamin-dependent enzymes. *Curr. Opin. Struct. Biol.* **2004,** *8* (5), 477-83.

62.   Gruber, K.; Puffer, B.; Kräutler, B., Vitamin B$_{12}$-derivatives—enzyme cofactors and ligands of proteins and nucleic acids. *Chem. Soc. Rev.* **2011,** *40* (8), 4346-4363.

63.   Marsh, E. N.; Ballou, D. P., Coupling of cobalt-carbon bond homolysis and hydrogen atom abstraction in adenosylcobalamin-dependent glutamate mutase. *Biochemistry* **1998,** *37* (34), 11864-72.

64.   Huhta, M. S.; Chen, H.-P.; Hemann, C.; Hille, C. R.; Marsh, E. N. G., Protein–coenzyme interactions in adenosylcobalamin-dependent glutamate mutase. *Biochem. J.* **2001,** *355* (1), 131-137.

65.   Semialjac, M.; Schwarz, H., Computational Exploration of Rearrangements Related to the Vitamin B_{12}-Dependent Ethanolamine Ammonia Lyase Catalyzed Transformation. *J. Am. Chem. Soc.* **2002,** *124* (30), 8974-8983.

66.   Semialjac, M. a. S. H., Computational Study on Mechanistic Details of the Aminoethanol Rearrangement Catalyzed by the Vitamin B_{12}-Dependent Ethanolamine Ammonia Lyase: His and Asp/Glu Acting Simultaneously as Catalytic Auxiliaries. *J. Org. Chem.* **2003,** *68*, 6967-6983.

67.   Chowdhury, S.; Banerjee, R., Thermodynamic and Kinetic Characterization of Co−C Bond Homolysis Catalyzed by Coenzyme B_{12}-Dependent Methylmalonyl-CoA Mutase. *Biochemistry* **2000,** *39* (27), 7998-8006.

68.   Hay, B. P.; Finke, R. G., Thermolysis of the cobalt-carbon bond in adenosylcorrins. 3. Quantification of the axial base effect in adenosylcobalamin by the synthesis and thermolysis of axial base-free adenosylcobinamide. Insights into the energetics of enzyme-assisted cobalt-carbon bond homolysis. *J. Am. Chem. Soc.* **1987,** *109* (26), 8012-8018.

69.   Hay, B. P.; Finke, R. G., Thermolysis of the cobalt-carbon bond of adenosylcobalamin. 2. Products, kinetics, and cobalt-carbon bond dissociation energy in aqueous solution. *J. Am. Chem. Soc.* **1986,** *108* (16), 4820-4829.

70.   Doll, K. M.; Finke, R. G., A Compelling Experimental Test of the Hypothesis That Enzymes Have Evolved To Enhance Quantum Mechanical Tunneling in Hydrogen Transfer Reactions: The β-Neopentylcobalamin System Combined with Prior Adocobalamin Data. *Inor. Chem.* **2003,** *42* (16), 4849-4856.

71.   Sharma, P. K.; Chu, Z. T.; Olsson, M. H. M.; Warshel, A., A new paradigm for electrostatic catalysis of radical reactions in vitamin B_{12} enzymes. *Proc. Natl. Acad. Sci.* **2007,** *104* (23), 9661.

72.   Warshel, A.; Levitt, M., Theoretical studies of enzymic reactions: dielectric, electrostatic and steric stabilization of the carbonium ion in the reaction of lysozyme. *J. Mol. Biol.* **1976,** *103* (2), 227-49.

73.   De Ridder, D. J. A.; Zangrando, E.; Bürgi, H.-B., Structural behaviour of cobaloximes: planarity, an anomalous trans-influence and possible implications on Co-C bond cleavage in coenzyme-B_{12}-dependent enzymes. *J. Mol. Struct.: THEOCHEM* **1996,** *374* (1), 63-83.

74.   Bresciani-Pahor, N.; Forcolin, M.; Marzilli, L. G.; Randaccio, L.; Summers, M. F.; Toscano, P. J., Organocobalt B_{12} models: axial ligand effects on the structural and coordination chemistry of cobaloximes. *Coord. Chem. Rev.* **1985,** *63*, 1-125.

75.   Mancia, F.; Evans, P. R., Conformational changes on substrate binding to methylmalonyl CoA mutase and new insights into the free radical mechanism. *Structure* **1998,** *6* (6), 711-720.

76.   Toraya, T.; Ishida, A., Acceleration of cleavage of the carbon-cobalt bond of sterically hindered alkylcobalamins by binding to apoprotein of diol dehydrase. *Biochemistry* **1988,** *27* (20), 7677-7681.

77.   Vlasie, M. D.; Banerjee, R., Tyrosine 89 accelerates Co-carbon bond homolysis in methylmalonyl-CoA mutase. *J. Am. Chem. Soc.* **2003,** *125* (18), 5431-5.

78.   Alfonso-Prieto, M.; Biarnés, X.; Kumar, M.; Rovira, C.; Kozlowski, P. M., Reductive Cleavage Mechanism of Co−C Bond in Cobalamin-Dependent Methionine Synthase. *J. Phys. Chem. B* **2010,** *114* (40), 12965-12971.

79.   Kozlowski, P. M.; Kamachi, T.; Kumar, M.; Nakayama, T.; Yoshizawa, K., Theoretical Analysis of the Diradical Nature of Adenosylcobalamin Cofactor−Tyrosine Complex in B_{12}-Dependent Mutases: Inspiring PCET-Driven Enzymatic Catalysis. *J. Phys. Chem. B* **2010,** *114* (17), 5928-5939.

80.   Kumar, M.; Kozlowski, P. M., Role of Tyrosine Residue in the Activation of Co−C Bond in Coenzyme B_{12}-Dependent Enzymes: Another Case of Proton-Coupled Electron Transfer? *J. Phys. Chem. B* **2009,** *113* (27), 9050-9054.

81.   Kumar, N.; Liu, S.; Kozlowski, P. M., Charge Separation Propensity of the Coenzyme B_{12}–Tyrosine Complex in Adenosylcobalamin-Dependent Methylmalonyl–CoA Mutase Enzyme. *J. Phys. Chem. Lett.* **2012,** *3* (8), 1035-1038.

82.   Grate, J. H.; Schrauzer, G. N., Chemistry of cobalamins and related compounds. 48. Sterically induced, spontaneous dealkylation of secondary alkylcobalamins due to axial base coordination and conformational changes of the corrin ligand. *J. Am. Chem. Soc.* **1979,** *101* (16), 4601-4611.

83.   Brown, K. L., The enzymatic activation of coenzyme B_{12}. *Dalton Trans.* **2006,** (9), 1123-1133.

84.   Masuda, J.; Shibata, N.; Morimoto, Y.; Toraya, T.; Yasuoka, N., How a protein generates a catalytic radical from coenzyme $B_{(12)}$: X-ray structure of a diol-dehydratase-adeninylpentylcobalamin complex. *Structure (London, England : 1993)* **2000,** *8* (7), 775-788.

85.   Toraya, T., Enzymatic Radical Catalysis: Coenzyme B_{12}-Dependent Diol Dehydratase. *Chem. Rec.* **2002,** *2* (5), 352-366.

86.   Mancia, F.; Keep, N. H.; Nakagawa, A.; Leadlay, P. F.; McSweeney, S.; Rasmussen, B.; secke, P. B.; Diat, O.; Evans, P. R., How coenzyme B_{12} radicals are generated: the crystal structure of methylmalonyl-coenzyme A mutase at 2 å resolution. *Structure* **1996,** *4* (3), 339-350.

87.   Pesavento, R. P.; Van Der Donk, W. A., Tyrosyl radical cofactors. In *Advances in Protein Chemistry*, Academic Press: 2001; Vol. 58, pp 317-385.

88.   Barry, B. A.; Babcock, G. T., Tyrosine radicals are involved in the photosynthetic oxygen-evolving system. *Proc. Natl. Acad. Sci.* **1987,** *84* (20), 7099.

89. Lee, Y.-K.; Whittaker, M. M.; Whittaker, J. W., The Electronic Structure of the Cys-Tyr• Free Radical in Galactose Oxidase Determined by EPR Spectroscopy. *Biochemistry* **2008,** *47* (25), 6637-6649.

90. Ferguson-Miller, S.; Babcock, G. T., Heme/Copper Terminal Oxidases. *Chem. Rev.* **1996,** *96* (7), 2889-2908.

91. Marohnic, C. C.; Crowley, L. J.; Davis, C. A.; Smith, E. T.; Barber, M. J., Cytochrome b5 Reductase: Role of the si-Face Residues, Proline 92 and Tyrosine 93, in Structure and Catalysis. *Biochemistry* **2005,** *44* (7), 2449-2461.

92. Barker, H. A.; Weissbach, H.; Smyth, R. D., A coenzyme containing pseudoivitamin B$_{(12)}$. *Proc. Natl. Acad. Sci. U. S. A.* **1958,** *44* (11), 1093-1097.

93. Weissbach, H.; Ladd, J. N.; Volcani, B. E.; Smyth, R. D.; Barker, H. A., Structure of the adenylcobamide coenzyme: degradation by cyanide, acid, and light. *J. Biol. Chem.* **1960,** *235*, 1462-73.

94. Pratt, J. M., 988. The chemistry of vitamin B12. Part II. Photochemical reactions. *J. Chem. Soc. (Resumed)* **1964,** (0), 5154-5160.

95. Pratt, J. M.; Whitear, B. R. D., Photolysis of methylcobalamin. *J. Chem. Soc. A* **1971,** (0), 252-255.

96. Jarrett, J. T.; Drennan, C. L.; Amaratunga, M.; Scholten, J. D.; Ludwig, M. L.; Matthews, R. G., A protein radical cage slows photolysis of methylcobalamin in methionine synthase from Escherichia coli. *Bioorg. Med. Chem.* **1996,** *4* (8), 1237-46.

97.   Walker, L. A.; Jarrett, J. T.; Anderson, N. A.; Pullen, S. H.; Matthews, R. G.; Sension, R. J., Time-Resolved Spectroscopic Studies of B_{12} Coenzymes: The Identification of a Metastable Cob(III)alamin Photoproduct in the Photolysis of Methylcobalamin. *J. Am. Chem. Soc.* **1998,** *120* (15), 3597-3603.

98.   Allwyn G. Cole, L. M. Y., Joseph J. Shiang, Neil A. Anderson, Larry A. Walker, II, Mark M. Banaszak Holl, and Roseanne J. Sension, Time-Resolved Spectroscopic Studies of B_{12} Coenzymes: A Comparison of the Primary Photolysis Mechanism in Methyl-,Ethyl-, *n*-Propyl-, and 5'-Deoxyadenosylcobalamin. *J. Am. Chem. Soc.* **2001,** *124* (3), 434-441.

99.   Sension, R. J.; Harris, D. A.; Stickrath, A.; Cole, A. G.; Fox, C. C.; Marsh, E. N., Time-resolved measurements of the photolysis and recombination of adenosylcobalamin bound to glutamate mutase. *J. Phys. Chem. B.* **2005,** *109* (38), 18146-52.

100.   Shiang, J. J.; Walker, L. A.; Anderson, N. A.; Cole, A. G.; Sension, R. J., Time-Resolved Spectroscopic Studies of B_{12} Coenzymes: The Photolysis of Methylcobalamin Is Wavelength Dependent. *J. Phys. Chem. B* **1999,** *103* (47), 10532-10539.

101.   Walker, L. A.; Shiang, J. J.; Anderson, N. A.; Pullen, S. H.; Sension, R. J., Time-Resolved Spectroscopic Studies of B_{12} Coenzymes: The Photolysis and Geminate Recombination of Adenosylcobalamin. *J. Am. Chem. Soc.* **1998,** *120* (29), 7286-7292.

102.   Robertson, W. D.; Warncke, K., Photolysis of adenosylcobalamin and radical pair recombination in ethanolamine ammonia-lyase probed on the micro- to millisecond time

scale by using time-resolved optical absorption spectroscopy. *Biochemistry* **2009,** *48* (1), 140-7.

103.   Warncke, K.; Utada, A. S., Interaction of the substrate radical and the 5'-deoxyadenosine-5'-methyl group in vitamin $B_{(12)}$ coenzyme-dependent ethanolamine deaminase. *J. Am. Chem. Soc.* **2001,** *123* (35), 8564-72.

104.   Robertson, W. D.; Wang, M.; Warncke, K., Characterization of protein contributions to cobalt-carbon bond cleavage catalysis in adenosylcobalamin-dependent ethanolamine ammonia-lyase by using photolysis in the ternary complex. *J. Am. Chem. Soc.* **2011,** *133* (18), 6968-77.

105.   Jones, A. R.; Hardman, S. J. O.; Hay, S.; Scrutton, N. S., Is There a Dynamic Protein Contribution to the Substrate Trigger in Coenzyme B_{12}-Dependent Ethanolamine Ammonia Lyase? *Angew. Chem., Int. Ed.* **2011,** *50* (46), 10843-10846.

106.   Jones, A. R.; Levy, C.; Hay, S.; Scrutton, N. S., Relating localized protein motions to the reaction coordinate in coenzyme B_{12}-dependent enzymes. *FEBS J.* **2013,** *280* (13), 2997-3008.

107.   Ortiz-Guerrero, J. M.; Polanco, M. C.; Murillo, F. J.; Padmanabhan, S.; Elías-Arnanz, M., Light-dependent gene regulation by a coenzyme B_{12}-based photoreceptor. *Proc. Natl. Acad. Sci.* **2011,** *108* (18), 7565.

108.   Padmanabhan, S.; Jost, M.; Drennan, C. L.; Elías-Arnanz, M., A New Facet of Vitamin B_{12}: Gene Regulation by Cobalamin-Based Photoreceptors. *Annu. Rev. Biochem.* **2017,** *86* (1), 485-514.

109.   Padmanabhan, S.; Pérez-Castaño, R.; Elías-Arnanz, M., B_{12}-based photoreceptors: from structure and function to applications in optogenetics and synthetic biology. *Curr. Opin. Struct. Biol.* **2019,** *57*, 47-55.

110.   Jost, M.; Fernandez-Zapata, J.; Polanco, M. C.; Ortiz-Guerrero, J. M.; Chen, P. Y.; Kang, G.; Padmanabhan, S.; Elias-Arnanz, M.; Drennan, C. L., Structural basis for gene regulation by a B_{12}-dependent photoreceptor. *Nature* **2015,** *526* (7574), 536-41.

111.   Jost, M.; Simpson, J. H.; Drennan, C. L., The Transcription Factor CarH Safeguards Use of Adenosylcobalamin as a Light Sensor by Altering the Photolysis Products. *Biochemistry* **2015,** *54* (21), 3231-3234.

112.   Zelder, F.; Zhou, K.; Sonnay, M., Peptide B_{12}: emerging trends at the interface of inorganic chemistry, chemical biology and medicine. *Dalton trans.* **2013,** *42* (4), 854-62.

113.   Bucher, D.; Sandala, G. M.; Durbeej, B.; Radom, L.; Smith, D. M., The Elusive 5′-Deoxyadenosyl Radical in Coenzyme-B_{12}-Mediated Reactions. *J. Am. Chem. Soc.* **2012,** *134* (3), 1591-1599.

114.   Lee, J. H.; Jung, M.-Y.; Oh, M.-K., High-yield production of 1,3-propanediol from glycerol by metabolically engineered Klebsiella pneumoniae. *Biotechnol. Biofuels* **2018,** *11* (1), 104.

115.   Smith, W. J.; Oien, N. P.; Hughes, R. M.; Marvin, C. M.; Rodgers, Z. L.; Lee, J.; Lawrence, D. S., Cell-Mediated Assembly of Phototherapeutics. *Angew. Chem., Int. Ed.* **2014,** *53* (41), 10945-10948.

116. Shell, T. A.; Shell, J. R.; Rodgers, Z. L.; Lawrence, D. S., Tunable Visible and Near-IR Photoactivation of Light-Responsive Compounds by Using Fluorophores as Light-Capturing Antennas. *Angew. Chem., Int. Ed.* **2014,** *53* (3), 875-878.

117. Shell, T. A.; Lawrence, D. S., Vitamin B$_{12}$: a tunable, long wavelength, light-responsive platform for launching therapeutic agents. *Acc. Chem. Res.* **2015,** *48* (11), 2866-74.

118. Rodgers, Z. L.; Hughes, R. M.; Doherty, L. M.; Shell, J. R.; Molesky, B. P.; Brugh, A. M.; Forbes, M. D. E.; Moran, A. M.; Lawrence, D. S., B$_{12}$-Mediated, Long Wavelength Photopolymerization of Hydrogels. *J. Am. Chem. Soc.* **2015,** *137* (9), 3372-3378.

119. Vreven, T.; Byun, K. S.; Komáromi, I.; Dapprich, S.; Montgomery, J. A.; Morokuma, K.; Frisch, M. J., Combining Quantum Mechanics Methods with Molecular Mechanics Methods in ONIOM. *J. Chem. Theory Comput.* **2006,** *2* (3), 815-826.

120. Padmakumar, R.; Padmakumar, R.; Banerjee, R., Evidence that Cobalt−Carbon Bond Homolysis is Coupled to Hydrogen Atom Abstraction from Substrate in Methylmalonyl-CoA Mutase. *Biochemistry* **1997,** *36* (12), 3713-3718.

121. Kornobis, K.; Kumar, N.; Lodowski, P.; Jaworska, M.; Piecuch, P.; Lutz, J. J.; Wong, B. M.; Kozlowski, P. M., Electronic structure of the S1 state in methylcobalamin: insight from CASSCF/MC-XQDPT2, EOM-CCSD, and TD-DFT calculations. *J. Comp. Chem.* **2013,** *34* (12), 987-1004.

122.   Lodowski, P.; Jaworska, M.; Andruniow, T.; Garabato, B. D.; Kozlowski, P. M., Mechanism of Co-C bond photolysis in the base-on form of methylcobalamin. *J. Phys. Chem. A* **2014,** *118* (50), 11718-34.

123.   Sension, R. J.; Harris, D. A.; Cole, A. G., Time-Resolved Spectroscopic Studies of B12 Coenzymes: Comparison of the Influence of Solvent on the Primary Photolysis Mechanism and Geminate Recombination of Methyl-, Ethyl-, n-Propyl-, and 5'-Deoxyadenosylcobalamin. *J. Phys. Chem. B* **2005,** *109* (46), 21954-21962.

124.   Peng, J.; Tang, K.-C.; McLoughlin, K.; Yang, Y.; Forgach, D.; Sension, R. J., Ultrafast Excited-State Dynamics and Photolysis in Base-Off B_{12} Coenzymes and Analogues: Absence of the trans-Nitrogenous Ligand Opens a Channel for Rapid Nonradiative Decay. *J. Phys. Chem. B* **2010,** *114* (38), 12398-12405.

125.   Jones, A. R.; Woodward, J. R.; Scrutton, N. S., Continuous wave photolysis magnetic field effect investigations with free and protein-bound alkylcobalamins. *J. Am. Chem. Soc.* **2009,** *131* (47), 17246-53.

126.   Andruniów, T.; Jaworska, M.; Lodowski, P.; Zgierski, M. Z.; Dreos, R.; Randaccio, L.; Kozlowski, P. M., Time-dependent density functional theory study of cobalt corrinoids: Electronically excited states of methylcobalamin. *J. Chem. Phys.* **2008,** *129* (8), 085101.

127.   Andruniów, T.; Lodowski, P.; Garabato, B. D.; Jaworska, M.; Kozlowski, P. M., The role of spin-orbit coupling in the photolysis of methylcobalamin. *J. Chem. Phys.* **2016,** *144* (12), 124305.

128.   Jaworska, M.; Lodowski, P.; Andruniów, T.; Kozlowski, P. M., Photolysis of Methylcobalamin: Identification of the Relevant Excited States Involved in Co−C Bond Scission. *J. Phys. Chem. B* **2007,** *111* (10), 2419-2422.

129.   Lodowski, P.; Jaworska, M.; Andruniów, T.; Kumar, M.; Kozlowski, P. M., Photodissociation of Co−C Bond in Methyl- and Ethylcobalamin: An Insight from TD-DFT Calculations. *J. Phys. Chem. B* **2009,** *113* (19), 6898-6909.

130.   Lodowski, P.; Jaworska, M.; Garabato, B. D.; Kozlowski, P. M., Mechanism of Co-C bond photolysis in methylcobalamin: influence of axial base. *J. Phys. Chem. A* **2015,** *119* (17), 3913-28.

131.   Kohn, W.; Sham, L. J., Self-Consistent Equations Including Exchange and Correlation Effects. *Phys. Rev.* **1965,** *140* (4A), A1133-A1138.

132.   Jones, R. O.; Gunnarsson, O., The density functional formalism, its applications and prospects. *Rev. Mod. Phys.* **1989,** *61* (3), 689-746.

133.   Runge, E.; Gross, E. K. U., Density-Functional Theory for Time-Dependent Systems. *Phys. Rev. Lett.* **1984,** *52* (12), 997-1000.

134.   Casida, M. E., *Recent Developments and Application of Modern Density Functional Theory*. Elsvevier: Amsterdam, 1996.

135.   Baerends, E. J.; Ricciardi, G.; Rosa, A.; van Gisbergen, S. J. A., A DFT/TDDFT interpretation of the ground and excited states of porphyrin and porphyrazine complexes. *Coord. Chem. Rev.* **2002,** *230* (1), 5-27.

136.   Dreuw, A.; Head-Gordon, M., Single-Reference ab Initio Methods for the Calculation of Excited States of Large Molecules. *Chem. Rev.* **2005,** *105* (11), 4009-4037.

137.   Garabato, B. D.; Lodowski, P.; Jaworska, M.; Kozlowski, P. M., Mechanism of Co-C photodissociation in adenosylcobalamin. *Phys. chem. chem. phys.* **2016,** *18* (28), 19070-82.

138.   Liu, H.; Kornobis, K.; Lodowski, P.; Jaworska, M.; Kozlowski, P. M., TD-DFT insight into photodissociation of the Co-C bond in coenzyme B_{12}. *Front. Chem.* **2014,** *1* (41), 1-12.

139.   Senn, H. M.; Thiel, W., QM/MM Methods for Biomolecular Systems. *Angew. Chem., Int. Ed.* **2009,** *48* (7), 1198-1229.

140.   Leach, A., *Molecular Modelling:Principles and Applications*. 2nd ed.; Pearson: 2001.

141.   Lin, H.; Truhlar, D. G., QM/MM: what have we learned, where are we, and where do we go from here? *Theor. Chem. Acc.* **2006,** *117* (2), 185.

142.   Sousa, S. F.; Fernandes, P. A.; Ramos, M. J., Computational enzymatic catalysis – clarifying enzymatic mechanisms with the help of computers. *Phys. chem. chem. phys.* **2012,** *14* (36), 12431-12441.

143.   van der Kamp, M. W.; Mulholland, A. J., Combined Quantum Mechanics/Molecular Mechanics (QM/MM) Methods in Computational Enzymology. *Biochemistry* **2013,** *52* (16), 2708-2728.

144.   Olsson, M. H. M.; Søndergaard, C. R.; Rostkowski, M.; Jensen, J. H., PROPKA3: Consistent Treatment of Internal and Surface Residues in Empirical pKa Predictions. *J. Chem. Theory Comput.* **2011,** *7* (2), 525-537.

145.   M. J. Frisch, G. W. T., H. B. Schlegel, G. E. Scuseria, M. A. Robb, J. R. Cheeseman, G. Scalmani, V. Barone, G. A. Petersson, H. Nakatsuji, X. Li, M. Caricato, A. Marenich, J. Bloino, B. G. Janesko, R. Gomperts, B. Mennucci, H. P. Hratchian, J. V. Ortiz, A. F. Izmaylov, J. L. Sonnenberg, D. Williams-Young, F. Ding, F. Lipparini, F. Egidi, J. Goings, B. Peng, A. Petrone, T. Henderson, D. Ranasinghe, V. G. Zakrzewski, J. Gao, N. Rega, G. Zheng, W. Liang, M. Hada, M. Ehara, K. Toyota, R. Fukuda, J. Hasegawa, M. Ishida, T. Nakajima, Y. Honda, O. Kitao, H. Nakai, T. Vreven, K. Throssell, J. A. Montgomery, Jr., J. E. Peralta, F. Ogliaro, M. Bearpark, J. J. Heyd, E. Brothers, K. N. Kudin, V. N. Staroverov, T. Keith, R. Kobayashi, J. Normand, K. Raghavachari, A. Rendell, J. C. Burant, S. S. Iyengar, J. Tomasi, M. Cossi, J. M. Millam, M. Klene, C. Adamo, R. Cammi, J. W. Ochterski, R. L. Martin, K. Morokuma, O. Farkas, J. B. Foresman, and D. J. Fox *Gaussian 09, Revision B*, Gaussian, Inc.: Wallingford CT, 2009.

146.   Becke, A. D., Density-functional exchange-energy approximation with correct asymptotic behavior. *Phys. Rev. A* **1988,** *38* (6), 3098-3100.

147.   Perdew, J. P., Density-functional approximation for the correlation energy of the inhomogeneous electron gas. *Phys. Rev. B* **1986,** *33* (12), 8822-8824.

148.   Kozlowski, P. M.; Kumar, M.; Piecuch, P.; Li, W.; Bauman, N. P.; Hansen, J. A.; Lodowski, P.; Jaworska, M., The Cobalt-Methyl Bond Dissociation in Methylcobalamin: New Benchmark Analysis Based on Density Functional Theory and Completely

Renormalized Coupled-Cluster Calculations. *J. Chem. Theory. Comput.* **2012,** *8* (6), 1870-94.

149.   Jensen, K. P.; Ryde, U., Theoretical Prediction of the Co−C Bond Strength in Cobalamins. *J. Phys. Chem. A* **2003,** *107* (38), 7539-7545.

150.   Dölker, N.; Morreale, A.; Maseras, F., Computational study on the difference between the Co–C bond dissociation energy in methylcobalamin and adenosylcobalamin. *J. Biol. Inorg. Chem.* **2005,** *10* (5), 509-517.

151.   Kuta, J.; Patchkovskii, S.; Zgierski Marek, Z.; Kozlowski Pawel, M., Performance of DFT in modeling electronic and structural properties of cobalamins. *J. Comput. Chem.* **2006,** *27* (12), 1429-1437.

152.   Stewart, J. J. P., Optimization of parameters for semiempirical methods V: Modification of NDDO approximations and application to 70 elements. *J. Mol. Model.* **2007,** *13* (12), 1173-1213.

153.   Maier, J. A.; Martinez, C.; Kasavajhala, K.; Wickstrom, L.; Hauser, K. E.; Simmerling, C., ff14SB: Improving the Accuracy of Protein Side Chain and Backbone Parameters from ff99SB. *J. Chem. Theory. Comput.* **2015,** *11* (8), 3696-3713.

154.   Eichkorn, K.; Weigend, F.; Treutler, O.; Ahlrichs, R., Auxiliary basis sets for main row atoms and transition metals and their use to approximate Coulomb potentials. *Theor. Chem. Acc.* **1997,** *97* (1), 119-124.

155.   Schäfer, A.; Huber, C.; Ahlrichs, R., Fully optimized contracted Gaussian basis sets of triple zeta valence quality for atoms Li to Kr. *J. Chem. Phys.* **1994,** *100* (8), 5829-5835.

156.   Kornobis, K.; Kumar, N.; Wong, B. M.; Lodowski, P.; Jaworska, M.; Andruniow, T.; Ruud, K.; Kozlowski, P. M., Electronically excited states of vitamin B_{12}: benchmark calculations including time-dependent density functional theory and correlated ab initio methods. *J. Phys. Chem. A* **2011,** *115* (7), 1280-92.

157.   Joseph J. Shiang, A. G. C., Roseanne J. Sension, Kun Hang, Yuxiang Weng, Jenna S. Trommel, Luigi G. Marzilli, and Tianquan Lian, Ultrafast Excited-State Dynamics in Vitamin B_{12} and Related Cob(III)alamins. *J. Am. Chem. Soc.* **2006,** *128*, 801-808.

158.   Lodowski, P.; Jaworska, M.; Andruniow, T.; Garabato, B. D.; Kozlowski, P. M., Mechanism of the S1 excited state internal conversion in vitamin B_{12}. *Phys. Chem. Chem. Phys.* **2014,** *16* (35), 18675-9.

159.   Miller, N. A.; Deb, A.; Alonso-Mori, R.; Garabato, B. D.; Glownia, J. M.; Kiefer, L. M.; Koralek, J.; Sikorski, M.; Spears, K. G.; Wiley, T. E.; Zhu, D.; Kozlowski, P. M.; Kubarych, K. J.; Penner-Hahn, J. E.; Sension, R. J., Polarized XANES Monitors Femtosecond Structural Evolution of Photoexcited Vitamin B_{12}. *J. Am. Chem. Soc.* **2017,** *139* (5), 1894-1899.

160.   Jarrett, J. T.; Amaratunga, M.; Drennan, C. L.; Scholten, J. D.; Sands, R. H.; Ludwig, M. L.; Matthews, R. G., Mutations in the B_{12}-Binding Region of Methionine Synthase: How the Protein Controls Methylcobalamin Reactivity. *Biochemistry* **1996,** *35* (7), 2464-2475.

161.   Miller, N. A.; Wiley, T. E.; Spears, K. G.; Ruetz, M.; Kieninger, C.; Krautler, B.; Sension, R. J., Toward the Design of Photoresponsive Conditional Antivitamins B_{12}: A Transient Absorption Study of an Arylcobalamin and an Alkynylcobalamin. *J. Am. Chem. Soc.* **2016,** *138* (43), 14250-14256.

162.   Ghosh, A. P.; Mamun, A. A.; Lodowski, P.; Jaworska, M.; Kozlowski, P. M., Mechanism of the photo-induced activation of CoC bond in methylcobalamin-dependent methionine synthase. *J. Photochem. Photobiol., B* **2018,** *189*, 306-317.

163.   Pettersen, E. F.; Goddard, T. D.; Huang, C. C.; Couch, G. S.; Greenblatt, D. M.; Meng, E. C.; Ferrin, T. E., UCSF Chimera—A visualization system for exploratory research and analysis. *J. Comput. Chem.* **2004,** *25* (13), 1605-1612.

164.   Mamun, A. A.; Toda, M. J.; Lodowski, P.; Jaworska, M.; Kozlowski, P. M., Mechanism of Light Induced Radical Pair Formation in Coenzyme B_{12}-Dependent Ethanolamine Ammonia-Lyase. *ACS Catal.* **2018**, 7164-7178.

165.   Mamun, A. A.; Toda, M. J.; Lodowski, P.; Kozlowski, P. M., Photolytic Cleavage of Co–C Bond in Coenzyme B_{12}-Dependent Glutamate Mutase. *J. Phys. Chem. B* **2019,** *123* (12), 2585-2598.

166.   Toda, M. J.; Lodowski, P.; Mamun, A. A.; Jaworska, M.; Kozlowski, P. M., Photolytic properties of the biologically active forms of vitamin B_{12}. *Coord. Chem. Rev.* **2019,** *385*, 20-43.

167.   Marques, H. M.; Ngoma, B.; Egan, T. J.; Brown, K. L., Parameters for the amber force field for the molecular mechanics modeling of the cobalt corrinoids. *J. Mol. Struct.* **2001,** *561* (1), 71-91.

168.   Adamo, C.; Jacquemin, D., The calculations of excited-state properties with Time-Dependent Density Functional Theory. *Chem. Soc. Rev.* **2013,** *42* (3), 845-56.

169.   Ciofini, I.; Le Bahers, T.; Adamo, C.; Odobel, F.; Jacquemin, D., Through-Space Charge Transfer in Rod-Like Molecules: Lessons from Theory. *J. Phys. Chem. C* **2012,** *116* (22), 11946-11955.

170.   Le Bahers, T.; Adamo, C.; Ciofini, I., A Qualitative Index of Spatial Extent in Charge-Transfer Excitations. *J. Chem. Theory Comput.* **2011,** *7* (8), 2498-2506.

171.   Adamo, C.; Le Bahers, T.; Savarese, M.; Wilbraham, L.; García, G.; Fukuda, R.; Ehara, M.; Rega, N.; Ciofini, I., Exploring excited states using Time Dependent Density Functional Theory and density-based indexes. *Coord. Chem. Rev.* **2015,** *304-305* (Supplement C), 166-178.

172.   Harris, D. A.; Stickrath, A. B.; Carroll, E. C.; Sension, R. J., Influence of Environment on the Electronic Structure of Cob(III)alamins: Time-Resolved Absorption Studies of the S_1 State Spectrum and Dynamics. *J. Am. Chem. Soc.* **2007,** *129* (24), 7578-7585.

173.   Garabato, B. D.; Kumar, N.; Lodowski, P.; Jaworska, M.; Kozlowski, P. M., Electronically excited states of cob(ii)alamin: insights from CASSCF/XMCQDPT2 and TD-DFT calculations. *Phys. Chem. Chem. Phys.* **2016,** *18* (6), 4513-26.

174.   v. Bünau, G., J. B. Birks: Photophysics of Aromatic Molecules. Wiley-Interscience, London 1970. 704 Seiten. Preis: 210s. *Ber. Bunsenges. Phys. Chem.* **1970,** *74* (12), 1294-1295.

175.   Bañuelos Prieto, J.; López Arbeloa, F.; Martínez Martínez, V.; Arbeloa López, T.; López Arbeloa, I., Structural and spectroscopic characteristics of Pyrromethene 567 laser dye. A theoretical approach. *Phys. Chem. Chem. Phys.* **2004,** *6* (17), 4247-4253.

176.   Alex R. Jones, C. L., Sam Hay, and Nigel S. Scrutton, Relating localized protein motions to the reaction coordinate in coenzyme B_{12}-dependent enzymes. *FEBS J.* **2013,** *280*, 2997-3008.

177.   Chen, Z.-G.; Ziętek, M. A.; Russell, H. J.; Tait, S.; Hay, S.; Jones, A. R.; Scrutton, N. S., Dynamic, Electrostatic Model for the Generation and Control of High-Energy Radical Intermediates by a Coenzyme B_{12}-Dependent Enzyme. *ChemBioChem* **2013,** *14* (13), 1529-1533.

178.   Ghosh, A. P.; Lodowski, P.; Chmielowska, A.; Jaworska, M.; Kozlowski, P. M., Elucidating the mechanism of cob(I)alamin mediated methylation reactions by alkyl halides: S_N^2 or radical mechanism? *J. Catal.* **2019,** *376*, 32-43.

179.   Ghosh, A. P.; Mamun, A. A.; Kozlowski, P. M., How does the mutation in the cap domain of methylcobalamin-dependent methionine synthase influence the photoactivation of the Co–C bond? *Phys. Chem. Chem. Phys.* **2019,** *21* (37), 20628-20640.

180.   Endicott, J. F.; Netzel, T. L., Early events and transient chemistry in the photohomolysis of alkylcobalamins. *J. Am. Chem. Soc.* **1979,** *101* (14), 4000-4002.

181.   Taylor, R. T.; Smucker, L.; Hanna, M. L.; Gill, J., Aerobic photoiysis of alkylcobalamins: Quantum yields and light-action spectra. *Arch. Biochem. Biophys.* **1973,** *156* (2), 521-533.

182.   Schrauzer, G. N.; Lee, L. P.; Sibert, J. W., Alkylcobalamins and alkylcobaloximes. Electronic structure, spectra, and mechanism of photodealkylation. *J. Am. Chem. Soc.* **1970,** *92* (10), 2997-3005.

183.   Schrauzer, G. N.; Sibert, J. W.; Windgassen, R. J., Photochemical and thermal cobalt-carbon bond cleavage in alkylcobalamins and related organometallic compounds. Comparative study. *J. Am. Chem. Soc.* **1968,** *90* (24), 6681-6688.

184.   Chen, E.; Chance, M. R., Continuous-wave quantum yields of various cobalamins are influenced by competition between geminate recombination and cage escape. *Biochemistry* **1993,** *32* (6), 1480-1487.

185.   Chen, E.; Chance, M. R., Nanosecond transient absorption spectroscopy of coenzyme B12. Quantum yields and spectral dynamics. *J. Biol. Chem.* **1990,** *265* (22), 12987-94.

186.   Jones, A. R., The photochemistry and photobiology of vitamin B_{12}. *Photochem. Photobiol. Sci.* **2017,** *16* (6), 820-834.

187.   Jones, A. R.; Russell, H. J.; Greetham, G. M.; Towrie, M.; Hay, S.; Scrutton, N. S., Ultrafast Infrared Spectral Fingerprints of Vitamin B_{12} and Related Cobalamins. *J. Phys. Chem. A* **2012,** *116* (23), 5586-5594.

188.   Wiley, T. E.; Arruda, B. C.; Miller, N. A.; Lenard, M.; Sension, R. J., Excited electronic states and internal conversion in cyanocobalamin. *Chin. Chem. Lett.* **2015,** *26* (4), 439-443.

189.   Wiley, T. E.; Miller, N. A.; Miller, W. R.; Sofferman, D. L.; Lodowski, P.; Toda, M. J.; Jaworska, M.; Kozlowski, P. M.; Sension, R. J., Off to the Races: Comparison of Excited State Dynamics in Vitamin B_{12} Derivatives Hydroxocobalamin and Aquocobalamin. *J. Phys. Chem. A* **2018,** *122* (33), 6693-6703.

190.   Wiley, T. E.; Miller, W. R.; Miller, N. A.; Sension, R. J.; Lodowski, P.; Jaworska, M.; Kozlowski, P. M., Photostability of Hydroxocobalamin: Ultrafast Excited State Dynamics and Computational Studies. *J. Phys. Chem. Lett.* **2016,** *7* (1), 143-7.

191.   Sension, R. J.; Cole, A. G.; Harris, A. D.; Fox, C. C.; Woodbury, N. W.; Lin, S.; Marsh, E. N., Photolysis and recombination of adenosylcobalamin bound to glutamate mutase. *J. Am. Chem. Soc.* **2004,** *126* (6), 1598-9.

192.   Hogenkamp, H. P. C.; Ladd, J. N.; Barker, H. A., The identification of a nucleoside derived from a coenzyme B12. *J. Biol. Chem.* **1962,** *237* (6), 1950-1952.

193.   Hogenkamp, H. P., The photolysis of methylcobalamin. *Biochemistry* **1966,** *5* (2), 417-22.

194.   Mok, C. Y.; Endicott, J. F., The photochemistry of organocobalt complexes containing tetraaza macrocyclic ligands. Cobalt-methyl homolysis and the nature of the cobalt-carbon bond. *J. Am. Chem. Soc.* **1978,** *100* (1), 123-129.

195. Schwartz, P. A.; Frey, P. A., 5'-Peroxyadenosine and 5'-Peroxyadenosylcobalamin as Intermediates in the Aerobic Photolysis of Adenosylcobalamin. *Biochemistry* **2007,** *46* (24), 7284-7292.

196. Endicott, J. F.; Ferraudi, G. J., A flash photolytic investigation of low energy homolytic processes in methylcobalamin. *J. Am. Chem. Soc.* **1977,** *99* (1), 243-245.

197. Ghosh, A. P.; Lodowski, P.; Bazarganpour, A.; Leks, M.; Kozlowski, P. M., Aerobic photolysis of methylcobalamin: structural and electronic properties of the Cbl–O–O–CH$_3$ intermediate. *Dalton Trans.* **2020,** *49* (13), 4114-4124.

198. Lee, C.; Yang, W.; Parr, R. G., Development of the Colle-Salvetti correlation-energy formula into a functional of the electron density. *Phys. Rev. B* **1988,** *37* (2), 785-789.

199. F. Weigend, M. H., H. Patzelt, and R. Ahlrichs, RI-MP2: Optimized Auxiliary Basis Sets and Demonstration of Efficiency. *Chem. Phys. Lett.* **1998,** *294*, 143-152.

200. TURBOMOLE 1988.

201. Ahlrichs, R.; Bär, M.; Häser, M.; Horn, H.; Kölmel, C., Electronic structure calculations on workstation computers: The program system turbomole. *Chem. Phys. Lett.* **1989,** *162* (3), 165-169.

202. Barone, V.; Cossi, M.; Tomasi, J., Geometry optimization of molecular structures in solution by the polarizable continuum model. *J. Comput. Chem.* **1998,** *19* (4), 404-417.

203.   Klamt, A.; Schuurmann, G., COSMO: a new approach to dielectric screening in solvents with explicit expressions for the screening energy and its gradient. *J. Chem. Soc., Perkin Trans. 2* **1993,** (5), 799-805.

204.   Andruniów, T.; Jaworska, M.; Lodowski, P.; Zgierski, M. Z.; Dreos, R.; Randaccio, L.; Kozlowski, P. M., Time-dependent density functional theory study of cobalt corrinoids: Electronically excited states of coenzyme B_{12}. *J. Chem. Phys.* **2009,** *131* (10), 105105.

205.   Andrew B. Stickrath, E. C. C., Xiaochuan Dai, D. Ahmasi Harris, Aaron Rury, Broc Smith, Kuo-Chun Tang, Jonathan Wert, and Roseanne J. Sension, Solvent-Dependent Cage Dynamics of Small Nonpolar Radicals: Lessons from the Photodissociation and Geminate Recombination of Alkylcobalamins. *J. Phys. Chem. A* **2009,** *113*, 8513-8522.

206.   Toraya, T., Radical Catalysis in Coenzyme B12-Dependent Isomerization (Eliminating) Reactions. *Chem. Rev.* **2003,** *103* (6), 2095-2128.

207.   Finke, R. G.; Hay, B. P., Thermolysis of adenosylcobalamin: a product, kinetic, and cobalt-carbon ($C_{5'}$) bond dissociation energy study. *Inorg. Chem.* **1984,** *23* (20), 3041-3043.

208.   Abend, A.; Illich, V.; Rétey, J., Further Insights into the Mechanism of Action of Methylmalonyl-CoA Mutase by Electron Paramagnetic Resonance Studies. *Eur. J. Biochem.* **1997,** *249* (1), 180-186.

209.   Dong, S.; Padmakumar, R.; Maiti, N.; Banerjee, R.; Spiro, T. G., Resonance Raman Spectra Show That Coenzyme B_{12} Binding to Methylmalonyl-Coenzyme A Mutase

Changes the Corrin Ring Conformation but Leaves the Co−C Bond Essentially Unaffected. *J. Am. Chem. Soc.* **1998,** *120* (38), 9947-9948.

210.   Schopf, P.; Mills, M. J. L.; Warshel, A., The entropic contributions in vitamin B_{12} enzymes still reflect the electrostatic paradigm. *Proc. Natl. Acad. Sci.* **2015,** *112* (14), 4328.

211.   Ruetz, M.; Campanello, G. C.; Purchal, M.; Shen, H.; McDevitt, L.; Gouda, H.; Wakabayashi, S.; Zhu, J.; Rubin, E. J.; Warncke, K.; Mootha, V. K.; Koutmos, M.; Banerjee, R., Itaconyl-CoA forms a stable biradical in methylmalonyl-CoA mutase and derails its activity and repair. *Science* **2019,** *366* (6465), 589.

212.   Brooks, A. J.; Vlasie, M.; Banerjee, R.; Brunold, T. C., Spectroscopic and computational studies on the adenosylcobalamin-dependent methylmalonyl-CoA mutase: evaluation of enzymatic contributions to Co-C bond activation in the Co^{3+} ground state. *J. Am. Chem. Soc.* **2004,** *126* (26), 8167-80.

213.   Tao, P.; Schlegel, H. B., A toolkit to assist ONIOM calculations. *J. Comput. Chem.* **2010,** *31* (12), 2363-2369.

214.   Toda, M. J.; Mamun, A. A.; Lodowski, P.; Kozlowski, P. M., Why is CarH photolytically active in comparison to other B_{12}-dependent enzymes? *J. Photochem. Photobiol., B* **2020,** *209*, 111919.

215.   Svensson, M.; Humbel, S.; Froese, R. D. J.; Matsubara, T.; Sieber, S.; Morokuma, K., ONIOM: A Multilayered Integrated MO + MM Method for Geometry Optimizations and Single Point Energy Predictions. A Test for Diels−Alder Reactions and $Pt(P(t-Bu)_3)2$ + H_2 Oxidative Addition. *J. Phys. Chem.* **1996,** *100* (50), 19357-19363.

216.   Hornak, V.; Abel, R.; Okur, A.; Strockbine, B.; Roitberg, A.; Simmerling, C., Comparison of multiple Amber force fields and development of improved protein backbone parameters. *Proteins: Struct., Funct., Bioinf.* **2006,** *65* (3), 712-725.

217.   Kwiecien, R. A.; Khavrutskii, I. V.; Musaev, D. G.; Morokuma, K.; Banerjee, R.; Paneth, P., Computational Insights into the Mechanism of Radical Generation in B_{12}-Dependent Methylmalonyl-CoA Mutase. *J. Am. Chem. Soc.* **2006,** *128* (4), 1287-1292.

218.   Gruber, K.; Reitzer, R.; Kratky, C., Radical Shuttling in a Protein: Ribose Pseudorotation Controls Alkyl-Radical Transfer in the Coenzyme B_{12} Dependent Enzyme Glutamate Mutase. *Angew. Chem., Int. Ed.* **2001,** *40* (18), 3377-3380.

219.   Durbeej, B.; Sandala, G. M.; Bucher, D.; Smith, D. M.; Radom, L., On the Importance of Ribose Orientation in the Substrate Activation of the Coenzyme B_{12}-Dependent Mutases. *Chem. Eur. J.* **2009,** *15* (34), 8578-8585.

220.   Mamun, A. A., Computational modeling of photolysis and catalysis reactions in vitamin B_{12}-dependent enzymes. *Electronic Theses and Dissertations* **2020,** (Paper 3406).

221.   Hay, B. P.; Finke, R. G., Thermolysis of the Co-C bond in adenosylcobalamin (coenzyme B_{12})—IV. Products, kinetics and Co-C bond dissociation energy studies in ethylene glycol. *Polyhedron* **1988,** *7* (16), 1469-1481.

222.   Jensen, K. P.; Ryde, U., How the Co−C Bond Is Cleaved in Coenzyme B_{12} Enzymes: A Theoretical Study. *J. Am. Chem. Soc.* **2005,** *127* (25), 9117-9128.

223.   Lexa, D.; Saveant, J. M., Electrochemistry of vitamin B_{12}. 3. One-electron intermediates in the reduction of methylcobalamin and methylcobinamide. *J. Am. Chem. Soc.* **1978,** *100* (10), 3220-3222.

224.   Lexa, D.; Saveant, J. M., The electrochemistry of vitamin B_{12}. *Acc. Chem. Res.* **1983,** *16* (7), 235-243.

225.   Birke, R. L.; Huang, Q.; Spataru, T.; Gosser, D. K., Electroreduction of a Series of Alkylcobalamins: Mechanism of Stepwise Reductive Cleavage of the Co−C Bond. *J. Am. Chem. Soc.* **2006,** *128* (6), 1922-1936.

226.   Percy, B. R., The theory of reactions involving proton transfers. *Proc. R. Soc. Lond. A,* **1936,** 154, 414–429

227.   Silverstein, T. P., Marcus Theory: Thermodynamics CAN Control the Kinetics of Electron Transfer Reactions. *J. Chem. Educ.* **2012,** *89* (9), 1159-1167.

228.   Mayer, J. M., Simple Marcus-Theory-Type Model for Hydrogen-Atom Transfer/Proton-Coupled Electron Transfer. *J. Phys. Chem. Lett.* **2011,** *2* (12), 1481-1489

229.   Zhou, H. X.; Szabo, A., Microscopic formulation of Marcus' theory of electron transfer. *J. Chem. Phys.* **1995,** *103* (9), 3481-3494.

230.   Weinberg, D. R.; Gagliardi, C. J.; Hull, J. F.; Murphy, C. F.; Kent, C. A.; Westlake, B. C.; Paul, A.; Ess, D. H.; McCafferty, D. G.; Meyer, T. J., Proton-Coupled Electron Transfer. *Chem. Rev* **2012,** *112* (7), 4016-4093.

231.   Ghosh, A P.; Toda, M. J.; Kozlowski P.M., What triggers the cleavage of the Co-C$_{5'}$ bond in coenzyme B$_{12}$-dependent itaconyl-CoA methylmalonyl-CoA mutase? ACS Catal. **2021**, 11 (13), 7943−7955
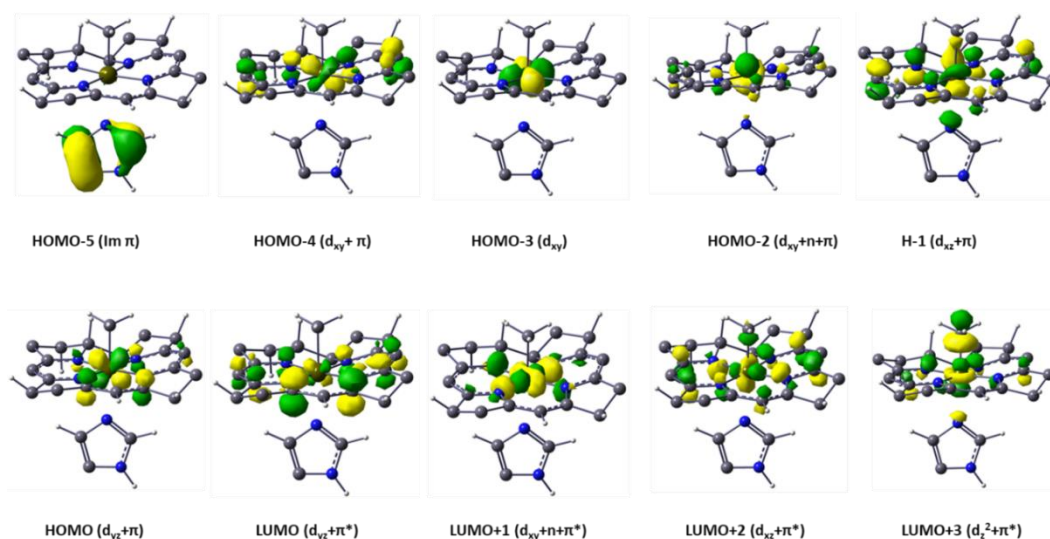
APPENDIX

Figure A1. HOMO and LUMO molecular orbitals for the lowest vertical singlet electronic transitions shown in table 1.
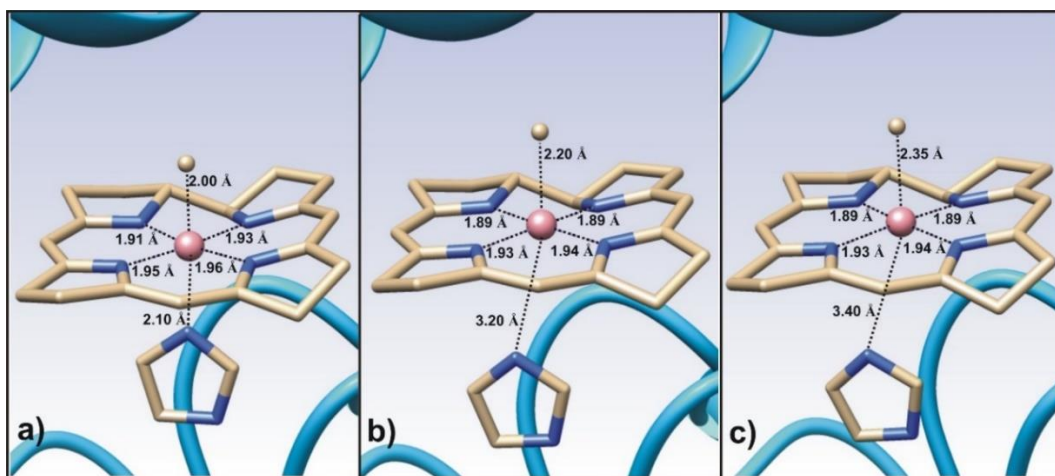

Figure A2. Corresponding ground state optimized geometries of MeCbl inside MetH with various axial bond lengths of selected points on the S_1 PES (Figure 2.4a), **(a)** I (S_{1min}) **(b)** IIB (S_{1min}) **(c)** IIIB (S_{1min}). QM region shown using the ball-and-stick model and MM region shown in ribbons.
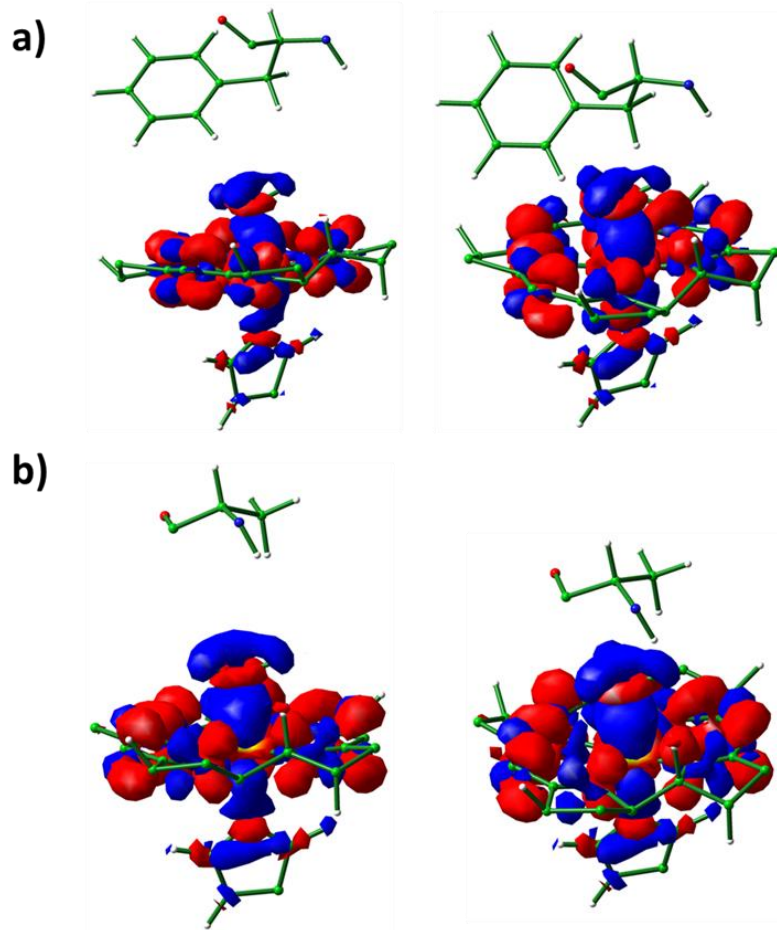
Figure A3. Plot of electron density differences between S_0 and S_1 states for **(a)** WT-MetH **(b)** F708A-MetH at $S_{(1min)}$ MLCT point. Results obtained from TD-DFT calculations. Isosurface plot value 0.002 was used.
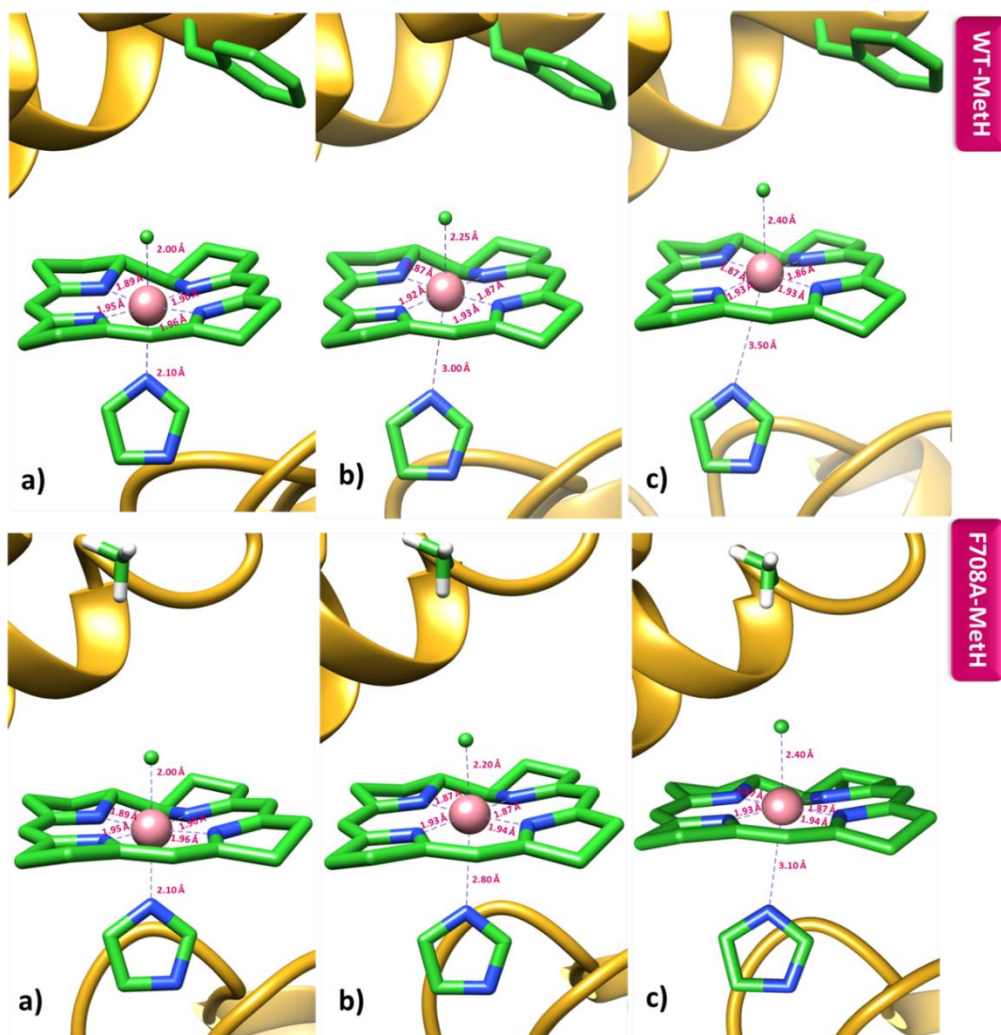
Figure A4. Corresponding ground state optimized geometries of WT-MetH and F708A-MetH with various axial bond lengths of selected points on the S_1 PESs (Figure 5a), **(a)** I (S_{1min}) **(b)** IIB (MECP) **(c)** IIIB (S_{1min}). QM region shown using the ball and stick model and MM region shown in ribbons.
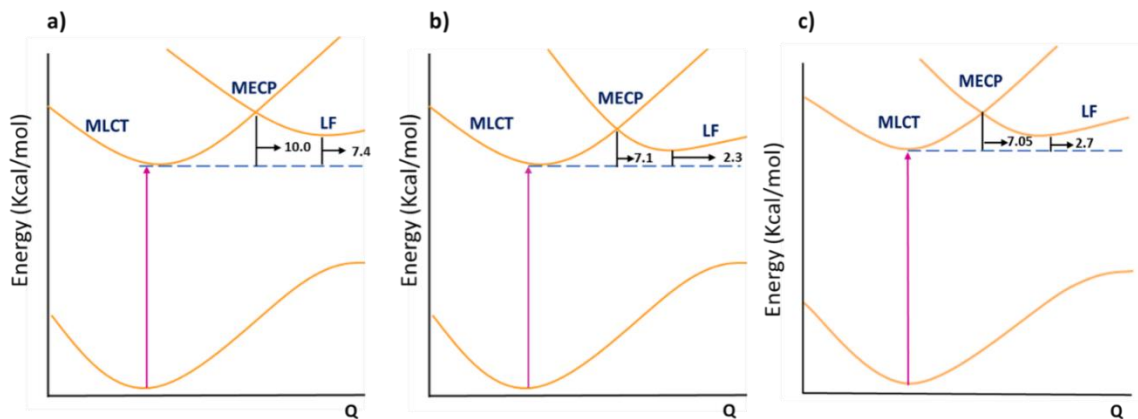
Figure A5. Relative energetics of the MLCT and LF state for (a) WT-MetH (b) F708A-MetH (c) Im−[Co^{III}(corrin)]−Me$^+$ of isolated MeCbl cofactor in solution.
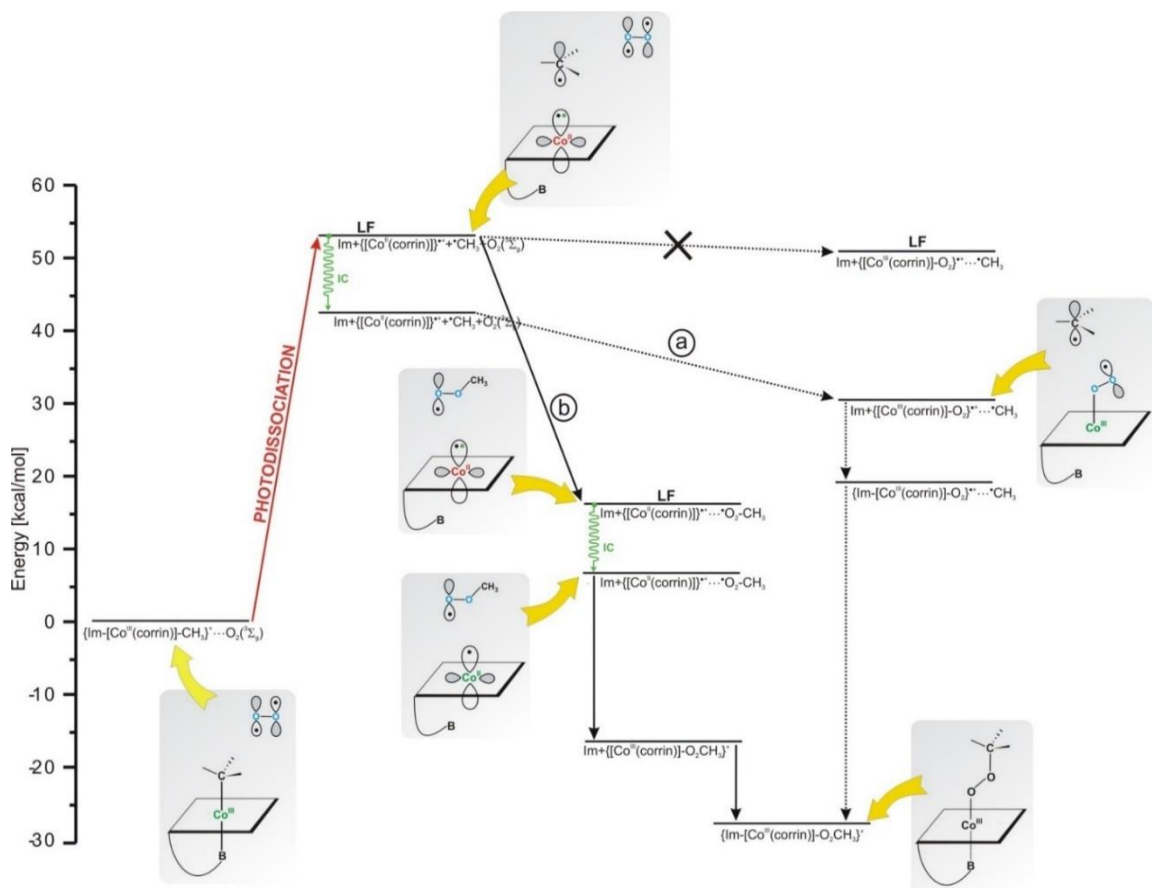

Figure A6. Energy diagram of photolytic reaction along paths a and b (path a, b of Scheme 2) showing the involvement of electronically excited states in MeCbl photoreaction in the presence of oxygen and the formation of [(Im-[Co^{III}(corrin)]-OO-CH$_3$)$^+$] complex.
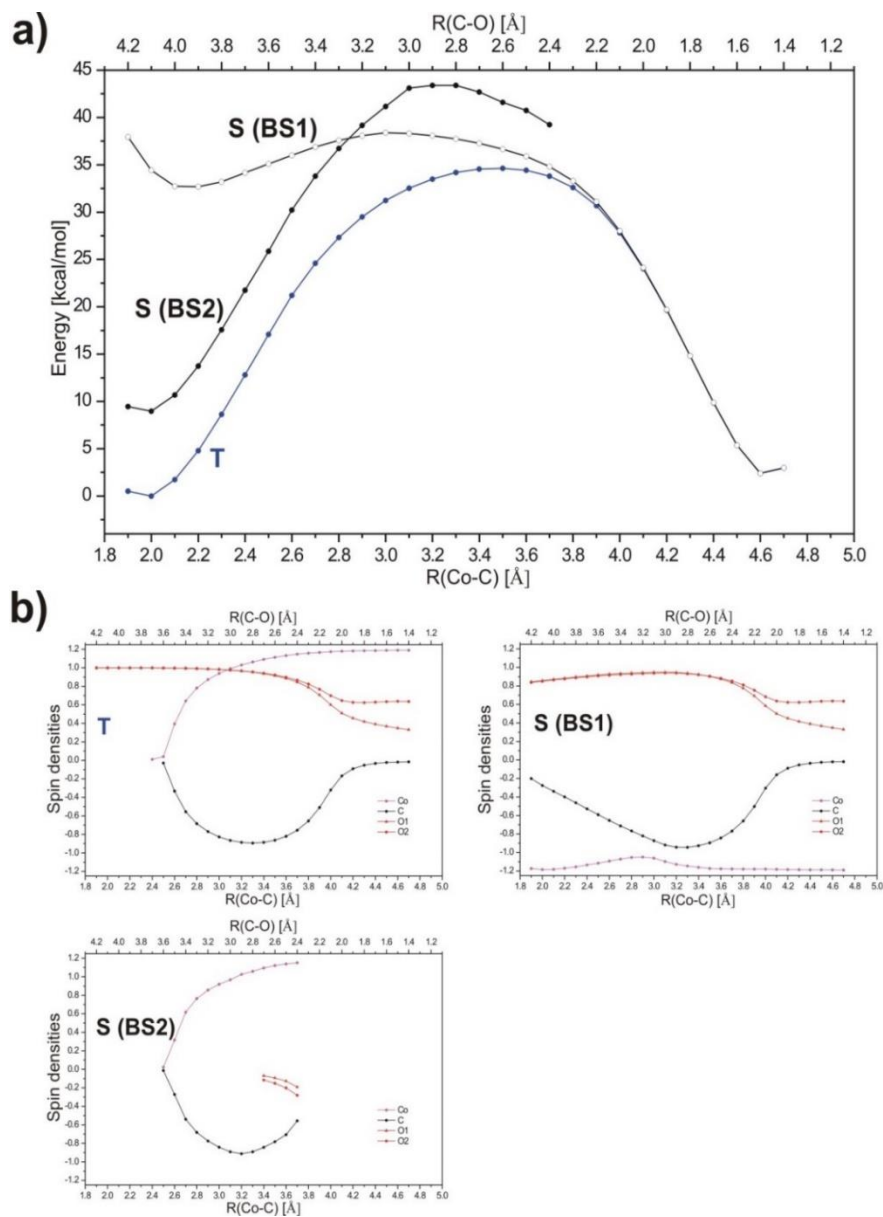
Figure A7. (a) Potential energy curves along reaction path for ([Co^{III}(corrin)]- CH$_3$)$^+$ + O$_2$ → ([Co^{II}(corrin)])$^{+•}$ + $^•$O-O-CH$_3$ model reaction. Based on the UDFT/BP86 level of theory, the three electronic states were considered, namely the triplet state (T) and two singlet states with broken symmetry wave function (S(BS1), S(BS2)). The distribution of spin in the reaction system schematically can be presented as follows: ↑Co ⋯ C↓⋯↑O-O↑ for T, ↓Co ⋯ C↓⋯↑O-O↑ or ↑Co ⋯ C↑⋯↓O-O↓ for S(BS1), and ↑Co ⋯ C↓⋯↑O-O↓ for S(BS2). (b) Mülliken spin densities on cobalt, carbon, and oxygen atoms, directly involved in the reaction.

Figure A8. Corresponding optimized geometries of the I (T_{1min}) and II (T_{1min}) on the PES (Figures 4a and 4b).
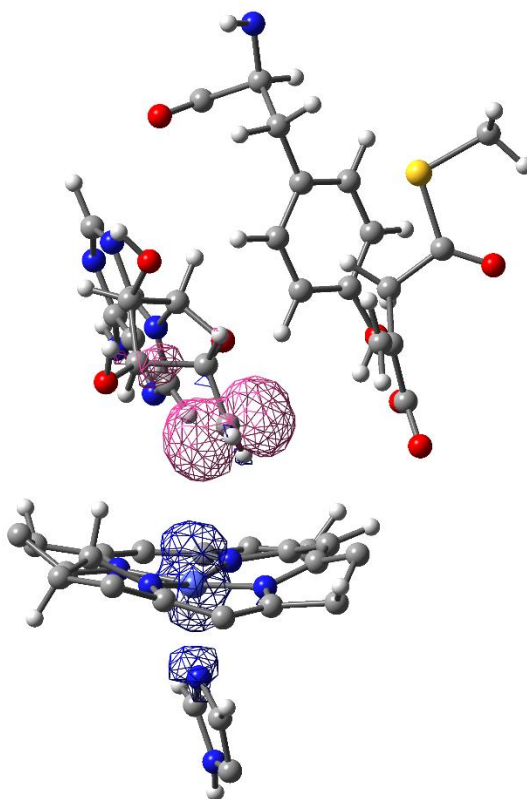
Figure A9. Spin density localization picture of Co/ $C_{5'}$ diradical in the MCM-[I-CoA] enzyme
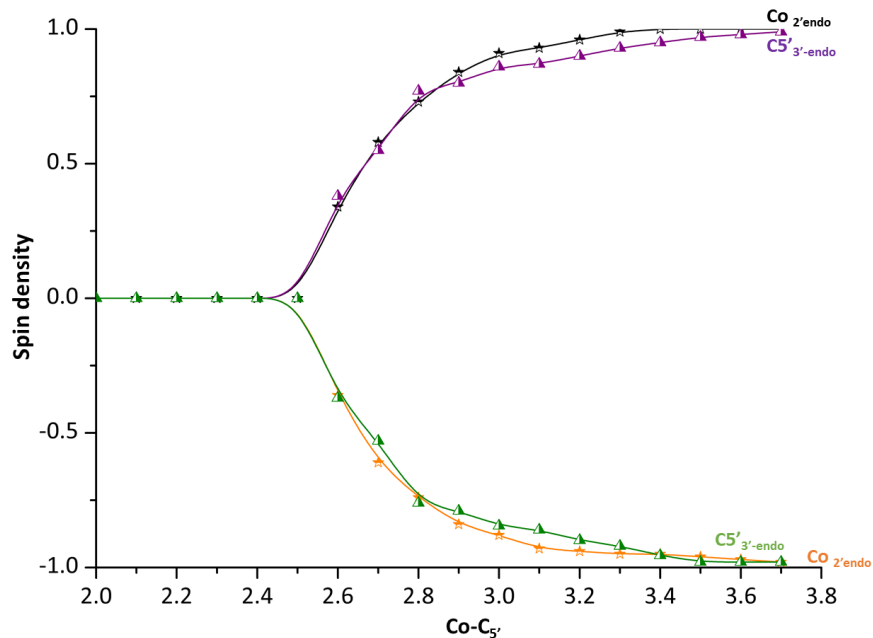
Figure A10. Spin density distribution of the Co-C$_{5'}$ bond throughout the cleavage in MCM-[I-CoA].
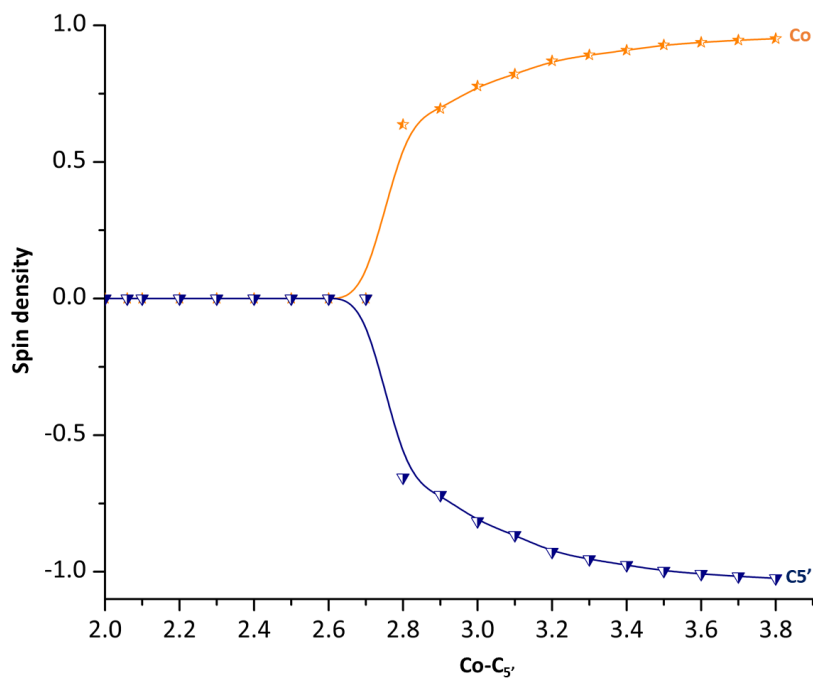
Figure A11. Spin density distribution of the Co-C$_{5'}$ bond throughout the cleavage in substrate-free MCM.

LIST OF ABBREVIATIONS

Vitamin B_{12} CNCbl

Coenzyme B_{12} AdoCbl

CNCbl   Cyanocobalamin

CH_3Cbl Methylcobalamin

AdoCbl   5'-deoxy 5'-adenosylcobalamin

H_2OCbl Aquacobalamin

OHCbl   Hydroxycobalamin

Cbl   Cobalamin

HC   Haptocorrin

DBI   dimethybenzimadazole

Im   Imidazole

GLM   Glutamate mutase

EAL   Ethanolamine ammonia-lyase

DDH   Dioldehydratse

GDH   Glycerol dehydratase

MCM   Methylmalonyl Co-C mutase

MetH   Methionine synthase

CH_3-H4folate   Methyltetrahydrofolate

HOMO	Highest occupied molecular orbital
LUMO	Lowest unoccupied molecular orbital
CT	Charge transfer
BDE	Bond dissociation energy
KIE	Kinetic isotope effect
Met	Methionine
Hcy	Homocysteine
H4-folate	Tetrahydrofolate
His	Histidine
Glu	Glutamate
Tyr	Tyrosine
EPR	Electron paramagnetic resonance
rR	Resonance Raman
RP	Radical pairs
TAS	Transient absorption spectroscopy
QM	Quantum mechanics
QM/MM	Quantum mechanics/Molecular mechanics
HL	High layer
ML	Middle layer
LL	Low layer
DFT	Density functional theory
TD-DFT	Time-dependent density functional theory
CC	Coupled cluster

MP2   Møller-Plesset second order perturbation

ONIOM   Our own N layer integrated molecular modeling

CASSCF   Complete active space self-consistent field

LMCT   Ligand-to-metal charge transfer

MLCT   Metal-to-ligand charge transfer

MC-XQDPT2   Second-order multiconfigurational quasi degenerate perturbation

theory

LR-CT   Long range-charge transfer

GGA   Generalized gradient approximation

QY   Quantum yield

PDB   Protein data bank

LF   Ligand field

MECP   Minimum energy crossing point

CURRICULUM VITAE

Arghya Pratim Ghosh
2200 James Guthrie Ct, Apt 8, Louisville, KY, 40217
Phone: 502-3418718
arghyapratim.chemistry@gmail.com

ACADEMIC BACKGROUNDS

Ph.D. Candidate in Chemistry   **(**Jan 2017**-**Dec 2021)
Department of Chemistry, University of Louisville, KY

M.S. Physical Chemistry   (Jan 2017- Feb 2020)
Department of Chemistry, University of Louisville, KY

Master of Science (M.Sc.) in Chemistry
Physical Chemistry specialization   (Aug 2014- June 2016)
Visva-Bharati University, West-Bengal, India

B.Sc. Chemistry   (Aug 2011- June 2014)
Visva-Bharati University, West-Bengal, India

RESEARCH HIGHLIGHTS

Graduate Student (Ph.D. Candidate)   (Jan 2017-Dec 2021)
University of Louisville
Advisor- Pawel M. Kozlowski, University of Louisville, Louisville, KY, USA

Applies methods of computational chemistry to study transition metal systems with an emphasis on understanding the photochemical behavior associated with derivatives of vitamin B_{12}.

(a) Enzymatic catalysis in vitamin B_{12}-dependent enzymes

Investigated the origin of the Co-C bond activation in the enzymatic reactions catalyzed by AdoCbl-dependent MCM using the combined quantum mechanics/molecular mechanics (QM/MM) approach method.

(b) Photochemical properties of Metalloenzymes
Using a QM/MM approach, we investigated the photolytic properties and mechanistic insights of the activation of an organometallic Co-C bond within the Methionine synthase (MetH) enzyme. The effect of the mutation on the photoactivation of the Co-C bond was also investigated.

(c) Photochemical properties of vitamin B_{12} derivative in solution

The photolytic properties of methylcobalamin in the presence of oxygen were investigated using density functional theory (DFT), time-dependent density functional theory (TD-DFT), and CASSCF.

(d) Cob(I)alamin mediated methyl transfer reactions

Elucidated the mechanism of cob(I)alamin mediated methyl transfer using DFT

Master Research (June 2015 – April 2016)
Master Research Project with **Dr. Manas Ghosh**
Visva-Bharati University, India

Optical properties of an impurity-doped quantum dot, under the influence of Gaussian white noise

Summer Research (May 2014 – July 2014)
Summer project student with **Dr. Suman Chakraborty**
CSIR-NCL, Pune, India

Molecular Dynamic study of the effect of pH on structural properties of the protein, polypeptide chain, and relevant free energy surfaces

PUBLICATIONS

1. **Ghosh, A P**.; Toda, M. J.; Kozlowski P.M. "What triggers the cleavage of the Co-C$_{5'}$ bond in coenzyme B$_{12}$-dependent itaconyl-CoA methylmalonyl-CoA mutase?" ACS Catal. 2021, 11, 7943−7955

2. Malinowski, A.; **Ghosh, A P**.; Edwards. S.; Jaroszynska-Wolinska, J.; Kozlowski P.M. "Methyl transfer reactions catalyzed by cobalamin-dependent enzymes: Insight from molecular docking" J. Mol. Graph. Model., 2021, 104, 107831

3. **Ghosh, A P**.; Lodowski, P; Bazarganpour, A; Leks, M; Kozlowski P.M. "Aerobic photolysis of methylcobalamin: structural and electronic properties of Cbl-O-O-CH$_3$ intermediate" Dalton Trans. 2020, 49, 4114-4124

4. **Ghosh, A P**.; Mamun Abdullah Al; Kozlowski P.M. "How does the mutation in the cap domain of methylcobalamin-dependent methionine synthase influence the photoactivation of the Co-C bond?" Phys. Chem. Chem. Phys., 2019, 21, 20628-20640

5. **Ghosh, A P**.; Lodowski, P; Jaworska M; Kozlowski P.M. "Elucidating the mechanism of cob(I)alamin mediated methylation reaction by alkyl halides: S$_N^2$ or radical mechanism?" J.Catal., 2019, 376, 32-43

6. **Ghosh, A P**.; Mamun Abdullah Al; Lodowski, P; Jaworska M; Kozlowski P.M. "Mechanism of the photo-induced activation of Co-C bond in methylcobalamin-dependent methionine synthase" J. Photochem. Photobiol. B, Biol., 2018, 189, 306-317

7. **Ghosh, A.P**.; Mandal, A; Sarkar S; and Ghosh M; "Influence of position-dependent effective mass on the nonlinear optical properties of impurity-doped Quantum dots in presence of Gaussian white noise" Optics Communications, 2016, 367, 325-334

8. Sarkar S; **Ghosh, A.P**; Mandal A; and Ghosh M; "Modulating nonlinear optical properties of impurity doped Quantum dots via the interplay between anisotropy and Gaussian white noise" Superlattices and Microstructures, 2016, 90, 297-307

9. Mandal A, Sarkar S; **Ghosh, A.P**; "Analyzing total optical absorption coefficient of impurity doped quantum dots in presence of noise with special emphasis on electric field, magnetic field, and confinement potential" Chem. Phys., 2015, 463, 149-158

10. Sarkar S; **Ghosh, A.P**; Mandal A; and Ghosh M; "Noise-Modulated Effects of Anisotropy and Position Dependent Effective Mass on the Oscillator Strength of Impurity Doped Quantum Dots" Journal of Advances in Nanomaterials, 2016, 1, 64-72

11. **Ghosh, A. P.;** Toda, M. J., Kozlowski, P. M. "Photolytic Properties of B_{12}-Dependent Enzymes: A Theoretical Perspective." In book: Vitamins and Hormones: Vitamin B_{12}. Volume 119, Academic Press/Elsevier. 2021 (In press)

12. **** Toda, M. J., **Ghosh, A. P.,** Parmar, S., Kozlowski, P.M. "Computational Investigations of B_{12}-Dependent Enzymatic Reactions" In book: Methods in Enzymology (MIE) Volume 667: B_{12} Enzymes, Elsevier (In press)

13. **Ghosh, A. P**.; Lodowski, P; Kozlowski P.M. "Aerobic photolysis of methylcobalamin: unraveling the photoreaction mechanism" Under review

POSTER AND ORAL PRESENTATIONS

1. **Arghya P. Ghosh**, Abdullah Al Mamun, Pawel M Kozlowski. "Effect of mutation on the photolytic properties of methylcobalamin-dependent methionine synthase- QM/MM study" Graduate Student Regional Research Conference, 2020 (Poster)

2. **Arghya P. Ghosh**, Abdullah Al Mamun, Pawel M Kozlowski. "Effect of mutation on the photolytic properties of methylcobalamin-dependent methionine synthase- QM/MM study" 51st Midwest Theoretical Chemistry Conference, University of Norte Dame, June 2019 (Poster)

3. **Arghya P. Ghosh**, Pawel M Kozlowski. "Light-induced activation of organo-metallic Co-C bond in MeCbl-dependent Methionine Synthase- QM/MM Study" 63th Biophysical Society Annual Meeting Regional Meeting, Baltimore, Maryland, March 2019 (Poster)

4. **Arghya P. Ghosh**, Pawel M Kozlowski. "How mutation in cap domain controls the photo-activation of Co-C bond in MeCbl-dependent methionine synthase?" Graduate Student Regional Research Conference, 2019 (Oral)

5. **Arghya P. Ghosh**, Pawel M Kozlowski. "Computational modeling of photo-induced activation of organo-metallic Co-C bond in MeCbl-dependent Methionine Synthase- QM/MM Study" Brown Bag Series Grad talk, University of Louisville (Oral)

6. **Arghya P. Ghosh**, Pawel M Kozlowski. "Light-induced activation of organo-metallic Co-C bond in MeCbl-dependent Methionine Synthase- QM/MM Study" 70th ACS Regional meeting, Augusta, Georgia Oct-Nov 2018 (Poster)

7. **Arghya P. Ghosh**, Pawel M Kozlowski. "Elucidating the mechanism of alkylation reaction involving Cob(I)alamin by Alkyl halide: S_N2 or radical mechanism?" 255th ACS National meeting, New Orleans, Louisiana, March 2018 (Poster)

8. **Arghya P. Ghosh**, Pawel M Kozlowski. "Elucidating the mechanism of alkylation reaction involving Cob(I)alamin by Alkyl halide: S_N2 or radical mechanism?" Graduate Student Regional Research Conference, 2018 (Poster)

9. **Arghya P. Ghosh**, Manas Ghosh "Analyzing non-linear optical properties of impurity-doped quantum-dot with the influence of position-dependent effective mass in presence of gaussian white noise" National Symposium On 'Recent Advances in Chemistry Research' West-Bengal, India, March 04, 2016

TECHNICAL SKILLS

- **Technical Expertise:** Quantum chemical calculations, Density Functional Theory (DFT), Time-dependent Density Functional Theory (TD-DFT), Multireference Self-Consistent Field Calculations (CASSCF), Multiscale modeling (QM/MM), Molecular Dynamics (MD) simulation, Parallel/HPC computing.
- **Quantum Chemistry codes:** Gaussian, Orca.
- **Molecular Dynamics:** Amber, Gromacs
- **Visualization software:** Chimera, Gaussview, VMD, Chemcraft, Avagadro
- **Plotting software and data analysis:** Origin, Gnuplot
- **Programming languages:** Python and Linux shell scripting
- **Operating systems:** Linux, and Windows

AWARDS

University of Louisville Graduate Network in A&S (GNAS) Research fund award   (Spring 2019)
University of Louisville Graduate Student Council (GSC) Travel Award   (Fall 2019)
University of Louisville Graduate Student Council (GSC) Travel Award   (Fall 2018)
University of Louisville Prestigious GSC Research Grant Award   (Spring 2018)
University of Louisville International Center Tuition Support Award   (Spring 2018)
University of Louisville International Center Tuition Support Award   (Fall 2018)
University of Louisville Graduate Network in A&S (GNAS) Research fund award   (Fall 2018)
University of Louisville, Department of Chemistry Conference travel award   (Fall 2018)
University of Louisville Graduate Student Council (GSC) Travel Award   (Spring 2018)
Best-applied project award in Eastern India Science and Engineering Fair   (2014)
CSIR-NCL, Summer Research Fellowship   (Summer 2014)

TEACHING EXPERIENCES

Graduate Teaching assistant   Spring 2017 – Fall 2021
Department of Chemistry, University of Louisville, KY, USA
- CHEM-101- Intro to Chemistry

- CHEM-207 and CHEM-208- Intro to Chemical Analysis (laboratory experiments)
- CHEM-466 (Advance Physical Chemistry)- Thermodynamics, statistical thermodynamics, chemical equilibrium, and reaction kinetics from a molecular point of view
- CHEM-470- Laboratory experiments and related lecture on properties of gases, thermochemistry, kinetics, electrochemistry, laser techniques in chemical processes, spectroscopic methods, including UV-VIS, FTIR, and EPR

PROFESSIONAL MEMBERSHIP

- American Chemical Society   2017-present
- Biophysical Society   2018-present
- Member of VIBHA India   2020-Present

COLLABORATORS

Dr. Piotr Lodowski (University of Silesia, Poland), Dr. Maria Jaworska (University of Silesia, Poland), Dr. Justyna Wolinska (Lublin University of Technology)